CHAPTER 1: INTRODUCTION

Alzheimer's disease (AD) is the most common cause of late life dementia and represents the fourth leading cause of death in the developed world (Soto, 1999). In 2006, the worldwide prevalence of AD was 26.6 million (Brookmeyer et al., 2007). In Malaysia, approximately 20,000 Malaysians are currently diagnosed with the illness. AD prevalence is approximately 1 % between 65 and 69 years and is higher than 50 % in individuals over 95 years (Racchi et al., 2008).

AD is characterized by severe memory loss and cognitive impairment, with the degenerative loss of basal forebrain cholinergic neurons (Fodale et al., 2006) and extensive reduction of cholinergic acetyltransferase (ChAT) activity in the cerebral cortex hippocampus (Davies and Maloney, 1976). Besides the damage in the cholinergic system, the formation and growth of brain amyloid lesions, the senile plaques, is also widely believed to be a crucial event in the pathogenesis of AD (Schaeffer et al., 2011). Current therapies include the use of acetylcholine (ACh) precursors, muscarinic agonists and acetylcholinesterase (AChE) inhibitors (Amenta et al., 2001).

The principal role of AChE is the termination of nerve impulse transmission at the cholinergic synapses by rapid hydrolysis of ACh. Hence AChE inhibitors can be used to increase the amount of acetylcholine present in the synapses between cholinergic neurons in order to improve cholinergic function in AD patients (Jung and Park, 2007). Although the AChE inhibitors donepezil, galantamine, rivastigmine and tacrine have been approved by the Food and Drug Administration (FDA) in the United States, these drugs have only modest effects on clinical benefit and do not prevent disease progression (Vardy et al., 2005).

Reports that the ability of AChE to promote amyloid formation is inhibited by propidium and decamethonium, point to involvement of the peripheral anionic binding site in the interaction of the enzyme with amyloid beta (Aβ) peptide (Inestrosa et al., 1996). Furthermore, several AChE inhibitors have been found to activate the non-amyloidogenic pathway and thus to reduce Aβ production (Racchi et al., 2004). They affect the expression and/or the metabolic processing of amyloid precursor protein (APP) essential for amyloid beta generation. Recent studies also indicate that AChE induces the aggregation of prion protein with a similar dependence on the peripheral anionic site (PAS) (Inestrosa et al., 2008).

Hence suitably-designed AChE inhibitors have the potential to become drug candidates which are capable of not only reducing the symptoms of AD, but also preventing disease progression.

AIMS OF STUDY

Most studies that have been carried out on AChE focus on the catalytic site of the enzyme. In this study, in addition to the catalytic site (CAS), the PAS will also be included in order to identify novel anticholinesterase compounds which are not only effective in reducing the symptoms of AD, but also preventing disease progression.

In the current study, virtual screening on commercially available compound libraries was performed to determine the binding mode of these inhibitors to the AChE. The AChE inhibitory activity of each compound was evaluated. Those compounds which showed promising activity were further evaluated for β-amyloid aggregation inhibitory activity.

The specific objectives of this study are as follows:-

1. To perform virtual screening on commercially available compound libraries to predict their anticholinesterase activity.

2. To optimise assays to determine inhibition of AChE and Aβ peptide aggregation.

3. To assay selected compounds for inhibition of AChE and Aβ peptide aggregation.

CHAPTER 2: LITERATURE REVIEW

2.1 THERAPEUTIC STRATEGY IN ALZHEIMER'S DISEASE TREATMENT

There are two main approaches for treatment of Alzheimer's disease (AD):-

(a) Cholinergic hypothesis and enhancement of cholinergic function

The findings that AD is associated with impairment in the cholinergic system led to the cholinergic hypothesis, which relates the neuronal degeneration with the loss of cholinergic neurotransmission (Terry and Buccafusco, 2003). Therefore, increasing cholinergic transmission may enhance cognitive function **(Figure 2.1)** (Alhomida et al., 2000). Cholinergic deficits in AD patient can be enhanced through various mechanisms of action in different parts of the cholinergic neurotransmission system.

Choline precursors, such as phosphatidylcholine, aimed at increasing the bioavailability of choline, ACh (acetylcholine) releasers, which facilitate the release of ACh from presynaptic end terminals, nicotinic agonists which enhance ACh release and acetylcholinesterase (AChE) inhibitors can be used to help overcome cholinergic deficits in AD patients. So far, the use of AChE inhibitors seems to be the most effective method for reducing the symptoms of the disease. Their mode of action is to block the AChE enzyme thereby stimulating cholinergic activity and enhancing cognitive function (Racchi et al., 2004).
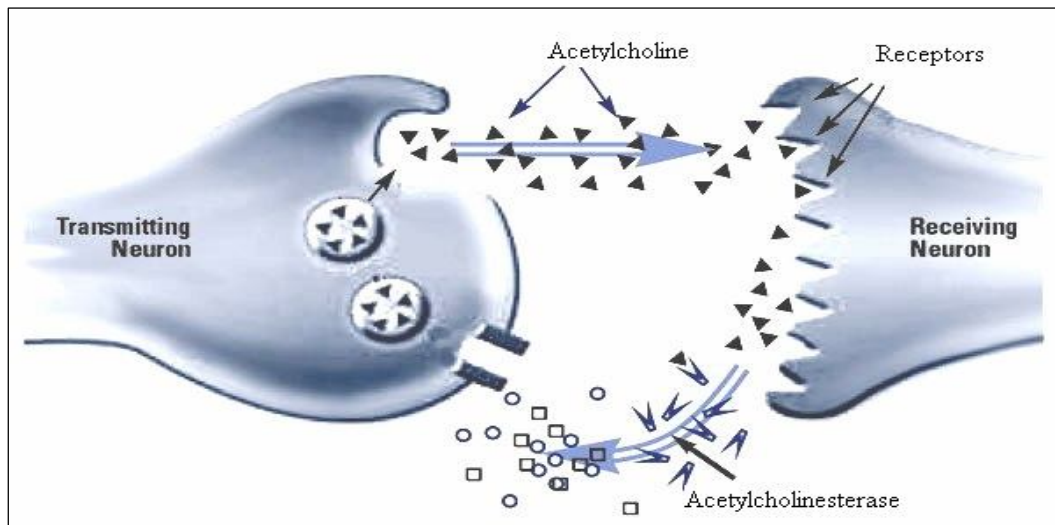
Figure 2.1: The mechanism of cholinergic neurotransmission. After signaling, acetylcholine is released from receptors and broken down by acetylcholinesterase to be recycled in a continuous process. Adapted from http://www.vrp.com/why-vrp on 28th April, 2012)

(b) Reduction or prevention of deposition of amyloid peptides

Amyloid beta (Aβ) peptide is a main component of senile plaques and fibrillary tangles that constitute one of the neurohistopathological features of AD. The Aβ peptide (39–43 amino acids) is generated by the proteolytic processing of the amyloid precursor protein (APP) (Inestrosa et al., 1996). APP is processed by one of two pathways: the amyloidogenic pathway leading to the production of Aβ (involving β and γ secretase) and the non-amyloidogenic pathway (involving α and γ secretase) (Vardy et al., 2005). The non-amyloidogenic pathway precludes the accumulation of Aβ (Tang, 2005) **(Figure 2.2).**

Incorporation of AChE into Alzheimer's amyloid aggregates results in the formation of stable complexes that change the biochemical and pharmacological properties of the enzyme and increase the neurotoxicity of Aβ fibrils (Inestrosa et al., 1996). Association of AChE with Aβ and the formation of amyloid fibrils can be inhibited by peripheral anionic site (PAS) ligands such as propidium (Inestrosa et al.,

1996). Reduction of Aβ production, either through inhibition of β and γ secretase or through activation of α secretase, is also a potential therapeutic approach for AD (Vardy et al., 2005).
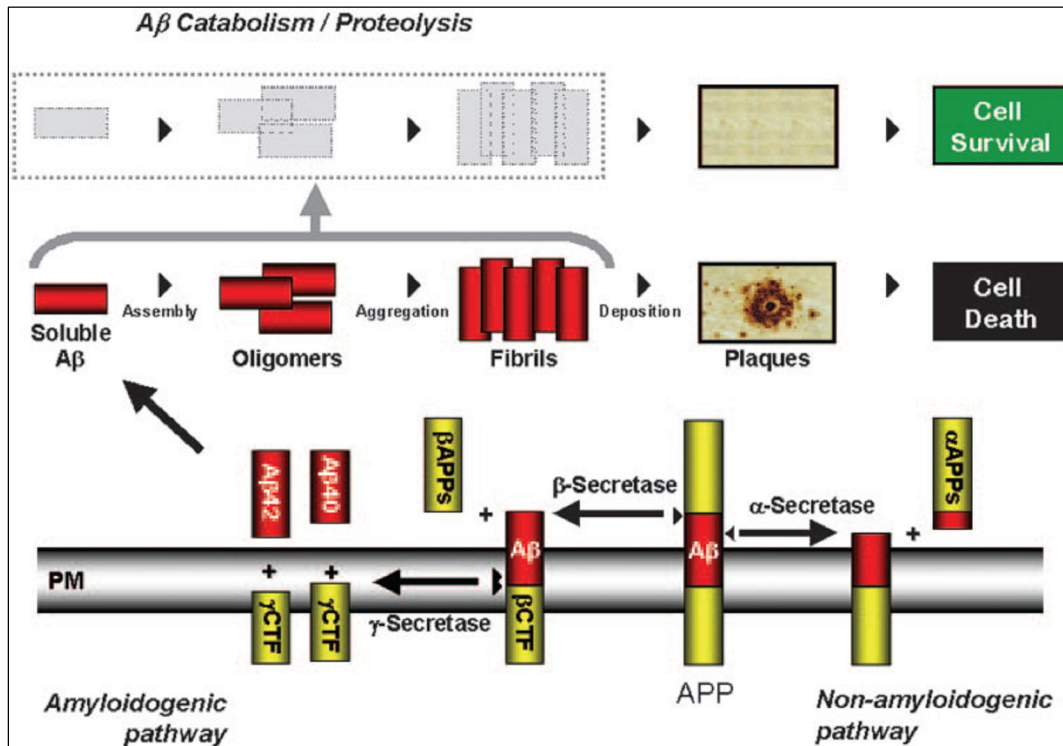

Figure 2.2: The amyloid cascade hypothesis. The APP is processed by β and γ secretases via the amyloidogenic pathway to yield a variety of toxic Aβ-containing species, ultimately resulting in neuronal cell death. These amyloidogenic species can be degraded by a number of catabolic proteases such as neprilysin, IDE and plasmin, thereby clearing Aβ and preventing cell death. The non-amyloidogenic pathway results from α secretase cleavage within the Aβ sequence of APP (adapted from Jacobsen et al., 2005).
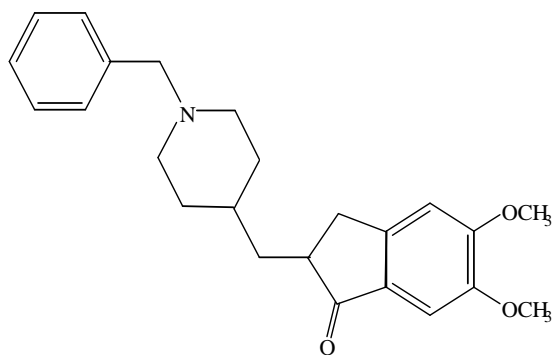
2.2 ACETYLCHOLINESTERASE INHIBITORS

Several AChE inhibitors are available for the treatment of mild to moderate AD namely donepezil, galantamine, rivastigmine and tacrine **(Figure 2.3)**. Tacrine was the first compound to come into clinical use, but it has now been replaced by the second generation inhibitors which are safer and have longer lasting effects. Rivastigmine is irreversible inhibitor whereas donepezil, galantamine and tacrine are reversible inhibitors. An inhibitor such as donepezil may bind to both the catalytic site (CAS) and PAS while others such as tacrine have higher affinity for the CAS compared to the PAS.

The important binding groups for an AChE inhibitor appear to be a positively charged nitrogen and a hydrogen-bonding group, separated by a lipophilic region. Since a positively charged nitrogen is common in many alkaloids at body pH, it is not surprising that many of the most powerful AChE inhibitors come from this class of compounds (Houghton and Howes, 2005).

(-)-Huperzine A is a natural compound (alkaloid) first isolated from Chinese medicine *Huperzia serrata* in 1986 (Filho et al., 2006). The protopine and palmatine from the aerial parts of *Corydalis speciosa* (Kim et al., 2004) are also alkaloids that have been isolated and were reported to inhibit AChE activity.

However, a number of other natural products which do not contain any nitrogen, have been found to be AChE inhibitors such as the triterpene ursolic acid (Chung et al., 2001), the flavonoid linarin (Fan et al., 2008), the sterol haloxysterol B (Ahmed et al., 2006) and the coumarin decursin (Kang et al., 2003). Non-nitrogen containing compounds may provide information on other features which are necessary for the activity.
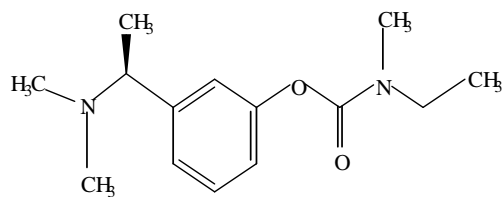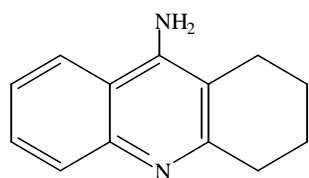
Donepezil
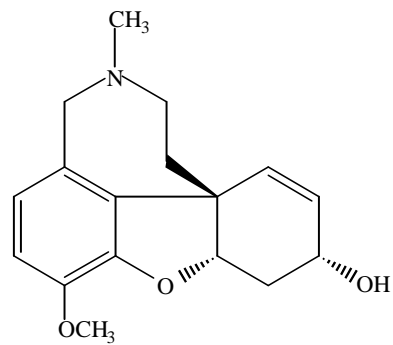
(-)-Galantamine
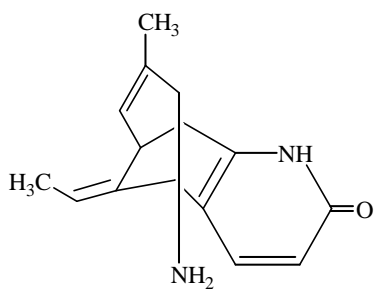
(-)-Huperzine A

Rivastigmine

Tacrine

Figure 2.3: Acetylcholinesterase inhibitors.

2.3 VARIOUS ROLES OF ACETYLCHOLINESTERASE INHIBITORS

AChE interacts with the Aβ peptide and promotes amyloid fibrils formation by a hydrophobic environment close to the PAS of the enzyme (De Ferrari et al., 2001). This can be inhibited by PAS ligands such as propidium (Inestrosa et al., 1996). However knowledge of the relationship between AChE activity and Aβ toxicity is still limited.

A number of studies on designing and synthesizing new dual acting compounds have been carried out. For example, it has been reported that piperidine derivaties and donepezil- tacrine hybrid related derivatives have dual inhibitory potency against AChE and $Aβ_{1-42}$ peptide aggregation that could bind simultaneously to the PAS and CAS binding site of the enzyme (Kwon et al., 2007; Alonso et al., 2005).

There is some evidence that some molecules may protect neurons from neurodegenerative insults including deposition of Aβ. Donepezil has been found to exert a neuroprotective effect by reducing the amount of the toxic form of Aβ in septal neuron cultures, independent of inhibition of AChE activity (Kimura et al., 2005). Likewise another compound (-)-huperzine A **(Figure 2.3)** has been demonstrated to protect neuronal and glial cells against cytotoxicity of Aβ (Zhang et al., 2002).

A remarkable inhibition of MSA (maximum size of aggregation) was obtained with propidium iodide, suggesting that AChE triggers PrP 106–126 and Aβ aggregation through a similar mechanism. Huprines (AChE inhibitor) also significantly decreased MSA induced by AChE as well (Pera et al., 2006), suggesting the PAS of the AChE is involved both in the Aβ and PrP pro-aggregating effect.

Pakaski et al. (2000) reported that metrifonate (AChE inhibitor) can increase the cell-associated APP level in a basal forebrain neuronal culture and also elevate the amount of APP secreted into medium thus suggesting that AChE inhibitors modulate APP processing via a stimulatory effect on Protein kinase C (PKC). It has also been stated that the effects of Huperzine A on the elevation of acetylcholine levels might contribute to an increase in secreted amyloid precursor protein-α (sAPPα) release because it might stimulate the muscarinic acetylcholine receptors M1 and M3 mediating the PKC pathway (Yan et al., 2007).

2.4 MOLECULAR MODELING STUDIES ON ACETYLCHOLINESTERASE

The X-ray crystallographic structure of the *Torpedo californica* acetylcholinesterase (*Tc*AChE) (Protein Data Bank (PDB) code: 1acj) (Sussman et al., 1991) **(Figures 2.4 & 2.5)** an enzyme monomer with 537 amino acids, shows that the CAS consists of the Ser200-His440-Glu327 triad. It is located near the bottom of a deep, narrow cavity, named the 'active-site gorge', lined by 14 aromatic residues. Of these 14 residues, Trp84 and Phe330 are involved in the so called 'anionic' subsite of the CAS, making π-cation interactions with the quaternary amino group of the substrate (Harel et al., 1993). Trp279 and Tyr70 contribute to the PAS at the mouth of the gorge (Eichler et al., 1994) and Trp233, Phe288 and Phe290 contribute to the acyl pocket (Harel et al., 1996). The structure of recombinant monomeric mouse acetylcholinesterase (mAChE) in complex with fasciculin-II (FAS-II) (PDB code: 1mah), provided the first mammalian cholinesterase template. A close structural similarity is observed between mAChE and *Tc*AChE (Bourne et al., 1995).
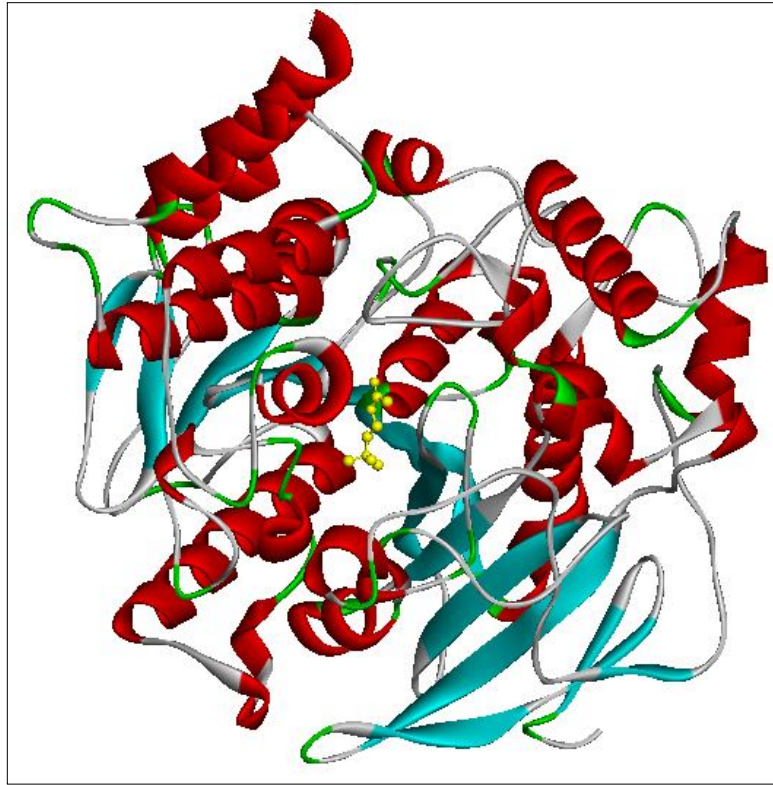
Figure 2.4: Ribbon diagram of *Tc*AChE complex with ACh, displayed as a ball-and-stick model, docked in the active site (adapted from Silman and Sussman, 2008).
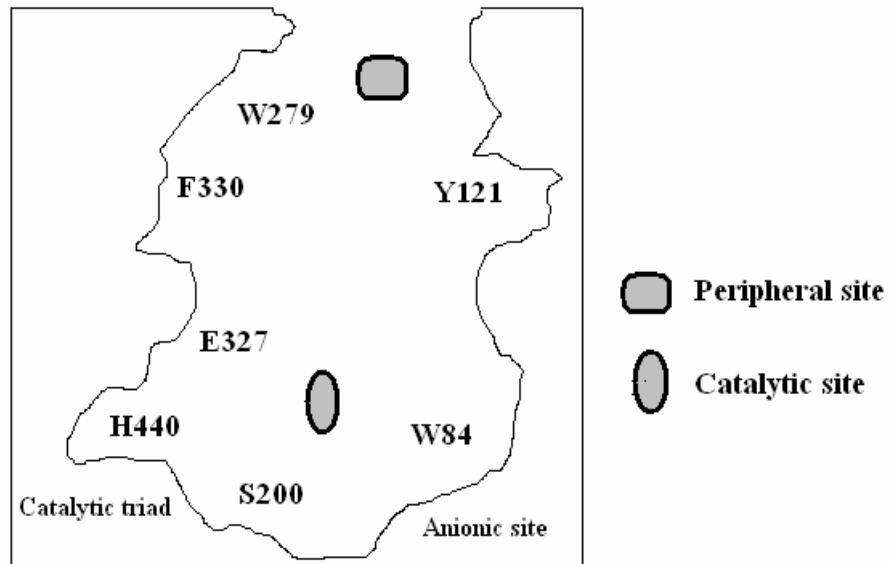

Figure 2.5: Schematic cross-sections through the active-site gorge of *Tc*AChE, showing the principal residues involved in the CAS and PAS and the catalytic triad (adapted from Silman and Sussman, 2008).

The amino acid sequence of human acetylcholinesterase (hAChE) has been determined (Soreq et al., 1990) and shown to have high homology with the *Tc*AChE. In particular, the residues constituting the surface of the ligand-binding pocket are identical except for Phe330, which is replaced by Tyr337 in the hAChE **(Figure 2.6)** (Belluti et al., 2009; Yamamoto et al., 1994). The x-ray crystallographic structure of hAChE in complex with FAS-II (PDB code: 1b41) (Kryger et al., 2000) revealed corresponding residues in hAChE and *Tc*AChE **(see figure 2.7 for comparison of the structures)**. Conservation of the amino-acid residues lining the active site gorge is very high: 26 residues are identical, two are similar, *viz.* Thr83(*Ser*81) and Tyr337(*Phe*330), and only two residues, both at the mouth of the gorge, are different in hAChE and mAChE *versus Tc*AChE, *viz.* Thr75(*Glu*73) and Leu76(*Gln*74) **(Table 2.1)**. In AChE from bovine erythrocytes, the Phe330 in *Tc*AChE is replaced by Tyr330.

Table 2.1: The identity and numbering of the residues in the different species.

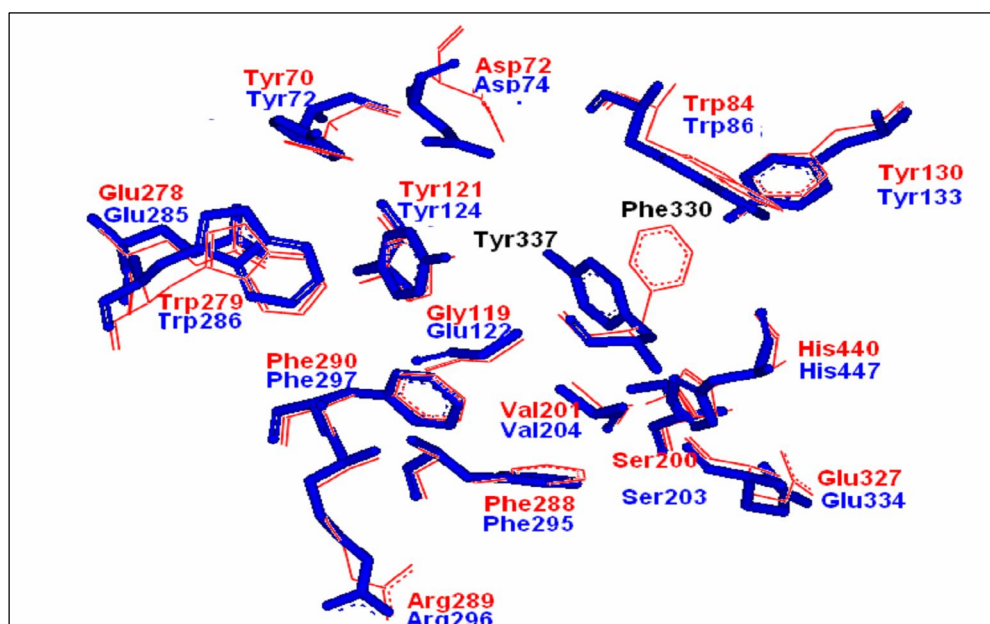| Binding sites	Species & Residues involved		
	*Tc*AChE	mAChE	HAChE
Acyl pocket	Trp233		
	Phe288	Phe295	Phe295
	Phe290	Phe297	Phe297
CAS	Trp84	Trp86	Trp86
	Phe330	Tyr337	Tyr337
	Ser200	Ser203	Ser203
	His440	His447	His447
	Glu327	Glu334	Glu334
PAS	Tyr70	Tyr72	Tyr72
	Glu73	Thr75	Thr75
	Gln74	Leu76	Leu76
	Trp279	Trp286	Trp286

Figure 2.6: Superimposition of the structures of hAChE (blue) and *Tc*AChE (red) (Liu et al., 2009).
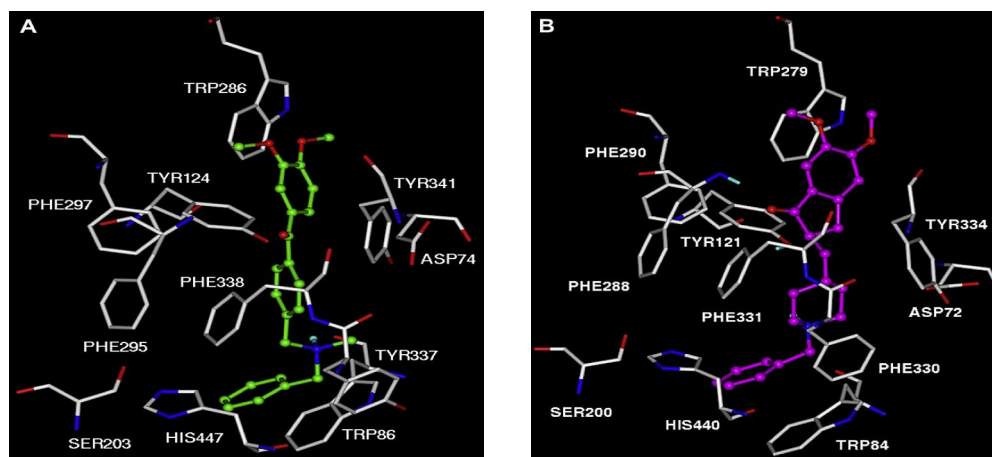
Figure 2.7: Docking model of a donepezil analogue with hAChE **(A)** and *Tc*AChE **(B)** (Belluti et al., 2009).

The complex formed between huperzine A and single-site and double site mutants of recombinant hAChE (rhAChE) showed that Tyr at position 337 is essential for inhibition of rhAChE by huperzine A (Ashani et al., 1994). Docking studies using *Tc*AChE have shown that inhibitors such as donepezil-tacrine hybrids and indole-tacrine heterodimers also are stacked against the aromatic rings of Trp84 and Tyr330 at the catalytic site and Trp279 at the PAS (Alonso et al., 2005; Munoz-Ruiz et al., 2005).

Comparison of the effects of 'peripheral site' ligands such as propidium and fasciculin (FAS) on *Tc*AChE and chicken AChE has indicated that they are more effective inhibitors of *Tc*AChE due to the absence of the two aromatic residues Tyr70 and Trp279 in the chicken enzyme (Eichler et al., 1994; Harel et al., 1995). FAS association with several mutant forms of recombinant DNA derived AChE from mouse have shown that the aromatic residues Tyr72, Tyr124 and Trp286 have the most marked influence on FAS binding (Radic et al., 1994).

2.5 DOCKING

Docking is a process which brings two molecular structures together so that binding occurs. The binding site is the part of the protein where the ligand binds. The binding site can be identified by looking at the crystal structure of the protein bound with a known inhibitor. The conformation of the ligand in the binding site is called the binding mode. Generally, protein-ligand docking software consists of two main components that work together, a search algorithm and a scoring function. The search algorithm generates a large number of poses of a molecule in the binding site while the scoring function calculates a score or binding affinity for a particular pose. Scoring functions can be divided into forcefield-based, empirical and knowledge-based potentials. There are a number of docking programmes available such as AutoDock (Morris et al., 1998), Dock (Kuntz et al., 1982), Drawin, E-Hits, FlexX (Rarey et al., 1996), FRED, Glide (Friesner et al., 2004), Gold (Jones et al., 1997), LigandFit, QXP, Slide and Surflex-Dock.

2.6 VIRTUAL SCREENING

In drug discovery, the physical screening of large libraries of chemicals against a biological target (high-throughput screening) is a dominant technique for the identification of new lead compounds. An alternative approach, known as virtual screening is to computationally screen large libraries of chemicals for compounds that complement targets of known structure, and experimentally test those that are predicted to bind well. This approach has been found to produce hit rates (ligands discovered per molecules tested) significantly greater than those obtained with high-throughput screening (Shoichet, 2004).

2.6.1 Virtual screening can be divided into two:-

(a) Structure based virtual screening

Involves automated and fast docking of a large number of chemical compounds against a protein-binding or active site (Reddy et al., 2007).

(b) Ligand based virtual screening

Databases of chemical structures are searched to find compounds that are similar to known actives (similarity searching) or posses a pharmacophore or substructure in common with a known active (pharmacophore substructure searching) (Reddy et al., 2007).

Docking algorithms for structure based virtual screening can be broadly classified into three categories **(Figure 2.8)**:-

(a) Searching the conformational space during docking

(b) Searching the conformational space before docking

(c) Incremental docking
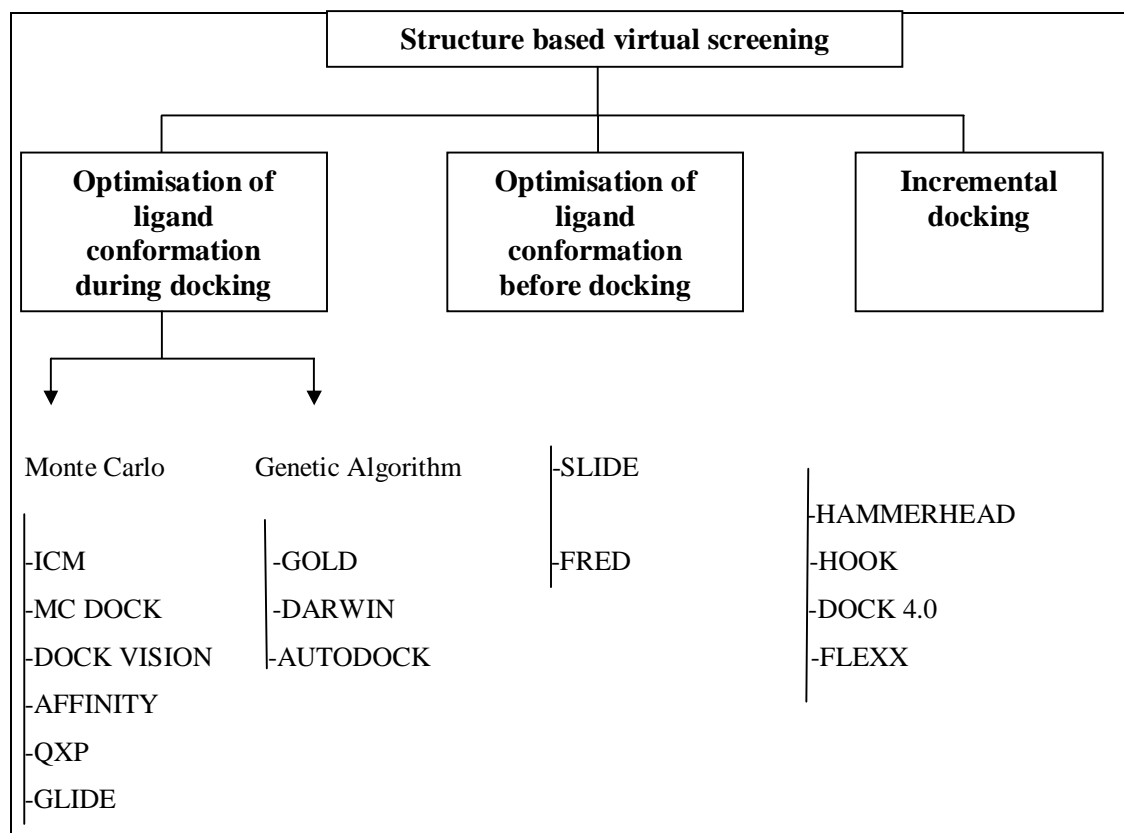
Figure 2.8: Classification of various methods of structure based virtual screening (http://www.slideshare.net/baoilleach/proteinligand-docking).

Virtual screening methods have been applied in recent years in order to find lead compounds for many targets such as Human Immunodeficiency Virus (HIV), AChE, Severe Acute Respiratory Syndrome (SARS), Cystein protease and *Mycobacterium tuberculosis* (MTB). In particular, there have been several successful cases reported for the synthesis of potential AChE inhibitors by the virtual screening procedure.

Taking AChE as target, a structure based pharmacophore model was generated and screening was conducted over 110 000 natural products which resulted in identification of effective AChE inhibitors, scopoletin and scopolin (Rollinger et al., 2004). In another study, virtual screening of about 160 000 commercially available compounds against the X-ray crystallographic structure of AChE was performed by Mizutani & Itai (2004) by employing a new method called ADAM & EVE. This study

found 13 compounds which had IC_{50} values between 0.5 and 10 μM and almost all their core structures are very different from those of known inhibitors.

CHAPTER 3: ACETYLCHOLINESTERASE MODEL BUILDING, SELECTION OF PROTEIN CRYSTAL STRUCTURES AND VIRTUAL SCREENING OF UNKNOWN LIGANDS

3.1 INTRODUCTION

The Brookhaven Protein Data Bank (PDB) is a repository of protein crystal structures, often in complexes with inhibitors. The PDB contains several crystal structures of acetylcholinesterase (AChE) such as human acetylcholinesterase (hAChE), *Torpedo californica* acetylcholinesterase (*Tc*AChE), mouse acetylcholinesterase (mAChE) and bovine erythrocytes acetylcholinesterase.

In the current study, several crystal structures of AChE were extracted from the PDB and docked with known ligands to find the most suitable protein structure for virtual screening. The selected protein was then docked with large libraries of commercially available ligands using computational procedures in order to identify potential anticholinesterase compounds.

3.2 MATERIALS AND METHODS

Work station, molecular modeling software.

3.2.1 Model building and model selection of protein crystal structures

3.2.1.1 Preparation of protein file

The AChE crystal structures, hAChE in complex with fasciculin II (2.76 Å) (PDB ID: 1b41), *Tc*AChE in complex with aricept (2.50 Å) (PDB ID: 1eve), mAChE in complex with gallamine (2.20 A°) (PDB ID: 1n5m), mAChE in complex with decidium

(2.35 A°) (PDB ID: 1j07), mAChE in complex with succinylcholine (2.05 A°) (PDB ID: 2ha2) and mAChE in complex with propidium (2.25 A°) (PDB ID: 1n5r) were extracted from the PDB as pdb files. The heteroatoms and water molecules were removed using Discovery Studio Visualizer 3.1 (Accelrys, Inc, Sandiego, CA, USA). Hydrogen atoms were added and double coordinates were corrected using Hyper chem Pro 6.0 software. Some modifications were carried out on *Tc*AChE crystal structure, PDB ID: 1eve to better reflect the binding site sequence in hAChE, resulting in five different protein files as outlined below:-

(a) Without any replacement of residues or energy minimization

(b) With residue Phe330 replaced by Tyr

(c) With residue Phe330 replaced by Tyr followed by energy minimization using Swiss PDB Viewer (SPBV 4.01)

(d) With residue Phe330 replaced by Tyr, Ser81 replaced by Thr, Glu73 replaced by Thr and Gln74 replaced by Leu

(e) With residue Phe330 replaced by Tyr, Ser81 replaced by Thr, Glu73 replaced by Thr and Gln74 replaced by Leu followed by energy minimization using Swiss PDB Viewer (SPBV 4.01)

Then, again hydrogen atoms were added and non polar hydrogens were merged using AutoDock Tools 1.5.2 software. The protein files were checked for any missing atoms and atoms were added as necessary. Kollman charges were also added and the

values were recorded. Finally, AutoDock 4 type atoms were assigned to the proteins and the files were saved in pdbqt format.

3.2.1.2 Preparation of standard ligand file

Three dimensional structural models of 19 well known AChE inhibitors (**Figure 3.1**) were downloaded in mol2 format from Drug bank (http://drugbank.ca/) and Pub chem (http://www.ncbi.nlm.nih.gov/pccompound). These compounds were prepared in protonated form where appropriate for physiological pH. Then, the compounds were minimized through the Hyper chem Pro 6.0 software to the lowest energy. Ligand files were then saved in pdbqt format.

3.2.1.3 Preparation of grid parameter file (gpf)

The protein file and the selected ligand file were opened together in AutoDock Tools 1.5.2 software. A grid box was created by adjusting the defaults value to cover the entire protein. The spacing was set to a default value of 0.375, and the file extension was set as ".gpf". Gpf files were created for other ligands as well. The same process was repeated for all protein structures.

3.2.1.4 Preparation of the docking parameter file (dpf)

The protein file and the selected ligand file were opened together in AutoDock Tools 1.5.2 software. The docking parameters were set as number of ga runs = 100, number of individuals in population = 150 and maximum number of energy minimization (medium) = 2500000. Cluster tolerance (rmstol) value was set as 2.0 and Lamarckian genetic algorithm was used. The file extension was set as ".dpf". Dpf files were created for other ligands as well. The same process was repeated for all protein structures.

3.2.1.5 Running autodock

Running autodock using the Linux operating system requires a protein file, a ligand file, a gpf and a dpf file. Autogrid was run using the command line, autogrid4 –p filename.gpf –l filename.glg &. Autogrid was followed by autodock using the command line autodock4 –p filename.dpf –l filename.dlg &. The process was repeated for each protein and each ligand.

3.2.1.6 Docking analysis

Ligand - protein interactions were analyzed using Viewer Lite, Discovery Studio Visualizer 3.1 (Accelrys, Inc, Sandiego, CA, USA) and Ligplot 4.4.2 softwares. Ligands which showed high affinity for the enzyme and the most suitable protein for virtual screening were identified.

3.2.2 Virtual screening of unknown ligands

3.2.2.1 Preparation of protein file

The AChE crystal structure (PDB code: 1b41) was chosen for virtual screening.

3.2.2.2 Preparation of ligand file

The 'ZINC' database (http://zinc.docking.org/search/) was explored using decamethonium, MF268 and propidium as the backbone structure for the ligands to find commercially available ligands. About 830 unknown ligands in mol2 format were downloaded from ZINC database. The mol2 file was split and each ligand was named according to its ZINC id. These ligands were prepared in protonated form where appropriate for physiological pH.

3.2.2.3 Virtual screening

The number of evaluations for the virtual screening was set to 1750000, the population size was set to 150, the number of runs was set to 20, the spacing was set to 0.375 and the rmstol value was set to 2.0.

3.2.2.4 Docking analysis

The Autodock log file with the extention .dlg file for each ligand consisting of a clustering histogram where details such as cluster rank, lowest binding energy and number of cluster was obtained. A pdb file was created for each ligand from the dlg file. These pdb files and the protein file were opened in DS Visualizer software to analyse the ligand - protein interactions. The binding site of the ligand in the protein and the lowest binding energy were recorded. The residues involved in hydrogen bonding, Van der waals interactions and pi-pi interactions between the ligand and protein were recorded. Hydrophobic interactions were analyzed using Ligplot 4.4.2 software. Ligands which show high affinity for the enzyme were identified.
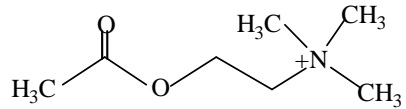
Acetylcholine
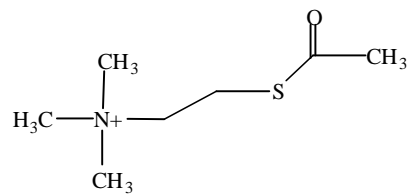
Acetylthio choline
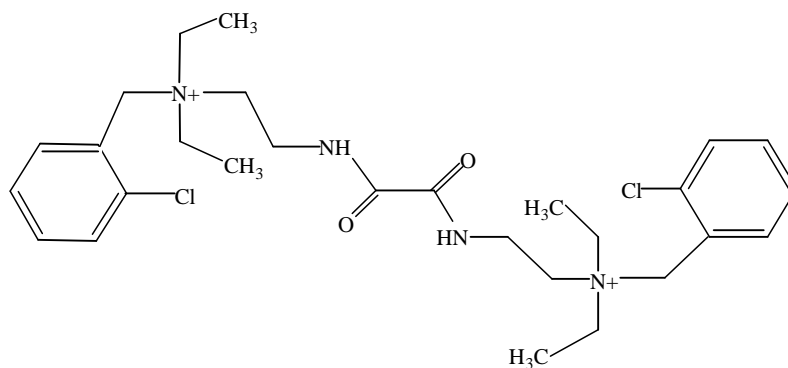
Ambenonium
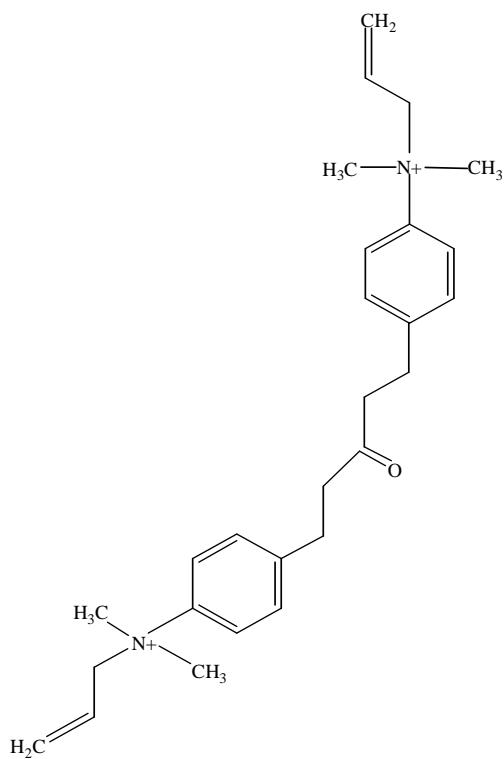
BW284C51
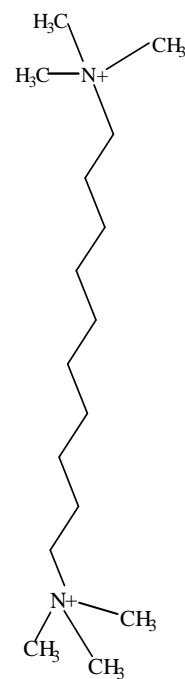
Decamethonium

Figure 3.1: Structures of known AChE ligands.
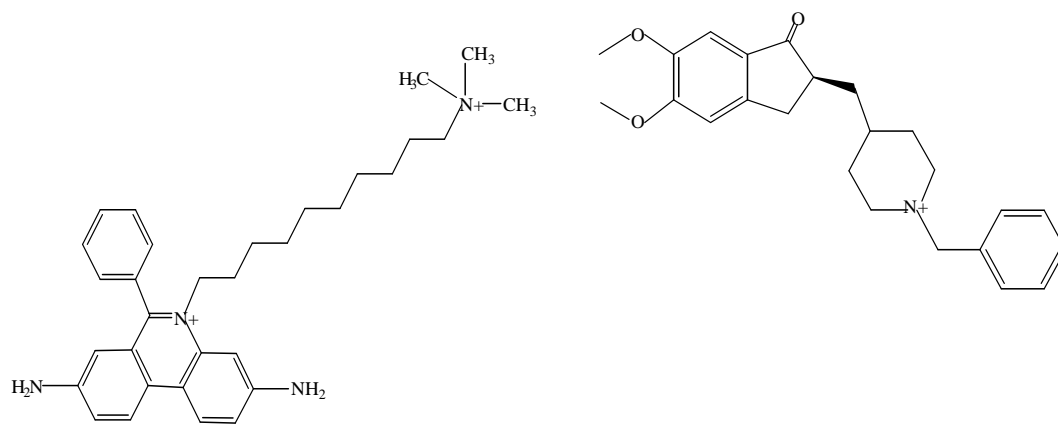
Decidium

Donepezil
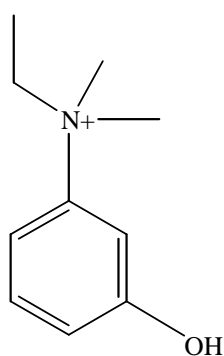
Edrophonium
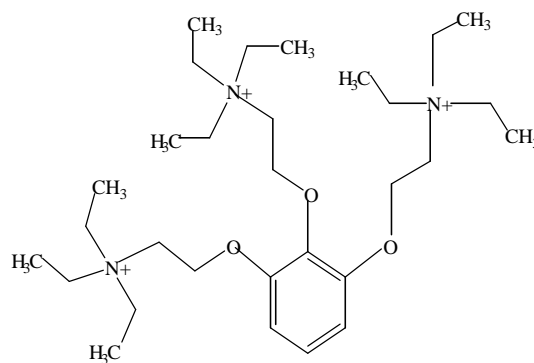
Gallamine
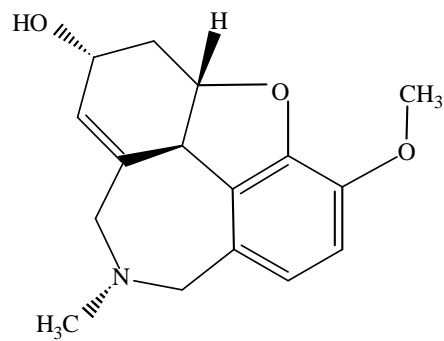
(-)-Galantamine
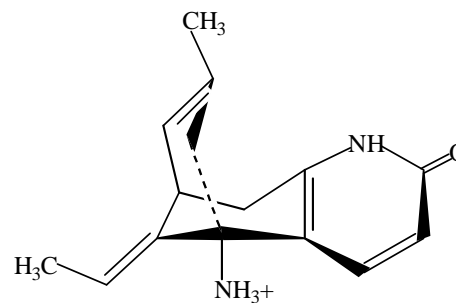
Huperzine A

Figure 3.1: Structures of known AChE ligands (continued).
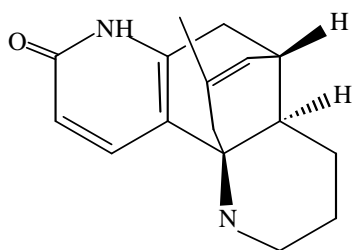
Huperzine B
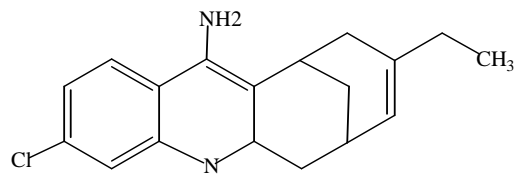
(-) - Huprine x
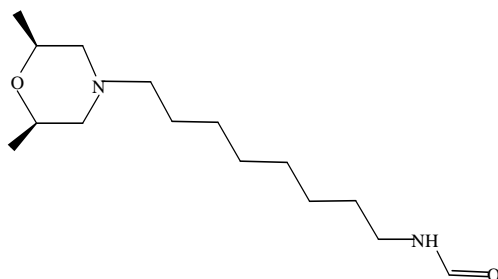
MF268
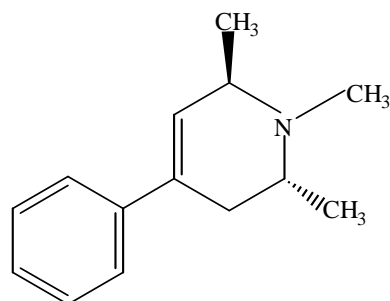
1-Methyl-4-phenyl-1, 2, 3, 6-
tetrahydropyridine (MPTP)
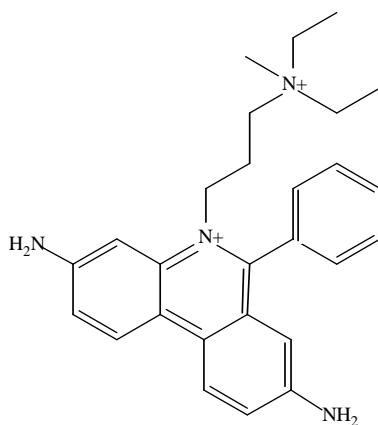
Propidium
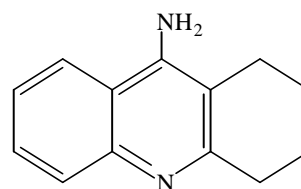
Tacrine

Figure 3.1: Structures of known AChE ligands (continued).
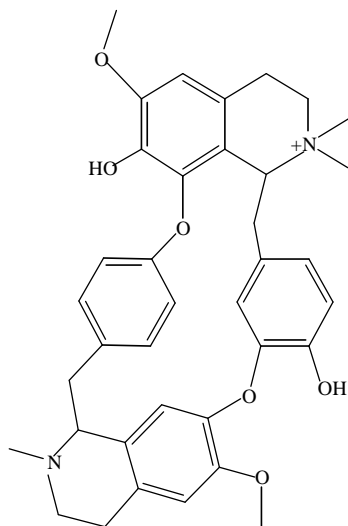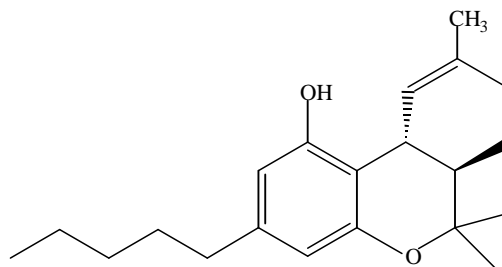
D-Tubocurarine   Tetrahydrocannabinol (Δ^9-THC)

Figure 3.1: Structures of known AChE ligands (continued).

3.3 RESULTS AND DISCUSSION

The protein crystal structures for model selection were chosen based on the resolution of the crystal structures. Ten crystal structures were investigated (**Tables 3.1–3.3**, **Appendices 1–27)** with 19 known ligands (**Figure 3.1**), comprising 7 PAS binding ligands, 9 CAS binding ligands and 3 both PAS and CAS binding ligands. The sequence identity between hAChE and mAChE is about 87 % and between hAChE and *Tc*AChE is about 53 % (Kryger et al., 2000). Therefore, the docking results were compared to mouse and *Tc*AChE in complex with ligand found in PDB.

The overall blind docking result **(Table 3.4)** indicated that 6 crystal structures (hAChE in complex with fasciculin II (2.76 Å) (PDB ID: 1b41), mAChE in complex with gallamine (2.20 A°) (PDB ID: 1n5m), mAChE in complex with decidium (2.35 A°) (PDB ID: 1j07), and modified models of *Tc*AChE in complex with aricept (2.50 Å) (PDB ID: 1eve) (b)–(d) **(see section 3.2.1.1)** [(except (e) which was compatible with PAS and both site (PAS & CAS) binders)] were compatible with PAS binding ligands.

mAChE in complex with succinylcholine (2.05 A°) (PDB ID: 2ha2) and mAChE in complex with propidium (2.25 A°) (PDB ID: 1n5r) were found to be compatible towards PAS and both site (PAS & CAS) binding ligands. *Tc*AChE in complex with aricept (2.50 Å) (PDB ID: 1eve) was compatible towards PAS, CAS and both site binding ligands **(Table 3.4)**. The ligplot analysis **(Appendices 28–30)** shows in detail the residues involved in hydrogen bonding and hydroph

obic interactions between the proteins and ligands.

The current study aimed at finding PAS binding ligands in addition to CAS binding ligands. Since the crystal structure of hAChE in complex with fasciculin II

(2.76 Å) (PDB ID: 1b41) was compatible with PAS binding ligands and the only crystal structure that available in PDB for hAChE, this crystal structure was chosen for the virtual screening studies. **Figure 3.2** shows the structures of top 21 compounds identified from virtual screening.
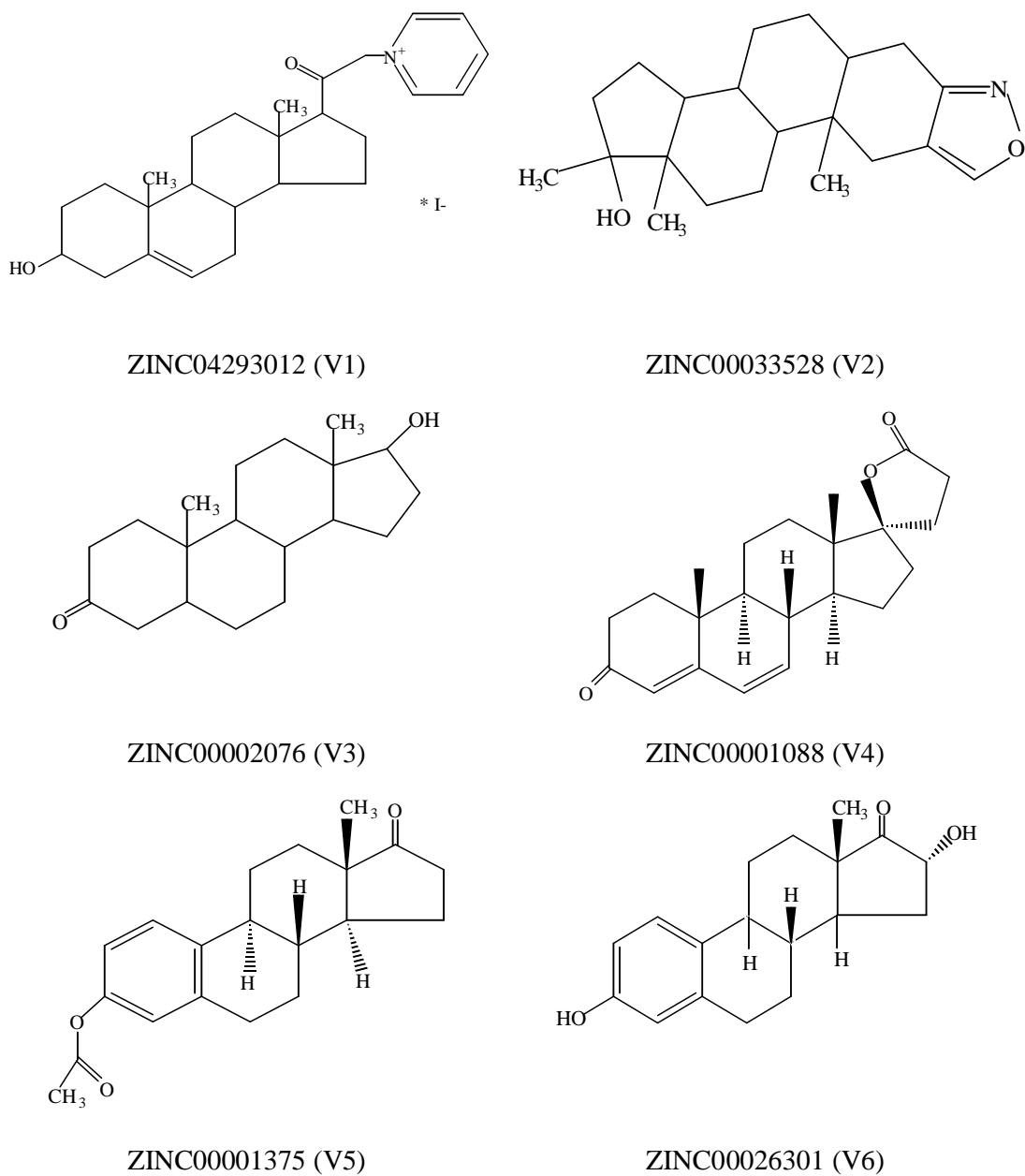
ZINC04293012 (V1)   ZINC00033528 (V2)

ZINC00002076 (V3)   ZINC00001088 (V4)

ZINC00001375 (V5)   ZINC00026301 (V6)

Figure 3.2: Structures of the top ligands identified from virtual screening for AChE binding activity.
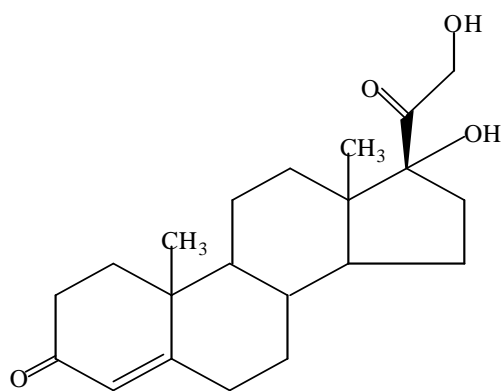
ZINC00001215 (V7)
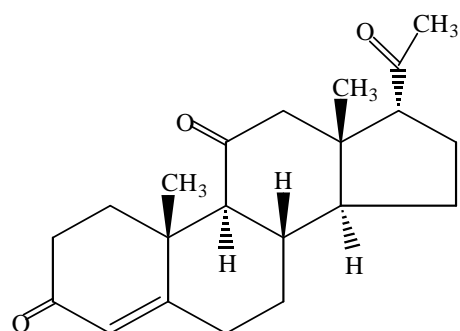
ZINC00002286 (V8)
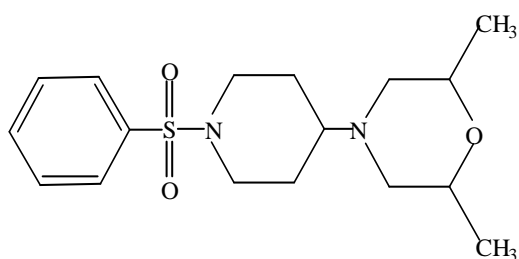
ZINC00550476 (V9)
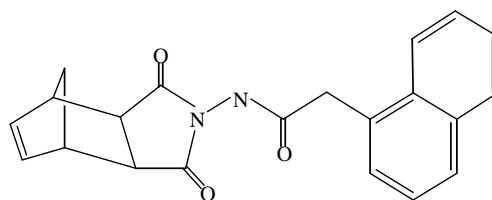
ZINC00033161 (V10)
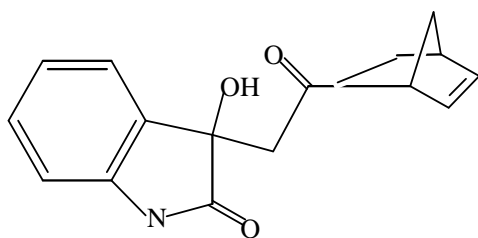
ZINC00032911 (V11)
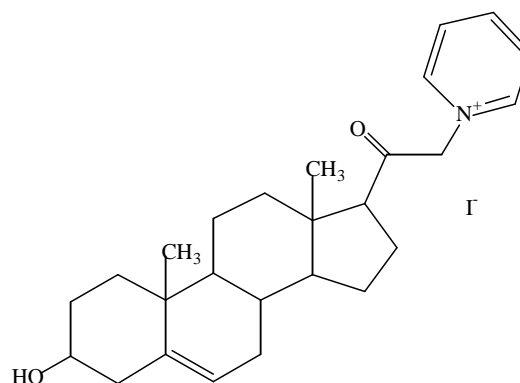
ZINC04293010 (V12)

Figure 3.2: Structures of the top ligands identified from virtual screening for AChE binding activity (continued).
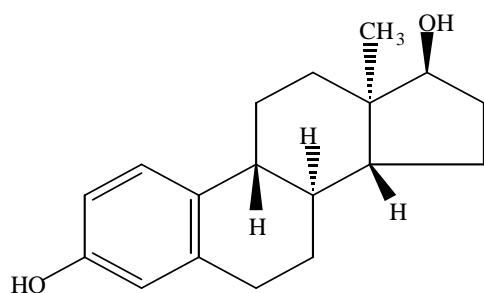
ZINC00001371 (V13)
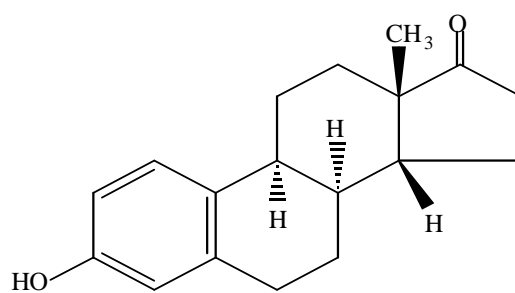
ZINC00031991 (V14)
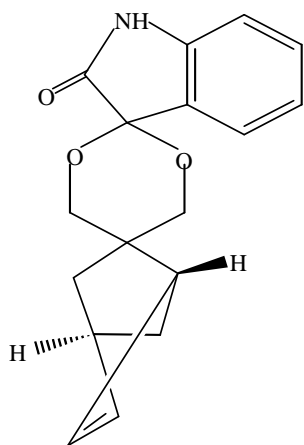
ZINC00032587 (V15)
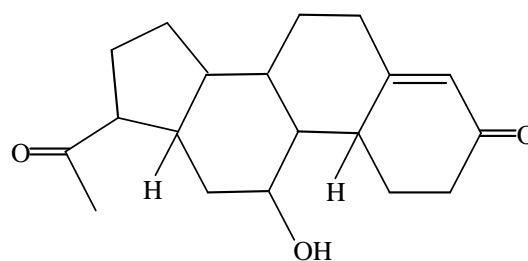
ZINC00002287 (V16)
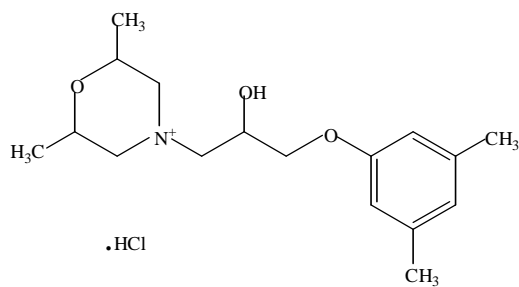
ZINC00211805 (V17)
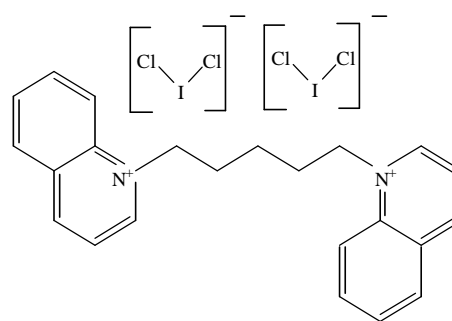
ZINC01668161 (V18)

Figure 3.2: Structures of the top ligands identified from virtual screening for AChE binding activity (continued).
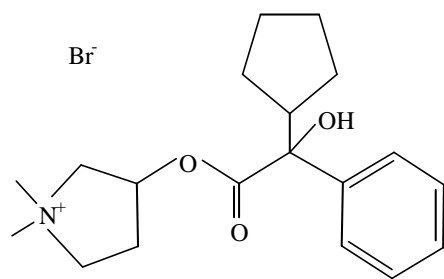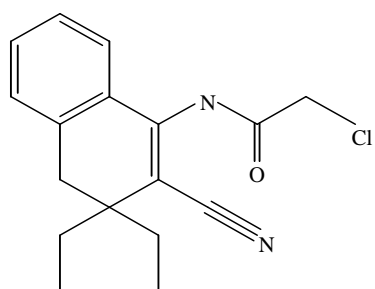
ZINC00000346 (V19)   ZINC00028128 (V20)
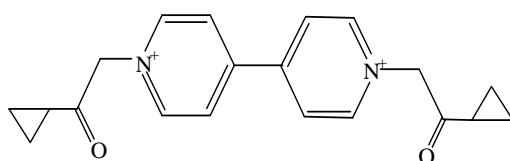
ZINC02190312 (V21)

Figure 3.2: Structures of the top ligands identified from virtual screening for AChE binding activity (continued).

Table 3.1: Results from the docking of standard ligands with a structure derived from the crystal structure of human AChE in complex with fasciculin II (2.76 Å) (PDB ID: 1b41) (arranged according to lowest binding energy).

Ligand	Cluster rank	Lowest binding energy (kcal/mol)	No. in cluster	Inhibition constant, K_i (µM)
(-)- Huprine x	1	-7.27	7	4.70
Huperzine B	1	-7.16	18	5.67
Huperzine A	1	-7.13	16	5.90
(-)-Galanthamine	1	-7.09	33	6.34
Δ^9-THC	1	-6.88	13	9.05
(-)- Huprine x	2	-6.69	22	12.56
Huperzine A	2	-6.53	52	16.23
Huperzine B	2	-6.47	67	18.18
Tacrine	1	-6.40	20	20.51
D-Tubocurarine	1	-6.01	3	39.39
Donepezil	1	-5.89	5	48.16
Tacrine	5	-5.86	35	51.07
MPTP	1	-5.58	33	81.25
Propidium	1	-5.48	3	95.81
Decidium	1	-5.39	1	111.35
BW284C5	1	-5.33	2	124.52
D-Tubocurarine	5	-5.32	8	126.71
MF268	1	-4.98	6	225.52
Edrophonium	1	-4.68	19	368.69
Edrophonium	2	-4.33	29	675.07
Acetylthiocholine	1	-3.77	33	1740.00
Acetylcholine	1	-3.76	36	1740.00
Decamethonium	1	-3.54	2	2540.00
Decamethonium	2	-3.39	14	3290.00
Ambenonium	1	-2.70	1	10550.00
Gallamine	1	+0.38	1	-

Table 3.2: Results from the docking of standard ligands with a structure derived from the crystal structure of human AChE in complex with fasciculin II (2.76 Å) (PDB ID: 1b41) (arranged according to highest number in cluster).

Ligand	Cluster rank	Lowest binding energy (kcal/mol)	No. in cluster	Inhibition constant, K_i (μM)
Huperzine B	2	-6.47	67	18.18
Huperzine A	2	-6.53	52	16.23
Acetylcholine	1	-3.76	36	1740.00
Tacrine	5	-5.86	35	51.07
Acetylthiocholine	1	-3.77	33	1740.00
(-)-Galanthamine	1	-7.09	33	6.34
MPTP	1	-5.58	33	81.25
Edrophonium	2	-4.33	29	675.07
(-)- Huprine x	2	-6.69	22	12.56
Tacrine	1	-6.40	20	20.51
Edrophonium	1	-4.68	19	368.69
Huperzine B	1	-7.16	18	5.67
Huperzine A	1	-7.13	16	5.90
Decamethonium	2	-3.39	14	3290
Δ^9-THC	1	-6.88	13	9.05
D-Tubocurarine	5	-5.32	8	126.71
(-)- Huprine x	1	-7.27	7	4.70
MF268	1	-4.98	6	225.52
Donepezil	1	-5.89	5	48.16
Propidium	1	-5.48	3	95.81
D-Tubocurarine	1	-6.01	3	39.39
BW284C51	1	-5.33	2	124.52
Decamethonium	1	-3.54	2	2540.00
Ambenonium	1	-2.70	1	10550.00
Decidium	1	-5.39	1	111.35
Gallamine	1	+0.38	1	-

Table 3.3: Results from the docking of standard ligands with a structure derived from the crystal structure of human AChE in complex with fasciculin II (2.76 Å) (PDB ID: 1b41). (PRINT FRM PAGE ADJUS)

CR	LIGAND																			
	ACL (CAS)		ACLTHIO (CAS / PAS)		AMB (PAS)		BW284C51 (BTH)		DECA (BTH)		DECI (PAS)		DONE (BTH)		EDR (CAS)		GALLMN (PAS)		(-)-GLNTM (CAS)	
	LBE	BS	LBE	BS	LBE	BS	LBE	BS	LBE	BS	LBE	BS	LBE	BS	LBE	BS	LBE	BS	LBE	BS
1	-3.76 (36)	PAS	-3.77 (33)	PAS	-2.70 (1)	PAS	-5.33 (2)	PAS	-3.54 (2)	BTH	-5.39 (1)	PAS	-5.89 (5)	PAS	-4.68 (19)	PAS	+0.38 (1)	PAS	-7.09 (33)	PAS
2	-3.39 (19)	PAS	-3.45 (15)	PAS	-0.88 (1)	PAS	-5.06 (3)	PAS	-3.39 (14)	PAS	-4.93 (1)	PAS	-5.55 (1)	PAS	-4.33 (29)	PAS	+0.49 (1)	PAS	-6.49 (8)	PAS
3	-2.96 (4)	O	-3.40 (2)	MDL	-0.67 (1)	O	-4.86 (1)	PAS	-3.20 (2)	BTH	-4.72 (2)	PAS	-5.27 (5)	PAS	-4.12 (11)	O	+0.55 (2)	PAS	-6.13 (2)	CAS
4	-2.87 (1)	O	-3.37 (13)	PAS	-0.51 (1)	O	-4.86 (1)	PAS	-3.07 (8)	PAS	-4.58 (1)	PAS	-5.00 (1)	PAS	-4.00 (4)	PAS	+0.78 (1)	PAS	-5.89 (1)	CAS
5	-2.84 (2)	O	-3.19 (7)	O	-0.51 (1)	O	-4.75 (1)	PAS	-2.96 (7)	PAS	-4.50 (1)	PAS	-4.90 (2)	PAS	-4.00 (3)	PAS	+0.98 (1)	PAS	-5.11 (2)	O
6	-2.76 (7)	O	-3.15 (5)	O	-0.31 (1)	PAS	-4.18 (1)	BTH	-2.87 (3)	O	-4.49 (1)	PAS	-4.86 (1)	O	-3.96 (4)	CAS	+0.99 (1)	O	-4.95 (11)	O
7	-2.76 (8)	O	-3.00 (1)	O	-0.07 (1)	O	-3.81 (2)	O	-2.70 (3)	O	-4.41 (2)	PAS	-4.83 (2)	PAS	-3.92 (7)	PAS	+1.00 (2)	PAS	-4.86 (1)	O
8	-2.74 (3)	O	-2.93 (2)	O	-0.01 (1)	PAS	-3.66 (1)	O	-2.58 (4)	PAS	-4.30 (1)	PAS	-4.82 (1)	PAS	-3.88 (1)	PAS	+1.04 (1)	O	-4.83 (2)	O
9	-2.68 (2)	CAS	-2.86 (1)	CAS	+0.00 (1)	O	-3.63 (4)	O	-2.47 (5)	PAS	-4.29 (1)	PAS	-4.80 (1)	PAS	-3.80 (3)	O	+1.08 (1)	PAS	-4.79 (2)	O
10	-2.59 (2)	O	-2.81 (1)	O	+0.12 (1)	O	-3.56 (1)	PAS	-2.06 (1)	O	-3.78 (1)	PAS	-4.80 (1)	PAS	-3.72 (1)	C	+1.11 (2)	O	-4.77 (1)	O
11–100		O		CAS/ O		PAS/ O		PAS/ O		PAS/ O		PAS/ O		PAS/ O		CAS/ O		PAS/ O		O
(*/100)		(2)		(67)		(9)		(1)		(4)		(25)		(-)		(10)		(24)		(3)
√/ X		X		√		√		X		√		√		X		X		√		X

CR = Cluster rank, PAS = Peripheral anionic site, CAS = Catalytic site, LBE = Lowest binding energy (kcal/mol), O = Bind to other site compared to PAS and CAS, MDL = Bind in between PAS and CAS, BTH = Bind at PAS and CAS, X = The binding location is incorrect according to literature, √ = The binding location is correct according to literature, (*/100) = Total conformation (the binding location is correct according to the literature) over 100 runs.

CR	HUPA (CAS)		HUPB (CAS)		(-)-HUP X (CAS)		MF268 (PAS)		MPTP (CAS)		PROP (PAS)		TAC (CAS)		Δ^9-THC (PAS)		TUBO (PAS)	
	LBE	BS	LBE	BS	LBE	BS	LBE	BS	LBE	BS	LBE	BS	LBE	BS	LBE	BS	LBE	BS
1	-7.13 (16)	CAS	-7.16 (18)	CAS	-7.27 (7)	PAS	-4.98 (6)	PAS	-5.58 (33)	PAS	-5.48 (3)	PAS	-6.40 (20)	CAS	-6.88 (13)	PAS	-6.01 (3)	PAS
2	-6.53 (52)	PAS	-6.47 (67)	PAS	-6.69 (22)	PAS	-4.53 (6)	PAS	-5.37 (21)	PAS	-5.48 (1)	PAS	-6.25 (12)	PAS	-6.44 (4)	PAS	-5.36 (7)	PAS
3	-6.51 (2)	CAS	-5.81 (2)	O	-6.65 (9)	PAS	-4.26 (1)	PAS	-5.36 (1)	MDL	-5.36 (4)	PAS	-6.14 (1)	CAS	-6.34 (3)	PAS	-5.35 (3)	PAS
4	-5.49 (3)	PAS	-5.59 (1)	O	-6.41 (4)	PAS	-4.16 (3)	PAS	-5.34 (2)	PAS	-5.09 (2)	PAS	-6.03 (6)	O	-5.94 (1)	PAS	-5.32 (3)	PAS
5	-5.29 (3)	O	-5.21 (4)	O	-6.36 (2)	PAS	-4.15 (1)	MDL	-5.30 (8)	PAS	-4.73 (3)	PAS	-5.86 (35)	PAS	-5.83 (1)	PAS	-5.32 (8)	PAS
6	-5.24 (3)	O	-5.17 (2)	O	-6.36 (18)	O	-4.11 (4)	PAS	-5.07 (2)	CAS	-4.59 (2)	PAS	-5.78 (7)	PAS	-5.72 (1)	PAS	-5.23 (2)	PAS
7	-5.20 (1)	O	-4.98 (1)	O	-5.29 (1)	O	-3.99 (2)	PAS	-4.93 (2)	PAS	-4.57 (1)	O	-5.69 (5)	PAS	-5.31 (1)	PAS	-5.19 (2)	PAS
8	-4.70 (1)	O	-4.52 (1)	O	-5.20 (1)	O	-3.77 (1)	PAS	-4.90 (2)	CAS	-4.57 (4)	PAS	-5.06 (4)	O	-5.17 (1)	O	-5.04 (2)	O
9	-4.65 (3)	O	-4.49 (1)	O	-5.01 (7)	O	-3.76 (1)	PAS	-4.21 (1)	O	-4.51 (1)	PAS	-5.01 (1)	O	-5.04 (2)	O	-5.03 (1)	PAS
10	-4.64 (1)	O	-4.36 (2)	O	-4.99 (1)	O	-3.70 (1)	PAS	-4.14 (3)	O	-4.24 (6)	O	-4.96 (3)	O	-4.80 (2)	O	-4.87 (1)	PAS
11–100		O		O		O		PAS/O		O		PAS/O		O		O		PAS/O
(*/100)		(18)		(18)		(-)		(45)		(4)		(22)		(21)		(24)		(36)
√/ X		√		√		X		√		X		√		√		√		√

CR = Cluster rank, PAS = Peripheral anionic site, CAS = Catalytic site, LBE = Lowest binding energy (kcal/mol), O = Bind to other site compared to PAS and CAS, MDL = Bind in between PAS and CAS, BTH = Bind at PAS and CAS, X = The binding location is incorrect according to literature, √ = The binding location is correct according to literature, (*/100) = Total conformation (the binding location is correct according to the literature) over 100 runs (continued).

Table 3.4: Suitability of the crystal structures towards PAS, CAS and BTH site binders. (PRINT FROM PAGE ADJUST -)

Model a	Model b	Model c
No. of ligands which the binding location is correct according to literature at CR 1 **- 11/19** **PAS** - 7/7 **CAS** - 3/9 **BTH** - 1/3 Conclusion : Good for **PAS** binders	No. of ligands which the binding location is correct according to literature at CR 1 **- 11/19** **PAS** - 4/7 **CAS** - 5/9 **BTH** - 2/3 Conclusion : Good for **PAS** , **CAS** & **BOTH SITE** binders	No. of ligands which the binding location is correct according to literature at CR 1 **- 11/19** **PAS** - 6/7 **CAS** - 3/9 **BTH** - 1/3 Conclusion : Good for **PAS** binders

Model d	Model e	Model f
No. of ligands which the binding location is correct according to literature at CR 1 **- 12/19** **PAS** - 7/7 **CAS** - 3/9 **BTH** - 1/3 Conclusion : Good for **PAS** binders	No. of ligands which the binding location is correct according to literature at CR 1 **- 12/19** **PAS** - 7/7 **CAS** - 3/9 **BTH** - 1/3 Conclusion : Good for **PAS** binders	No. of ligands which the binding location is correct according to literature at CR 1 **- 13/19** **PAS** - 6/7 **CAS** - 4/9 **BTH** - 2/3 Conclusion : Good for **PAS** binders

CR = Cluster rank, PAS =Peripheral anionic site, CAS = Catalytic site, BTH = Bind at PAS and CAS, Model **a** = HAChE in complex with fasciculin II (2.76 Å) (PDB ID: 1b41), Model **b** = TcAChE in complex with aricept (2.50 Å) (PDB ID: 1eve) (Without any replacement of residues or energy minimization), Model **c** = TcAChE in complex with aricept (2.50 Å) (PDB ID: 1eve) (with residue Phe330 replaced by Tyr), Model **d** = TcAChE in complex with aricept (2.50 Å) (PDB ID: 1eve) (with residue Phe330 replaced by Tyr followed by energy minimization using Swiss PDB Viewer (SPBV 4.01)), Model **e** = TcAChE in complex with aricept (2.50 Å) (PDB ID: 1eve) (with residue Phe330 replaced by Tyr, Ser81 replaced by Thr, Glu73 replaced by Thr and Gln74 replaced by Leu), Model **f** = TcAChE in complex with aricept (2.50 Å) (PDB ID: 1eve) (with residue Phe330 replaced by Tyr, Ser81 replaced by Thr, Glu73 replaced by Thr and Gln74 replaced by Leu followed by energy minimization using Swiss PDB Viewer (SPBV 4.01)).

Model g	Model h	Model i
No. of ligands which the binding location is correct according to literature at CR 1 - **6/19** **PAS** - 5/7 **CAS** - -/9 **BTH** - -/3 **Conclusion** : Good for **PAS** binders	No. of ligands which the binding location is correct according to literature at CR 1 - **8/19** **PAS** - 5/7 **CAS** - -/9 **BTH** - 2/3 **Conclusion** : Good for **PAS** and **BOTH** site binders	No. of ligands which the binding location is correct according to literature at CR 1 - **7/19** **PAS** - 5/7 **CAS** - -/9 **BTH** - 1/3 **Conclusion** : Good for **PAS** binders

Model j
No. of ligands which the binding location is correct according to literature at CR 1 - **9/19** **PAS**- 4/7 **CAS**- 1/9 **BTH**- 3/3 **Conclusion** : Good for **PAS** and **BOTH** site binders

CR = Cluster rank, PAS =Peripheral anionic site, CAS = Catalytic site, BTH = Bind at PAS and CAS, Model **g** = mAChE in complex with decidium (2.35 A°) (PDB ID: 1j07), Model **h** = mAChE in complex with propidium (2.25 A°) (PDB ID: 1n5r), Model **i** = mAChE in complex with gallamine (2.20 A°) (PDB ID: 1n5m), Model **j** = mAChE in complex with succinylcholine (2.05 A°) (PDB ID: 2ha2) (Continued).

Table 3.5: Docking results for compounds V1-V21 identified from virtual screening.

Compound	Docking studies		
	Binding energy (kcal /mol)	Binding site	K_i (μM)
V1	-8.72	PAS	0.40
V2	-8.51	PAS	0.58
V3	-8.34	PAS	0.77
V4	-8.30	PAS	0.83
V5	-7.92	PAS	1.56
V6	-7.76	PAS	2.04
V7	-7.75	PAS	2.09
V8	-7.50	PAS	3.16
V9	-7.35	PAS	4.08
V10	-7.34	PAS	4.18
V11	-7.31	PAS	4.40
V12	-7.29	PAS	4.56
V13	-7.25	PAS	4.86
V14	-7.23	PAS	5.01
V15	-7.16	PAS	5.65
V16	-7.13	PAS	5.90
V17	-7.09	PAS & CAS	6.40
V18	-7.08	PAS & CAS	6.42
V19	-7.00	PAS	7.41
V20	-7.00	PAS	7.39
V21	-5.60	PAS	78.91
Tacrine*	-6.40	CAS	20.51
Propidium*	-5.48	PAS	95.81

PAS = Peripheral anionic site, CAS = Catalytic site, *Standard inhibitor

Table 3.6: The molecular interactions of compounds identified from virtual screening.

Compound	No. in cluster	Molecular Interactions									Binding energy (kcal/mol)
		Hydrogen bonds length (Å)	Residues involved in hydrogen bonding	Residues involved in hydrophobic interaction			Residues involved in van der waals interaction			Residues involved in Pi-pi / Pi-sigma / Pi-cation interaction (A°)	
V1	1	2.95	O2…..OH-Tyr337	Trp286	Leu289	Glu292	Trp286	Leu289	Val294	**Pi-sigma**	-8.72
		3.03	O1…..N-Ser293	Val294	Phe295	Phe297	Phe295	Arg296	Phe297	Trp286-C18 (1.835)	
				Phe338	Tyr341	Gly342	Phe338	Tyr341	Gly342		
				Val365			Val365				
V2	8	2.93	O1…..OH-Tyr124	Tyr72	Trp286	Phe295	Tyr72	Tyr124	Phe295	**Pi-pi**	-8.51
				Phe297	Tyr337	Phe338	Arg296	Phe297	Tyr337	ligand-Trp286	
				Tyr341			Phe338	Tyr341		**Pi-sigma**	
										Tyr341-C3 (1.781)	
V3	14	2.77	O2…N-Phe295	Tyr72	Tyr124	Trp286	Tyr72	Tyr124	Val294	**Pi-sigma**	-8.34
				Phe297	Phe338	Tyr341	Phe297	Tyr337	Tyr341	Trp286-C7 (1.764)	
V4	9	-	-	Tyr124	Trp286	Leu289	Trp286	Val294	Phe295	-	-8.30
				Glu292	Ser293	Val294	Arg296	Phe297	Phe338		
				Phe295	Phe297	Phe338	Tyr341				
				Tyr341							
V5	6	2.72	O3…..N-Phe295	Tyr72	Trp286	Phe297	Tyr124	Val294	Phe297	**Pi-pi**	-7.92
				Phe338	Tyr341		Tyr337	Phe338	Tyr341	ligand-Trp286	
										Pi-sigma	
										Tyr341-C16 (1.712)	
V6	10	2.84	O1…..N-Phe295	Tyr72	Asp 74	Tyr 124	Tyr72	Tyr124	Trp286	**Pi-pi**	-7.76
				Trp286	Val294	Arg296	Val294	Phe297	Phe338	ligand-Trp286	
				Phe297	Tyr341	Tyr337				**Pi-sigma**	
				Phe338						Tyr341-C15 (1.670)	

Compound	No. in cluster	Molecular Interactions									Binding energy (kcal/mol)
		Hydrogen bonds length (Å)	Residues involved in hydrogen bonding	Residues involved in hydrophobic interaction			Residues involved in van der waals interaction			Residues involved in Pi-pi / Pi-sigma / Pi-cation interaction (A°)	
V7	4	2.71	O3…..N-Ser 293	Tyr124	Trp286	Leu289	Tyr124	Trp286	Leu289	-	-7.75
		3.12	O3…..O-Ser 293	Gln291	Glu292	Val294	Gln291	Val294	Phe295		
		3.19	O4….. O-Ser 293	Phe295	Arg296	Phe297	Arg296	Phe297	Phe338		
				Tyr337	Phe338	Tyr341	Tyr341				
V8	7	2.90	O1…..N-Phe295	Tyr72	Tyr124	Trp286	Tyr72	Tyr124	Trp286	-	-7.50
				Leu289	Val294	Arg296	Val294	Arg296	Phe297	**Pi-sigma**	
				Phe297	Tyr337	Phe338	Tyr337			Trp286-C20 (1.942)	
				Tyr341							
V9	3	2.65	N2…..O-Ser293	Tyr72	Asp74	Tyr124	Tyr72	Trp286	Leu289	**Pi-pi**	-7.35
				Trp286	Leu289	Pro290	Gln291	Glu292	Phe297	ligand-Trp286	
				Gln291	Glu292	Val294	Tyr341			ligand-Tyr341	
				Phe295	Arg296	Phe297					
				Phe338	Tyr341						
V10	7	2.70	O2…..N-Arg296	Tyr124	Trp286	His287	Tyr124	Trp286	Leu289	**Pi-sigma**	-7.34
		3.10	N1…..O-Ser293	Leu289	Pro290	Gln291	Pro290	Gln291	Glu292	Tyr341-C17 (1.707)	
				Glu292	Val294	Phe295	Phe297	Tyr337	Phe338		
				Phe297	Tyr337	Phe338					
				Tyr341							
V11	3	2.96	N1…..O-Tyr341	Tyr124	Trp286	Leu289	Tyr124	Trp286	Leu289	-	-7.31
		3.09	O2…..N-Arg296	Phe297	Val294	Tyr337	Phe297	Tyr337	Phe338		
		3.12	O3…..O-Arg296	Phe338							
		3.17	O2…..N-Phe295								
		3.18	O1…..N-Phe295								
		3.39	O3…..O-Ser293								
		3.51	O3…..N-Arg296								
		3.61	O3…..N-Phe295								
		3.82	O3.....OG-Ser293								

(continued)

Compound	No. in cluster	Molecular Interactions								Binding energy (kcal/mol)
		Hydrogen bonds length (Å)	Residues involved in hydrogen bonding	Residues involved in hydrophobic interaction			Residues involved in van der waals interaction			Residues involved in Pi-pi / Pi-sigma / Pi-cation interaction (A°)	
V12	2	2.94	O2…..OH-Tyr124	Trp286	His287	Leu289	His287	Leu289	Gln291	-	-7.29
		3.83	O2…..OH-Tyr337	Pro290	Gln291	Ser293	Ser293	Val294	Phe295		
				Val294	Phe295	Arg296	Arg296	Phe297	Phe338		
				Phe297	Phe338	Tyr341	Tyr341				
V13	7	-	-	Tyr72	Tyr124	Trp286	Tyr72	Phe295	Arg296	-	-7.25
				Val294	Phe295	Phe297	Phe297	Phe338			
				Tyr337	Phe338	Tyr341					
V14	9	3.01	O2…..OG-Ser293	Tyr124	Trp286	Leu289	Trp286	Leu289	Gln291	-	-7.23
				Val294	Phe295	Arg296	Val294	Phe295	Arg296		
				Phe297	Tyr337	Phe338	Phe297	Phe338	Tyr341		
				Tyr341							
V15	14	2.81	O1…..N-Phe295	Tyr124	Trp286	Leu289	Tyr124	Trp286	Leu289	**Pi-pi**	-7.16
		2.82	O1…..N-Arg296	Val294	Phe295	Tyr337	Phe297	Phe338	Tyr341	ligand-Trp286	
		2.96	N1…..OG-Ser293	Phe338	Tyr341						
V16	3	2.88	O1…..N-Phe295	Tyr72	Tyr124	Trp286	Tyr72	Tyr124	Trp286	-	-7.13
				Leu289	Val294	Arg296	Val294	Arg296	Phe297		
				Phe297	Tyr337	Phe338	Tyr337	Tyr341			
				Tyr341							
V17	1	2.75	N1…..OH-TYR124	Tyr72	Trp86	Gly120	Trp86	Gly120	Tyr133	**Pi-cation**	-7.09
		2.77	O3…..OH-TYR124	Gly121	Tyr133	Glu202	Tyr341	Trp286	Phe295	Tyr341-N1	
				Ser203	Trp286	Val294	Arg296	Phe297	Tyr337	His447:NE2 - ligand	
				Phe295	Arg296	Phe297	Phe338	Tyr341	His447		
				Tyr337	Phe338	Tyr341					
				His447	Gly448	Tyr449					
				Ile451							

(continued)

Compound	No. in cluster	Hydrogen bonds length (Å)	Residues involved in hydrogen bonding	Residues involved in hydrophobic interaction			Residues involved in van der waals interaction			Residues involved in Pi-pi / Pi-sigma / Pi-cation interaction (A°)	Binding energy (kcal/mol)
V18	1	-		Tyr72	Asp74	Trp86	Trp86	Gly120	Gly121	**Pi-pi**	-7.08
				Gly120	Gly121	Gly122	Ser125	Gly126	Tyr133	ligand-Trp286	
				Tyr124	Ser125	Gly126	Gly202	Ser203	Trp286	Tyr341-ligand	
				Leu130	Tyr133	Glu202	Val294	Phe295	Arg296		
				Ser203	Trp286	Val294	Phe297	Tyr337	Phe338		
				Phe295	Phe297	Tyr337	Tyr341				
				Phe338	Tyr341	His447					
				Gly448							
V19	2	3.34	O3…..O-Ser293	Tyr72	Tyr124	Trp286	Tyr124	Trp286	Leu289	**Pi-sigma**	-7.00
		3.44	O3…..O-Tyr341	Leu289	Val294	Phe295	Val294	Arg296	Phe297	Trp286-C19 (1.765)	
				Arg296	Phe297	Tyr337	Phe338			**Pi-cation**	
				Phe338						Trp286-N1	
										Trp286-N1	
V20	4	-	-	Tyr72	Asp74	Tyr124	Tyr72	Asp74	Tyr124	-	-7.00
				Trp286	Leu289	Ser293	Trp286	Leu289	Val294		
				Val294	Phe295	Arg296	Phe297	Tyr337	Phe338		
				Phe297	Tyr337	Phe338					
				Tyr341							
V21	1	2.95	O1…..OH-TYR72	Thr75	Leu76	Tyr124	Leu76	Tyr124	Trp286	**Pi-Pi**	-5.60
		2.98	O2…..N-Phe295	Trp286	Val294	Arg296	Val294	Phe297	Tyr337	ligand-Trp286	
				Phe297	Tyr337	Phe338	Phe338	Tyr341		ligand- Tyr72	
				Tyr341						**Pi-sigma**	
										Trp286-C7	

(continued)

In this study, in order to find PAS binding ligands for virtual screening, the ligands decamethonium (both PAS and CAS binder), decidium and MF268 (PAS binders) were used as a backbone structure to download ligands from ZINC database. **Tables 3.5** and **3.6** show docking results for top twenty one ligands from virtual screening. The lowest binding energy that could be obtain was -8.72 kcal/mol for compound **V1**. This value is much better than the binding energy for the ligands decamethonium, decidium and MF268 which were 3.54 kcal/mol, -4.30 kcal/mol and -3.94 kcal/mol, respectively.

Molecular interaction studies indicated that all ligands bound to PAS of the enzyme near the aromatic residue Trp286 except compound **V17** and compound **V18** which bound to PAS and CAS of the enzyme **(Table 3.5)**. Residues that mainly involved in hydrophobic interaction are Trp286, Phe295 (except for compounds **V3**, **V5**, **V6**, **V8**, **V11**, **V16** and **V21**), Phe297 (except for compound **V15**), Tyr337 (except for compounds **V1**, **V3**, **V4**, **V5**, **V9** and **V12**) and Phe338. Meanwhile, residues such as Trp286 (except for **V2**, **V3**, **V5**, **V12** and **V13**), Phe297 and Tyr341 (except for **V6**, **V8**, **V10**, **V11**, **V13**, **V19** and **V20**) are mostly involved in van der waals interaction.

Molecular interaction investigation also suggested that the residues Tyr72, Tyr124, Ser293, Phe295, Arg296, Tyr337 and Tyr341 are important for the hydrogen bonding between ligands and the protein. The residues Trp286 and Tyr341 are contributing for pi-sigma interaction, residues Tyr72, Trp286 and Tyr341 are involved in pi-pi interaction whereas the residues Trp286, Tyr341 and His447 are contributing for pi-cation interaction between the ligand and the protein.

Other than the usage of AChE inhibitors in the treatment of AD, peripherally acting AChE inhibitors are used in conditions such as glaucoma, constipation, spasmolysis, anaesthesiology and myasthenia gravis (Komloova et al., 2011). These conditions can be treated with peripherally acting AChE inhibitors that contain a positive charge in their structure (Komloova et al., 2011). Since these compounds do not penetrate blood-brain barrier, thus avoiding side effects. In this study, several compounds that have been identified from virtual screening contain a positive charge in their structure and therefore have potential for these other applications.
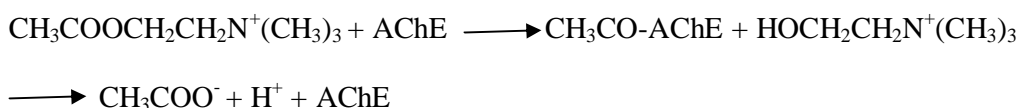
3.4 CONCLUSION

In this study our interest was to find PAS binding ligands. The blind docking results using a crystal structure of hAChE in complex with fasciculin II (PDB ID: 1b41) have shown that most of the PAS ligands bound near the aromatic residue Trp286. This is in agreement with site directed mutagenesis studies. The structure obtained from this crystal structure was found to be the most suitable for identifying PAS ligands and was chosen for virtual screening compared with other AChE model structures.

Based on the molecular interaction studies on the top twenty one ligands from the virtual screening, it can be concluded that Trp286, Phe295, Phe297, Tyr337 and Phe338 are mainly involved in hydrophobic contacts, the residues Trp286, Phe297 and Tyr341 are mostly contributing for van der waals interaction, residues Tyr72, Tyr124, Ser293, Phe295, Arg296, Tyr337 and Tyr341 are contributing for the hydrogen bonding while the residues such as Tyr72, Trp286, Tyr341, and His447 are important in pi-sigma, pi-pi and pi-cation interactions.

CHAPTER 4: OPTIMISATION OF HUMAN ACETYLCHOLINESTERASE INHIBITION ASSAY AND AMYLOID BETA PEPTIDE AGGREGATION ASSAY

4.1 INTRODUCTION

The principal biological role of acetylcholinesterase (AChE) (acetylcholine hydrolase, E.C. 3.1.1.7) is termination of impulse transmission at cholinergic synapses by rapid hydrolysis of the neurotransmitter acetylcholine (ACh) (Dvir et al., 2010).

$$CH_3COOCH_2CH_2N^+(CH_3)_3 + AChE \longrightarrow CH_3CO\text{-}AChE + HOCH_2CH_2N^+(CH_3)_3$$
$$\longrightarrow CH_3COO^- + H^+ + AChE$$

The catalytic activity of AChE is very high with each molecule of AChE degrading about 5000 molecules of acetylcholine (ACh) per second. The choline produced by the action of AChE is recycled, and transported, through reuptake, back into nerve terminals where it is used to synthesize new ACh molecules.

The standard method for determination of AChE activity is Ellman's method (Ellman et al., 1961), which measures the rate of production of thiocholine as acetylthiocholine is hydrolyzed. This is accomplished by the reaction of the thiol group with 5: 5-dithiobis-2-nitrobenzoate ion (DTNB) to produce the intense yellow coloured anion of 5-thio-2-nitro-benzoic acid.
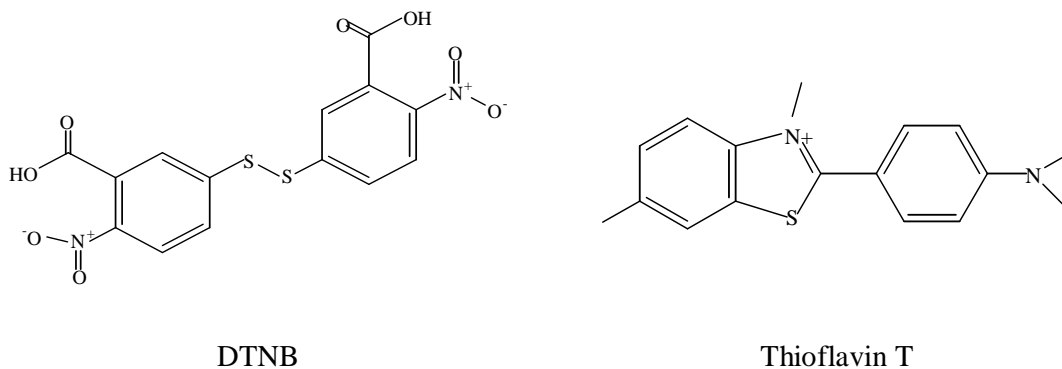
DTNB   Thioflavin T

Figure 4.1: Structures of DTNB and Thioflavin T.

Amyloid peptide aggregation can be determined using Thioflavin T (ThT) **(Figure 4.1)**, a cationic benzothiazole dye that shows enhanced fluorescence upon binding to amyloid fibrils (Khurana et al., 2005). The fluorescence spectra and binding properties of ThT were first characterized by Naiki et al. (1989), Naiki et al. (1990), Naiki et al. (1991), LeVine (1993) and LeVine (1997). They demonstrated that, upon binding of fibrils, ThT displays a dramatic shift of the excitation maximum (from 385 nm to 450 nm) and the emission maximum (from 445 nm to 482 nm) and that ThT fluorescence originates only from the dye bound to amyloid fibrils (Naiki et al., 1989; Levine, 1993).

In the current study, the Ellman assay and Thioflavin T-Based Fluorometric assay were adopted and optimized based on the method developed by Ellman (Ellman et al., 1961) and LeVine (Levine, 1993), respectively.

4.2 MATERIALS

Acetylcholinesterase from human recombinant (2,419 U/mg), lyophilized powder (E.C. No. 3.1.1.7), acetylthiocholine iodide (ATChI), 5, 5'-dithiobis[2-nitrobenzoic acid] (DTNB), tacrine hydrochloride (A79922), propidium iodide (P4170), thioflavin T, di-sodium hydrogen orthophosphate dodecahydrate ($Na_2HPO_4.12H_2O$), sodium dihydrogen orthophosphate ($NaH_2PO_4.2H_2O$), sodium hydroxide (NaOH), glycine, hydrochloric acid (HCl) 37%, dimethyl sulfoxide (DMSO), methanol (MeOH) and ethanol (EtOH) were purchased from Sigma-Aldrich (St. Louis, MO, USA). The chemicals were of analytical grade. Amyloid beta (Aß) peptide (1-40), lyophilized from HFIP solution was purchased from Anaspec (Fremont, CA, USA). Instruments used included a uv / fluorescence spectrophotometer and multiplate reader (Tecan Infinite M200).

4.3 METHODS

4.3.1 Optimisation of human acetylcholinesterase (hAChE) inhibition assay

4.3.1.1 Buffer preparation

0.1 M sodium phosphate buffer was prepared by mixing 47.35 mL of 0.2 M dibasic sodium phosphate and 2.65 mL of 0.2 M monobasic sodium phosphate. The volume was then made up to 100 mL with deionised water and adjusted to pH 8.0 with concentrated hydrochloric acid.

4.3.1.2 Enzyme preparation

Acetylcholinesterase from human recombinant (2,419 U/mg) was dissolved in 0.1 M sodium phosphate buffer pH 8.0 and the aliquots were kept at – 80 °C.

4.3.1.3 Acetylthiocholine iodide (ATChI) preparation

0.6 mM stock solution of acetylthiocholine iodide was freshly prepared by dissolving 1.0 mg of acetylthiocholine iodide powder in 6 mL of 0.1 M sodium phosphate buffer pH 8.0.

4.3.1.4 5,5'-dithiobis [2-nitrobenzoic acid] (DTNB) preparation

0.63 mM stock solution of 5,5'-dithiobis [2-nitrobenzoic acid] was freshly prepared by dissolving 0.5 mg of 5,5'-dithiobis [2-nitrobenzoic acid] powder in 1.23 mL of 0.1 M sodium phosphate buffer pH 8.0.

4.3.1.5 Assay

The AChE inhibition assay was performed in 96 well plates by the method of Ellman et al. (1961) and Li et al. (2009) with minor modifications, using acetylthiocholine as a substrate. 5, 5'-dithiobis [2-nitrobenzoic acid](DTNB) was used to measure cholinesterase activity. 110 μL of sodium phosphate buffer (pH 8.0) was added to the each well followed by 20 μL of sample, 50 μL of DTNB (0.126 mM) and 20 μL of AChE enzyme (0.6 u/ml). The mixture was incubated for 20 minutes at 37 ℃. The reaction was then initiated by the addition of 50 μL (0.120 mM) of acetylthiocholine iodide. The hydrolysis of acetylthiocholine was monitored by measuring the absorbance due to yellow 5-thio-2-nitrobenzoate anion at a wavelength of 412 nm every 30 s for 25 min. Each assay was performed in triplicate.
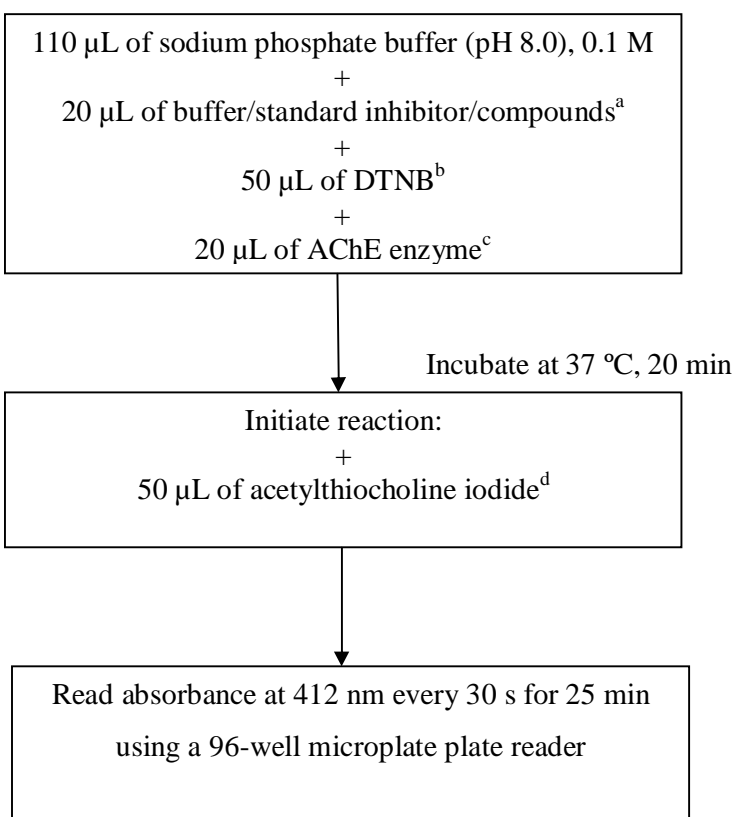
```
┌─────────────────────────────────────────────────────┐
│   110 µL of sodium phosphate buffer (pH 8.0), 0.1 M   │
│                          +                            │
│   20 µL of buffer/standard inhibitor/compounds[a]     │
│                          +                            │
│              50 µL of DTNB[b]                          │
│                          +                            │
│           20 µL of AChE enzyme[c]                     │
└─────────────────────────────────────────────────────┘
                          │
                          │       Incubate at 37 ºC, 20 min
                          ▼
┌─────────────────────────────────────────────────────┐
│                  Initiate reaction:                   │
│                          +                            │
│      50 µL of acetylthiocholine iodide[d]             │
└─────────────────────────────────────────────────────┘
                          │
                          ▼
┌─────────────────────────────────────────────────────┐
│   Read absorbance at 412 nm every 30 s for 25 min     │
│        using a 96-well microplate plate reader        │
└─────────────────────────────────────────────────────┘
```

Figure 4.2: The flow chart of the protocol optimised anticholinesterase assay.

[a]Final DMSO concentration of 0.1 % v/v

[b]Final DTNB concentration of 0.126 mM

[c]Final AChE enzyme concentration of 0.6 u/ml

[d]Final acetylthiocholine iodide concentration of 0.120 mM

4.3.1.6 Data analysis

The percent inhibition was calculated by the following expression: $(E–S)/E$ x 100), where E is the activity of the enzyme without test compound and S is the activity of the enzyme with test compound. Data from concentration-inhibition experiments of the inhibitors were transformed by nonlinear regression analysis, which gave estimates of the IC_{50} (concentration of drug producing 50 % inhibition of enzyme activity inhibition). Tacrine and propidium iodide were used as standard inhibitors. The computer program PRISM® Software, version 3.0 (GraphPad Software, Inc, San Diego, USA) was used to analyze these data.

4.3.2 Optimisation of Aß peptide aggregation assay

4.3.2.1 Buffer preparation

0.215 M sodium phosphate buffer was prepared by mixing 47.35 mL of 0.43 M dibasic sodium phosphate and 2.65 mL of 0.43 M monobasic sodium phosphate. The volume was then made up to 100 mL with deionised water and adjusted to pH 8.0 with concentrated hydrochloric acid.

50 mM glycine-sodium hydroxide (Gycine-NaOH) buffer was prepared by dissolving 0.375 g of glycine in 70ml of diionised water. Then, 2 mL of 0.2 M NaOH solution was added into the glycine solution. The volume was then made up to 100 mL with deionised water and adjusted to pH 8.5 with concentrated hydrochloric acid.

4.3.2.2 Preparation of Aß peptide stock solution

231 μM Aß peptide stock solution was prepared by dissolving 1 mg of Aß peptide (1-40) (lyophilized from HFIP solution) in DMSO. The solution was then aliquoted and stored at –20 °C until use.

4.3.2.3 Preparation of Thioflavin T (Th-T)

30 μM stock solution of Th-T was prepared by dissolving 0.28 mg of Th-T in 29.3 mL of deionised water. Then 3 μM of Th-T solution was prepared by diluting 500 μL of the stock solution with 500 μL of 50 mM glycine-NaOH buffer pH 8.5.

4.3.2.4 Assay

The Aß peptide aggregation assay was performed by the method of LeVine (1993) and Munoz-Ruiz et al. (2005) with minor modifications. The protocol of the assay as described here is based on the optimised parameters of **section 4.4**. Aß peptide (1-40), lyophilized from HFIP solution, was dissolved in DMSO to prepare a stock solution. Aliquots of Aß in DMSO were then incubated in constant rotation for 24 hours at room temperature in 0.215 M sodium phosphate buffer (pH 8.0) at a final Aß concentration of 5 μM in the presence or absence of compounds or propidium at 100 μM, used as a reference. To quantify amyloid fibril formation, the thioflavin T fluorescence method was used. Fluorescence was measured at 440 nm (λ excitation) and 485 nm (λ emission). To determine amyloid fibril formation, after incubation, the solution containing Aß or Aß plus AChE inhibitors were added to 50 mM gycine-NaOH buffer, pH 8.5, containing 3 μM thioflavin T in a final volume of 150 μL. Each assay was performed in triplicate.

4.3.2.5 Data analysis

The percent aggregation was calculated by the following expression: $100 - (IF_i/IF_o \times 100)$ where, IF_i and IF_o are the fluorescence intensities obtained for Aß in the presence and in the absence of inhibitor, respectively, after subtracting the fluorescence of the respective blanks.
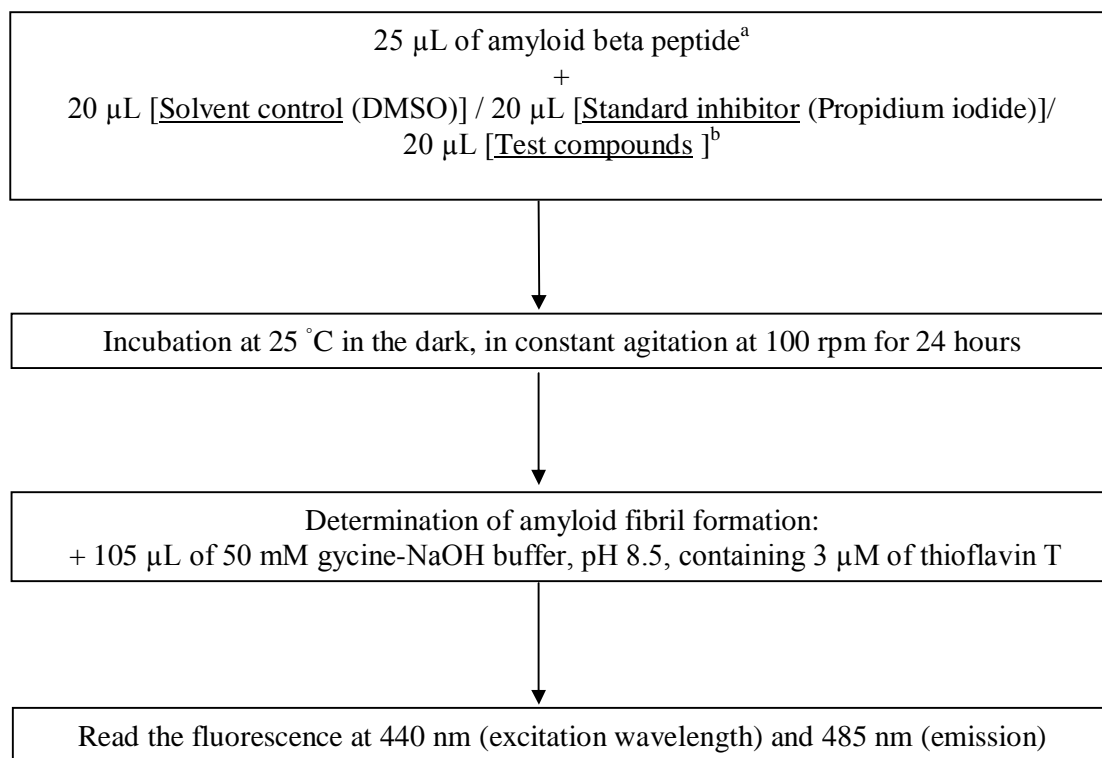
```
┌─────────────────────────────────────────────────────────────────────────┐
│                    25 µL of amyloid beta peptide[a]                       │
│                                    +                                      │
│  20 µL [Solvent control (DMSO)] / 20 µL [Standard inhibitor (Propidium    │
│                        iodide)]/                                          │
│              20 µL [Test compounds ][b]                                   │
└─────────────────────────────────────────────────────────────────────────┘
                                      │
                                      ▼
┌─────────────────────────────────────────────────────────────────────────┐
│  Incubation at 25 °C in the dark, in constant agitation at 100 rpm for    │
│  24 hours                                                                 │
└─────────────────────────────────────────────────────────────────────────┘
                                      │
                                      ▼
┌─────────────────────────────────────────────────────────────────────────┐
│              Determination of amyloid fibril formation:                   │
│  + 105 µL of 50 mM gycine-NaOH buffer, pH 8.5, containing 3 µM of         │
│  thioflavin T                                                             │
└─────────────────────────────────────────────────────────────────────────┘
                                      │
                                      ▼
┌─────────────────────────────────────────────────────────────────────────┐
│  Read the fluorescence at 440 nm (excitation wavelength) and 485 nm       │
│  (emission)                                                               │
└─────────────────────────────────────────────────────────────────────────┘
```

Figure 4.3: The flow chart of the protocol of amyloid beta peptide aggregation assay.

[a]Final amyloid beta peptide concentration of 5 µM

[b]Final DMSO concentration of 0.5% v/v

4.4 RESULTS AND DISCUSSION

4.4.1 Optimisation of hAChE inhibition assay

4.4.1.1 Determination of absorbance wavelength

Absorbance scanning was carried out from 0 to 60 min to select a suitable wavelength for the Ellman assay **(Figure 4.4 (a))**. The color development increased linearly until 60 minutes **(Figure 4.4 (b))** at 412 nm as reported earlier by Ellman et al. (1961). Therefore the wavelength 412 nm was chosen as the optimum wavelength for this assay.
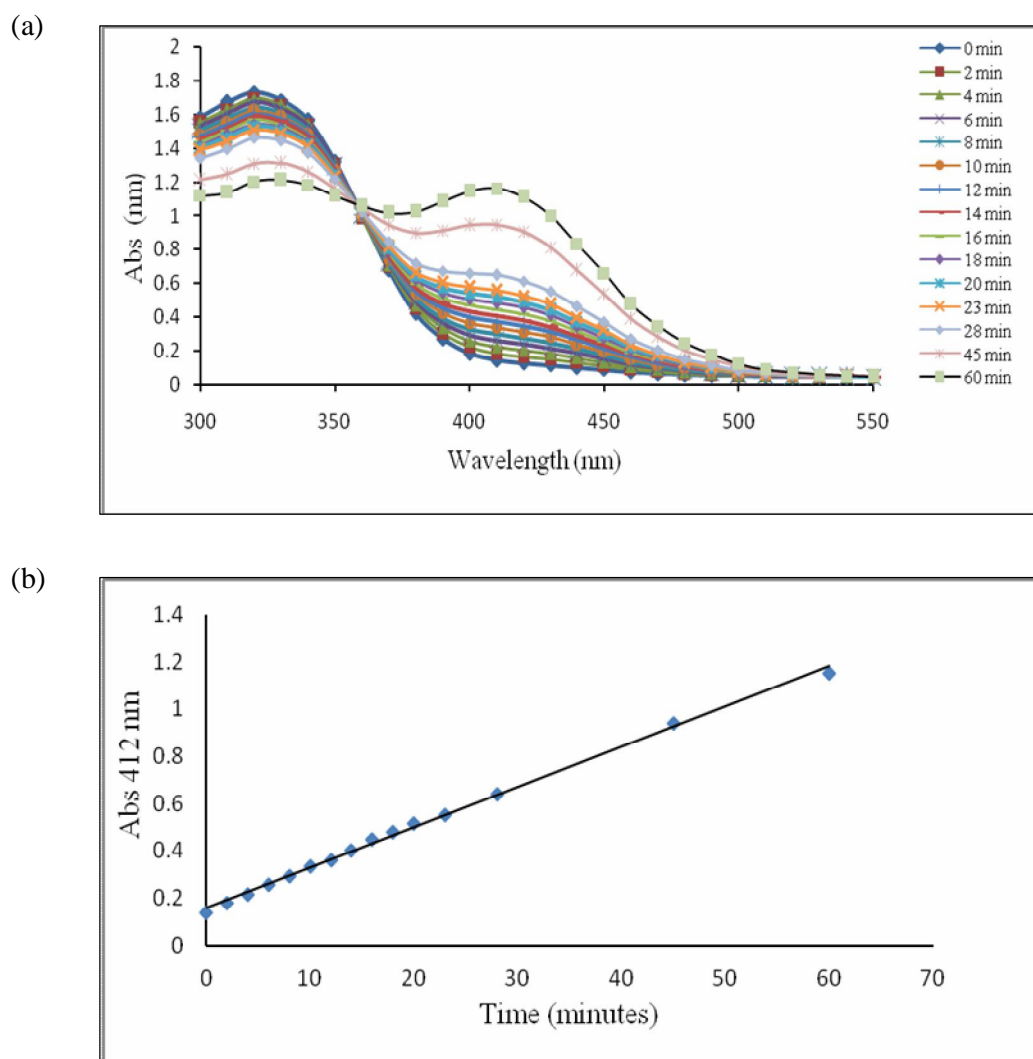
(a)

(b)

Figure 4.4: (a) Absorbance scanning (300 nm – 550 nm), **(b)** Absorbance at 412 nm against time measured over 60 min.

4.4.1.2 Optimisation of enzyme concentration

The effect of enzyme concentration on absorbance was determined using enzyme concentrations between 0 u/ml to 1.24 u/ml (**Figure 4.5**). It was observed that all concentrations of enzyme showed a linear response until 1 hour. The maximum absorbance that could reach by enzyme concentrations 0 to 0.31 u/ml until 1 hour was about 0.15 OD/min which was too low, meanwhile the OD/min at 1 hour was too high (>0.7) at enzyme concentration of 1.24 u/ml. Therefore, 0.62 u/ml enzyme was chosen as the optimum enzyme concentration for this assay.
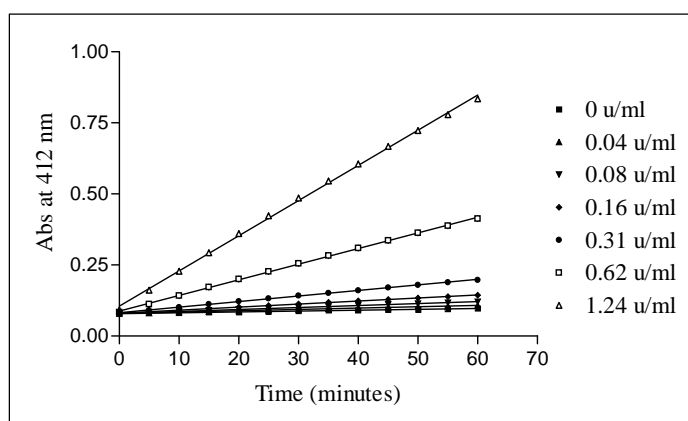
Figure 4.5: Absorbance against time at varying enzyme concentrations. Each data point is expressed as mean ± standard deviation (n=3).

4.4.1.3 Optimisation of substrate concentration

According to the Michaelis – Menten kinetics model, the K_m is the substrate concentration which results in an initial reaction velocity that is one-half the maximum velocity determined under saturating substrate concentration. In order for competitive inhibitors to be identified in a competition experiment that measures IC_{50} values, a substrate concentration around or below the K_m value must be used.

(a)
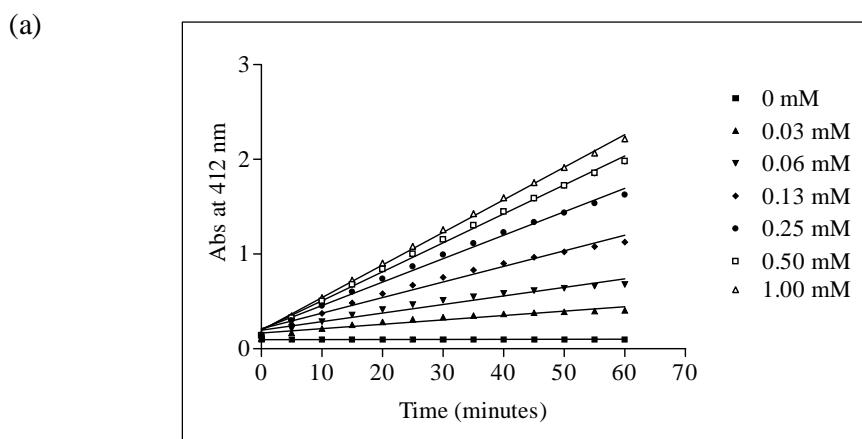
Figure 4.6 (a): Absorbance against time at varying substrate concentrations. Each data point is expressed as mean ± standard deviation (n=3).
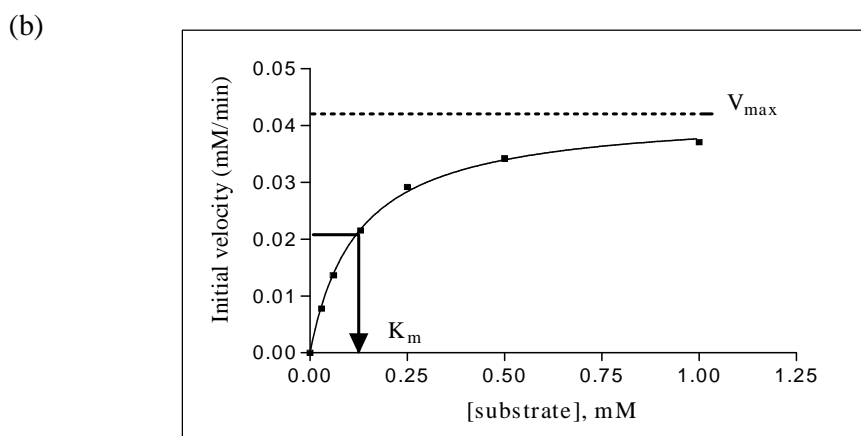
(b)

Figure 4.6 (b): Estimation of K_m value for the substrate.
Michaelis-Menten kinetics (relationship between initial rate and substrate concentration). Best-fit value: V_{max} = 0.042 mM/min, K_m = 0.123 mM, R^2 = 0.9983.

The concentration of substrate acetylthiocholine iodide was varied from 0–1 mM with a fixed concentration of enzyme (0.6 u/ml) to determine the K_m value of the substrate. All concentrations of acetylthiocholine iodide showed a linear response until 1 hour **(Figure 4.6 (a))**. The absorbances at 25 minutes were used to determine the rate of reaction and K_m value **(Figure 4.6 (b))**. The initial velocity (vo) for each reaction progress curves is equivalent to the slope of the line which is defined as the change in the amount of product formed divided by the change in time. The K_m value was

estimated as 0.12 mM and this value was used as the optimum concentration of substrate in the experiments that follow.

4.4.1.4 Optimisation of incubation time

The kinetic reaction was conducted with the enzyme and substrate concentrations fixed at 0.62 u/ml and 0.12 mM, respectively at two different temperatures, 25 °C **(Figure 4.7(a))** and 37 °C **(Figure 4.7(b))** for 1 hour to determine the optimum incubation time for this assay.
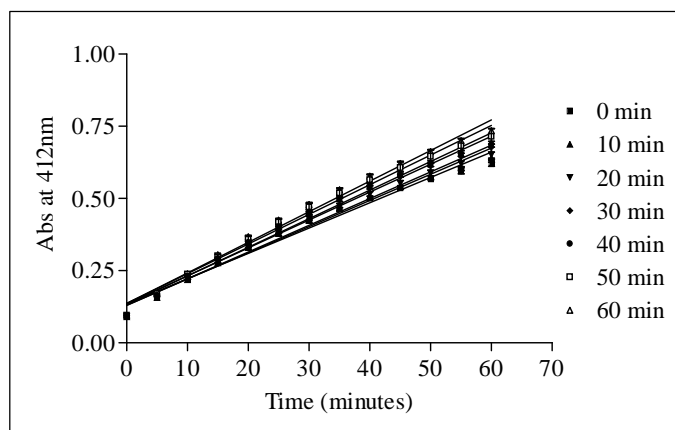
(a) 25 °C
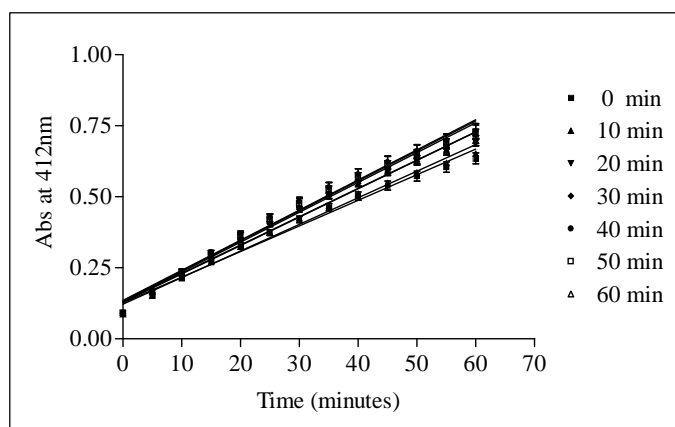
(b) 37 °C

Figure 4.7 (a) & (b): Optimisation of incubation time at 25 °C & 37 °C. Each data point is expressed as mean ± standard deviation (n=3).

All the incubation times showed a linear response until 1 hour. An incubation time of 20 minutes was chosen for the optimal reaction since there is not much difference in the changes of absorbance at various incubation times.

4.4.1.5 Optimisation of incubation temperature

The kinetic reaction was conducted for 1 hour with the enzyme and substrate concentrations fixed at 0.62 u/ml and 0.12 mM, respectively at two different temperatures, 25 ˚C and 37 ˚C **(Figure 4.8)** after 20 minutes of incubation.
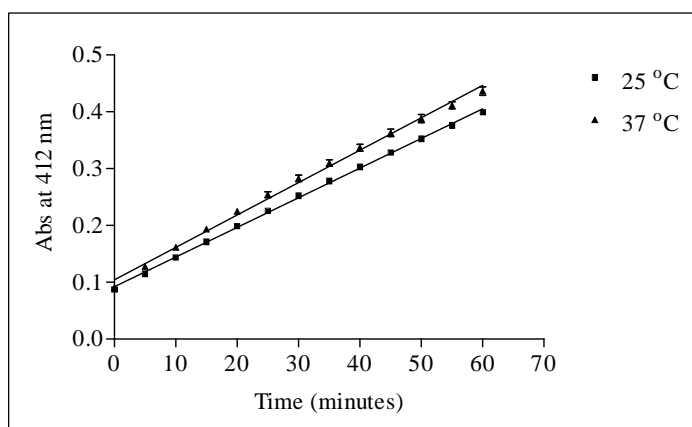
Figure 4.8: Optimisation of incubation temperature. Each data point is expressed as mean ± standard deviation (n=3). $R^2 = 0.9977$ (25 ℃) and $R^2 = 0.9912$ (37 ℃).

Reactions at both temperatures were linear until 1 hour. Since 37 ˚C is an ambient temperature for most biological reactions, it was chosen as the incubation temperature for optimal reaction.

4.4.1.6 Optimisation of solvent concentration

The kinetic reaction was conducted for 40 minutes, after 20 minutes of incubation at 37 ˚C (with the enzyme and substrate concentrations fixed at 0.62 u/ml and 0.12 mM, respectively and varying concentrations of dimethyl sulfoxide (DMSO), methanol (MeOH), and ethanol (EtOH) (0 % –1.0 % v/v)).

(a) Effect of DMSO
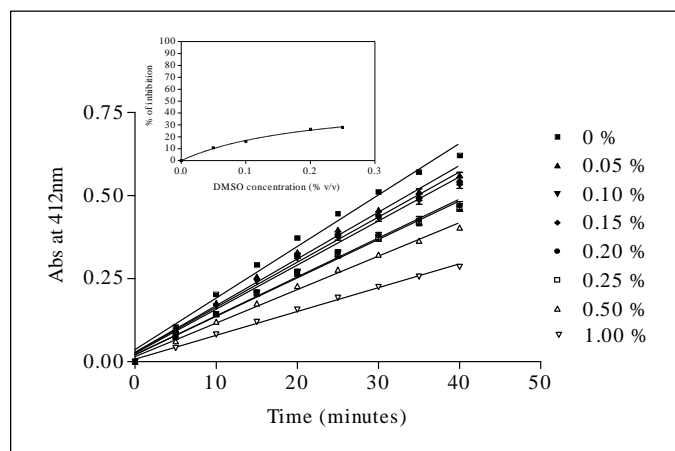
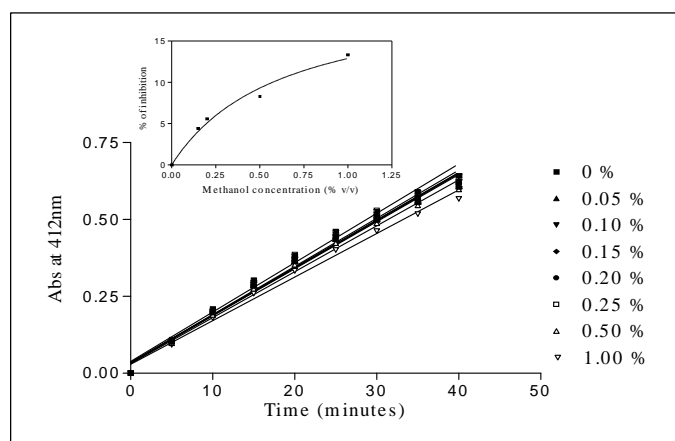**(b) Effect of methanol**

Figure 4.9 (a) & (b): Optimisation of solvent concentration. Each data point is expressed as mean ± standard deviation (n=3). R^2 = 0.9384 and 0.9739 for DMSO and methanol, respectively.
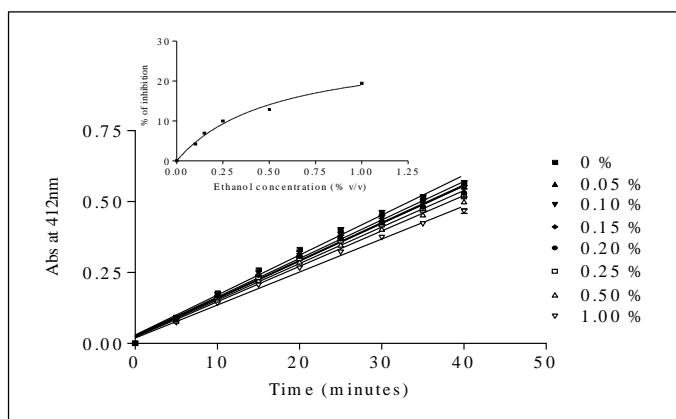
(c) Effect of ethanol

Figure 4.9 (c): Optimisation of solvent concentration. Each data point is expressed as mean ± standard deviation (n=3). $R^2 = 0.9513$.

The percentage of inhibition increased in a dose dependent manner with percentage of organic solvent **(Figure 4.9 (a)–(c))**. The maximum percentage of inhibition was observed at around 25 % at 0.25 % of v/v for DMSO, 14 % and 20 % at 1.0 % of v/v for MeOH and EtOH. DMSO is a universal solvent and can be used to dissolve most of the compounds. Therefore a final concentration of DMSO up to 0.1 % can be used with maximum percentage of inhibition at around 10–15 %.

4.4.1.7 Assay validation with standard inhibitors

The assay was validated with standard inhibitors tacrine and propidium using the optimised parameters as described earlier. The graph of % inhibition reaction reached a plateau at 95 % for tacrine and the IC_{50} was determined as 0.26 μM (**Figure 4.10**).

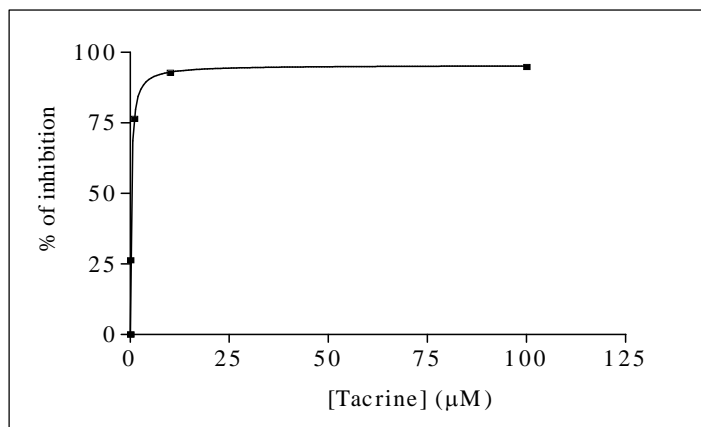**Figure 4.10:** Percentage inhibition of AChE against concentration of tacrine (0–100 μM). Each data point is expressed as mean ± standard deviation (n=3). Best-fit value: V_{max} = 95.40 %, IC_{50}= 0.26 μM, R^2 = 0.9987.
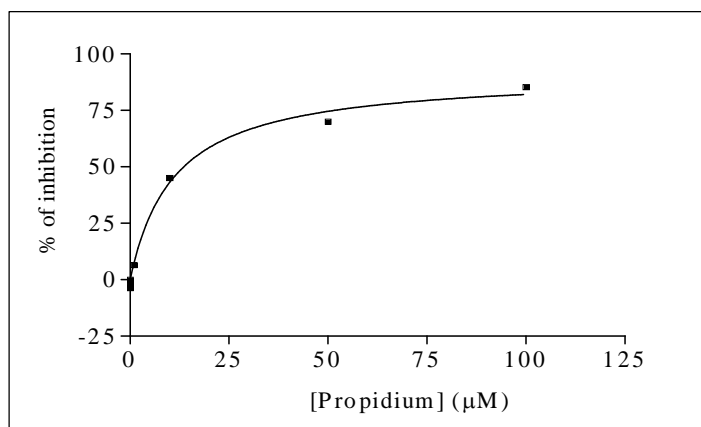

Figure 4.11: Percentage inhibition of AChE against concentration of propidium iodide (0–100 μM). Each data point is expressed as mean ± standard deviation (n=3). Best-fit value: V_{max} = 91.24 %, $IC_{50=}$ 11.20 μM, R^2 = 0.9929.

This value was comparable to the value previously reported for tacrine, 0.50 μM (Korabecny et al., 2011). The graph of % inhibition for propidium showed maximum inhibition of 91 % and the IC_{50} was determined as 11.20 μM **(Figure 4.11)**.

4.4.2 Optimisation of Aß peptide aggregation assay

4.4.2.1 Fluorescence intensity scanning

The Aß peptide aggregation assay was conducted as described in **section 4.3.2.4**. In order to find a suitable wavelength for fluorescence scanning, wells with various concentrations of Aß peptide (0, 0.03, 0.08, 0.15, 0.3, 0.6, 1.2, 2.4, 5, 10, 20 and 40 μM) were prepared. The fluorescence excitation spectrum was recorded between 400 to 470 nm (with emission fixed at 550 nm) while the emission scan was performed from 475 to 550 nm (with excitation wavelength fixed at 440 nm). The excitation and emission peaks that were obtained for the well that contained a final concentration of Aß peptide of 10 μM were 440 nm and 485 nm, respectively **(Figures 4.12 (a) & (b))** (More concentrated wells with fixed concentrations of 20 μM and 40 μM of Aß peptide gave signal overflow). These values were almost similar with the reported range (Bartolini et al., 2003).

(a) Excitation scanning
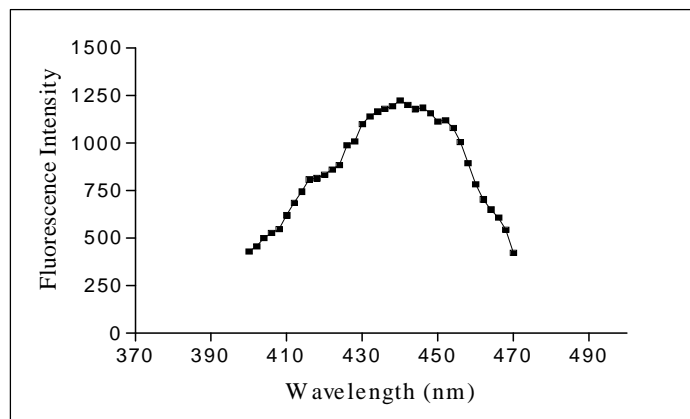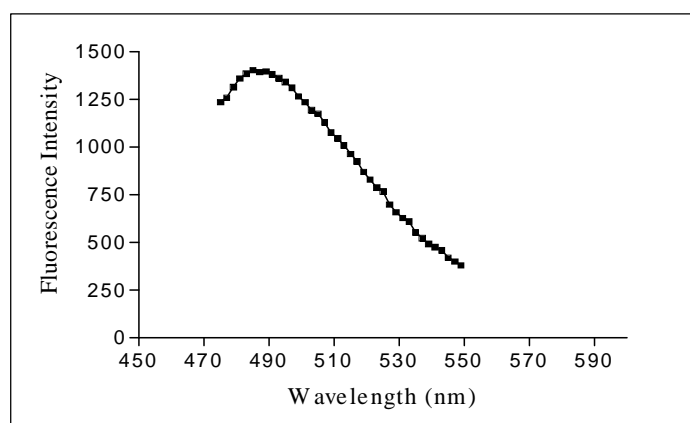

(a) Emission scanning

Figure 4.12 (a) & (b): Fluorescence intensity of thioflavin T ranged from wavelength of 400 nm to 470 nm (excitation scan), 470 nm to 550 nm (emission scan).

The excitation and emission peaks that were obtained above were applied further to determine the Z-position height and the value of optimal gain. Z-position scans were performed for both a signal and blank well in order to detect the volume in the well and to achieve the maximum signal to blank ratio thus increase the sensitivity of the instrument towards assay sample. The optimal gain value was achieved in order to improve the accuracy in fluorescence readings. The value of optimal Z-position height and optimal gain value that could obtain were 18325 µM and 166, respectively and these values were used in every subsequent experiment to make sure the readings were consistent.

4.4.2.2 Optimisation of Aß peptide concentration

The assay was conducted as described in **section 4.3.2.4** using various concentrations of Aß peptide (0, 0.03, 0.08, 0.15, 0.3, 0.6, 1.2, 2.4, 5, 10, 20 and 40 µM). Hexafluoroisopropanol (HFIP) has been shown to break down β-sheet structure, disrupt hydrophobic forces in aggregated amyloid preparations, and promote α-helical secondary structure (Bartolini et al., 2003). Therefore, in order to prevent pre-aggregation in the initial solution, Aß peptide (1 - 40), lyophilized from HFIP solution was used and then a stock solution was prepared by dissolving it in 100 % DMSO. The reason for stock solution prepared in 100 % DMSO was, at this concentration, DMSO does not promote thioflavin T fluorescence (Sabate et al., 2008) and contributes only minimum aggregation (Shen & Murphy, 1995; Bartolini et al., 2003).
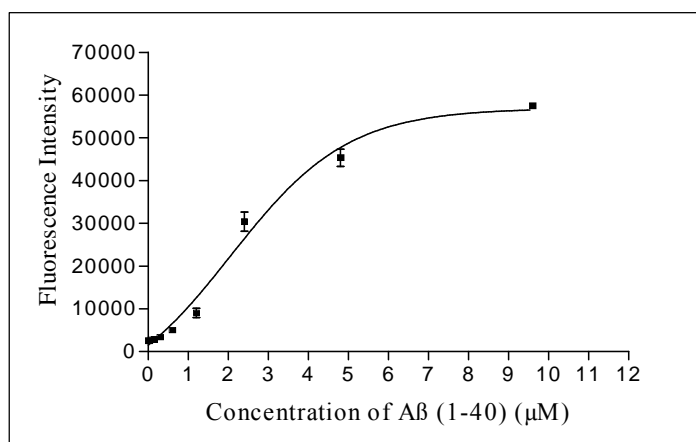

Figure 4.13: Graph of fluorescence intensity against Aß peptide (1-40) concentration. Each data point is expressed as mean ± standard deviation (n=3).

Figure 4.13 shows the non-linear relationship between fluorescence intensity and Aß peptide concentration. The fluorescence intensity increased until a concentration of 5 µM of Aß peptide concentration and slowly started to reach plateau at a concentration of 10 µM. At the final concentrations of 20 µM and 40 µM of Aß peptide (data not shown in graph), the signal gave overflow. Since the concentration of 5 µM

was quite near to the reported value (Levine, 1993) and (Munoz-Ruiz et al., 2005), it was chosen as the optimum concentration for the Aß peptide assay and was used in subsequent experiments.

4.4.2.3 Effect of solvent on Aß peptide aggregation

The experiment was conducted as described in **section 4.3.2.4** using a fixed concentration of Aß (5 μM) and various concentrations of DMSO (0–3 % v/v) as sample **(Figure 4.14 (a) & (b))**.
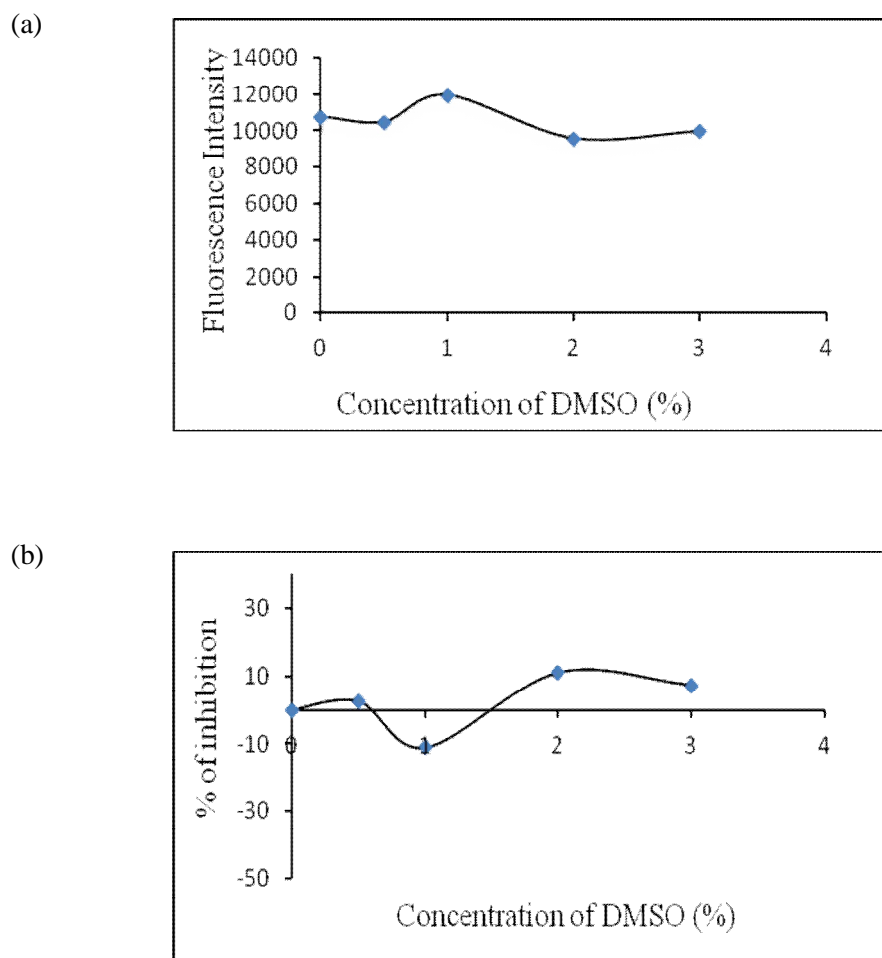
(a)

(b)

Figure 4.14 (a) & (b): Graphs of fluorescence intensity / % inhibition of Aß peptide aggregation against concentration of DMSO.

1 % of DMSO showed negative inhibition, whereas 0.5 % DMSO demonstrated the lowest inhibition value compared to the 2 and 3 % of DMSO. Avona test (Bonferroni's multiple comparison test) was carried out to determine whether there was any significant difference between the inhibition effects for 0.5, 1, 2 and 3 % of DMSO. The p value that was obtained was 0.83 (p > 0.05). This confirmed that there was no significant difference between 0.5, 1, 2 and 3 % of DMSO. Therefore 0.5 % DMSO (the lowest among 0.5, 1, 2 and 3 % of DMSO) was selected as the desired solvent concentration during preparation of different concentrations of test compounds.

4.4.2.4 Assay validation with standard inhibitor (Propidium Iodide)

The assay was validated with the standard inhibitor, propidium iodide using the optimised parameters as described earlier. Propidium iodide is known to be a potent inhibitor of Aß peptide aggregation (Munoz-Ruiz et al., 2005) and also does not affect the fluorescence intensity of ThT as the iodide does not exhibit a quenching effect on ThT (Bartolini et al., 2003). Therefore, it was selected as the standard inhibitor in this assay.

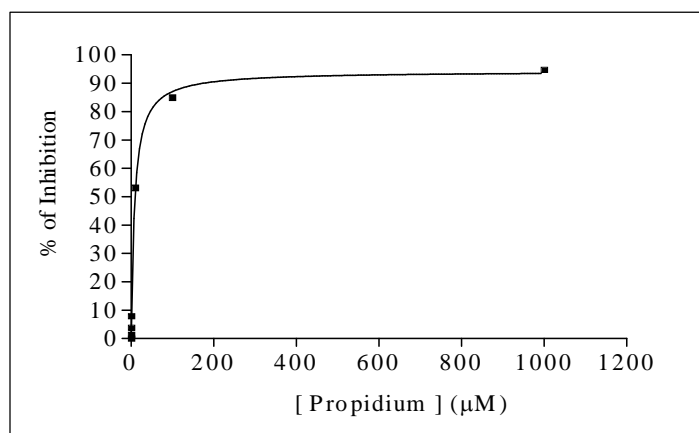
Figure 4.15: Graph of % inhibition of Aß peptide aggregation against concentration of propidium iodide. Each data point is expressed as mean ± standard deviation (n= 3). Best-fit value: V_{max} = 94.20 %, IC_{50}= 8.23 µM, R^2 = 0.9972.

Based on **Figure 4.15**, the reaction reached a plateau at 90 % inhibition and the IC_{50} of propidium was determined as 8.23 µM.

4.5 CONCLUSION

The human acetylcholinesterase inhibition assay was conducted by modifying the method of Ellman et al. (1961). Parameters such as enzyme concentration, substrate concentration, incubation time, incubation temperature and solvent were optimised. Different concentrations of substrate were used to determine the K_m value. This K_m value was used as the substrate concentration for this assay for competitive inhibitors to be identified in a competition experiment that measures IC_{50} values. The assay was validated with standard inhibitors to determine the assay reliability. In **Chapter 5**, compounds derived from the virtual screening study will be tested using this assay.

The Aß peptide assay was performed following the method of LeVine (1993) and Munoz-Ruiz et al. (2005) with minor modifications. Fluorescence intensity scanning was conducted followed by optimisation of Aß peptide concentration and determination of solvent concentration. The assay was validated with a standard inhibitor to determine the assay reliability. In **Chapter 5**, compounds derived from the virtual screening study that show promising anticholinesterase activity, will be tested using this assay.

CHAPTER 5: EVALUATION OF COMPOUNDS IDENTIFIED FROM VIRTUAL SCREENING AS INHIBITORS OF ACETYLCHOLINESTERASE AND AMYLOID BETA PEPTIDE AGGREGATION

5.1 INTRODUCTION

In the present study, a number of the compounds identified from virtual screening were triterpenes and steroids. Previous studies have discovered that some triterpenes and steroids are potential acetylcholinesterase (AChE) inhibitors **(Table 5.1)**. For an example, Kvaltinova et al. (1991) has reported that buxaminol-E, a steroidal alkaloid from *B. sempervirens* has good inhibitory activity towards AChE. A screening of pregnane-type steroidal alkaloids, from *Sarcococca hookeriana* against AChE was performed by Choudhary et al. (2005) and this study has found that these steroidal alkaloids had IC_{50} values between 1.6 and 59.0 µM. In another study, Axillaridine-A, a pregnane-type steroidal alkaloid from *Sarcococca saligna* was reported as potent anticholinesterase compound with IC_{50} value 5.2 µM (Khalid et al., 2004). Steroidal alkaloids such as epoxynepapakistamine-A, funtumafrine C and *N*-methylfuntumine from leaves of *Sarcococca coriacea* also found to have cholinesterase inhibitory with IC_{50} values ranging from 45.8 to >200.0 µM (Kalauni et al., 2002).

Screening was carried out by Atta ur et al. (2001) which resulted in identification of effective AChE inhibitors, triterpenoid alkaloids, from *Buxus papillosa*, with IC_{50} values ranging from 25.4 to 235.0 µM. Another triterpenoid alkaloid, (+)-*N*-tigloylbuxahyrcanine has been isolated from *Buxus hyrcana* and found to be the most potent against AChE with IC_{50} value 443.6 µM (Choudhary et al., 2003). 17-oxo-3-benzoylbuxadine, benzoylbuxadine, buxhyrcamine, homomoenjodarmine and spirofornabuxine are also triterpenoid alkaloids, found from the same plant which

69

exhibited better AChE inhibitory activity with IC_{50} values ranging from 6.3 to 19.5 µM (Ata et al., 2010). In another case, some tetracyclic triterpene with good AChE inhibitory profile were also identified by Rouleau et al. (2011).

In the present study, the Ellman assay was employed to measure the AChE activity of the compounds found from virtual screening. Compounds showing the greatest anticholinesterase activity were further tested using the thioflavin T-based fluorometric assay to study their self-induced amyloid beta (Aβ) peptide aggregation inhibitory activity.

Table 5.1: Previous findings on triterpenes and steroids as acetylcholinesterase inhibitors.

Compound	Plant	Activity	Reference
Hookerianamide-d Hookerianamide-E Hookerianamide-F Hookerianamide-G	*Sarcococca hookeriana*	1.6–59.0 µM	(Choudhary et al., 2005)
Axillaridine -A	*Sarcococca saligna*	5.2 µM	(Khalid et al., 2004)
Epoxynepapakistamine – A funtumafrine C *N*-methylfuntumine	*Sarcococca coriacea*	45.8– >200.0 µM	(Kalauni et al., 2002)
Buxakashmiramine Buxakarachiamine Buxahejramine Cyclovirobuxeine-A Cyclomicrophylline-A Semperviraminol	*Buxus papillosa*	25.4–235.0 µM	(Atta ur et al., 2001)
(+)-*N*-tigloylbuxahyrcanine	*Buxus hyrcana*	443.6 µM	(Choudhary et al., 2003)
17-oxo-3-benzoylbuxadine Buxhyrcamine Homomoenjodarmine Spirofornabuxine	*Buxus hyrcana*	6.3–19.5 µM	(Ata et al., 2010)
Tetracyclic triterpene	Synthesized compounds	0.003–> 10.0 µM	(Rouleau et al., 2011)

5.2 MATERIALS AND METHODS

Refer to **sections 4.2** and **4.3**

5.3 RESULTS AND DISCUSSION

5.3.1 Human acetylcholinesterase (hAChE) inhibition assay

The AChE inhibitory effects of the compounds were examined by the method of Ellman et al. (1961) using AChE from human recombinant acetylcholinesterase with tacrine and propidium as reference standards. The compounds were initially tested at a final concentration of 10 µM. Compounds that showed more than 25 % inhibition at 10 µM were further tested to determine their IC_{50} values and the data summarized in **Table 5.2**.

Table 5.2: Anticholinesterase activity of compounds V1–V21 identified from virtual screening together with data obtained from the molecular modeling studies.

Compound	Anti-cholinesterase activity (hAChE)			Docking studies	
	% Inhibition at 10 μM [a]	$IC_{50} \pm SEM$ (μM)	$K_i \pm SEM$ (μM)	K_i (μM)	Binding site
V1	27	12.4 ± 1.3	6.2 ± 0.7	0.40	PAS
V2	19	-	-	0.58	PAS
V3	5	-	-	0.77	PAS
V4	-	-	-	0.83	PAS
V5	-	-	-	1.56	PAS
V6	3	-	-	2.04	PAS
V7	-	-	-	2.09	PAS
V8	-	-	-	3.16	PAS
V9	-	-	-	4.08	PAS
V10	-	-	-	4.18	PAS
V11	1	-	-	4.40	PAS
V12	48	10.4 ± 2.5	5.2 ± 1.3	4.56	PAS
V13	8	-	-	4.86	PAS
V14	5	-	-	5.01	PAS
V15	5	-	-	5.65	PAS
V16	3	-	-	5.90	PAS
V17	-	-	-	6.40	PAS & CAS
V18	90	1.5 ± 0.2	0.8 ± 0.1	6.42	PAS & CAS
V19	-	-	-	7.41	PAS
V20	-	-	-	7.39	PAS
V21	38	14.7 ± 4.0	7.4 ± 2.0	78.91	PAS
Tacrine*	48	0.26 ± 0.01	0.13 ± 0.01	20.51	CAS
Propidium*	41	11.4 ± 1.3	5.7 ± 0.7	95.81	PAS

[a] Values are expressed as mean of triplicate, PAS = Peripheral anionic site, CAS = Catalytic site, *Standard inhibitor, - = No activity observed at 10 μM
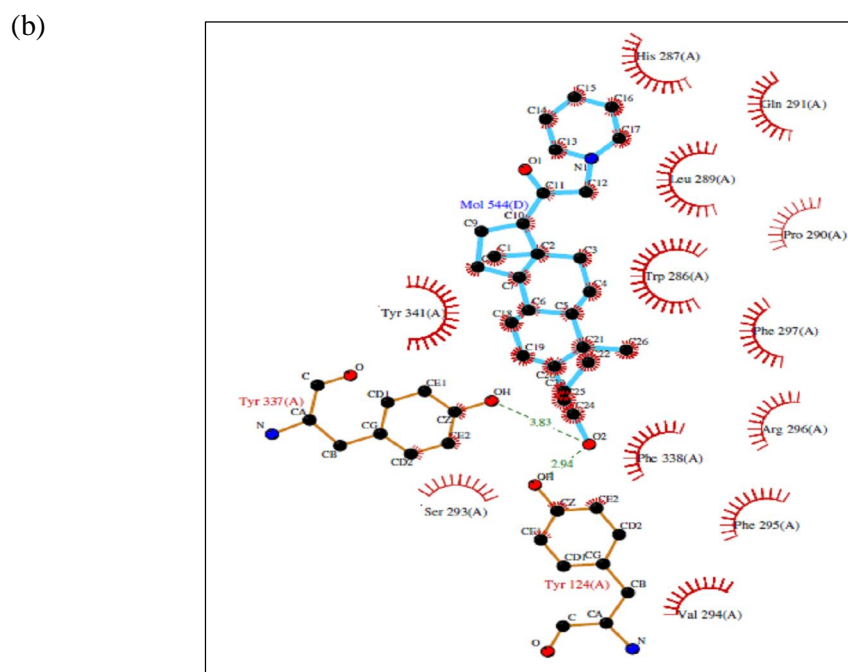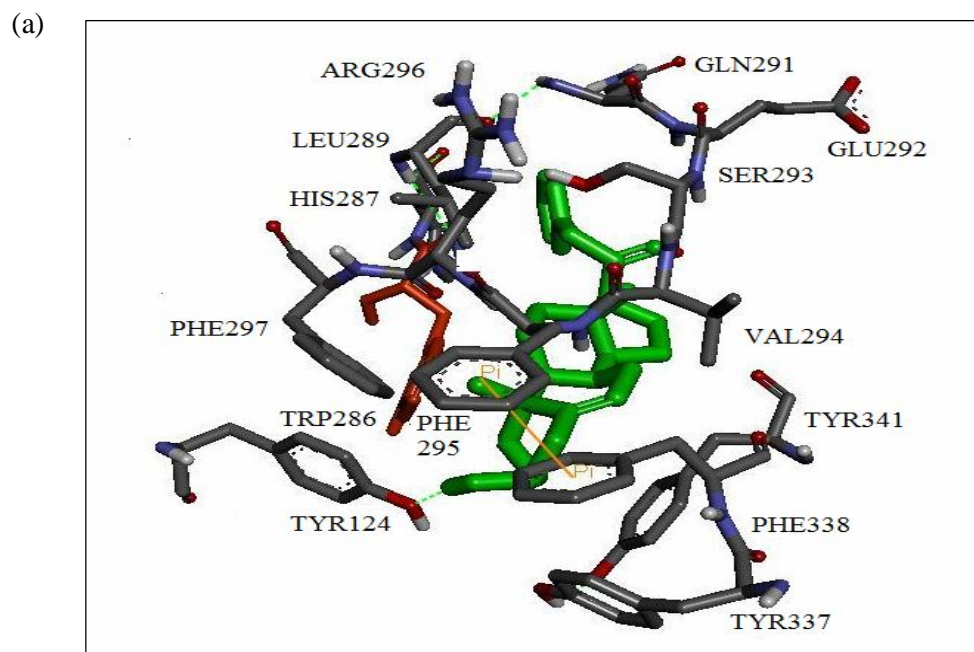
(a)

(b)

Figure 5.1: a) 3D representation of hAChE complex with compound **V1** (ZINC04293012) (purple) at the PAS region of the AChE. **b)** Ligplot analysis to show the molecular interactions (hydrophobic and hydrogen bonds) between the ligand and the protein.

(a)

(b)

Figure 5.2: a) 3D representation of hAChE complex with compound **V12** (ZINC04293010) (green) at the PAS region of the AChE. **b)** Ligplot analysis to show the molecular interactions (hydrophobic and hydrogen bonds) between the ligand and the protein.
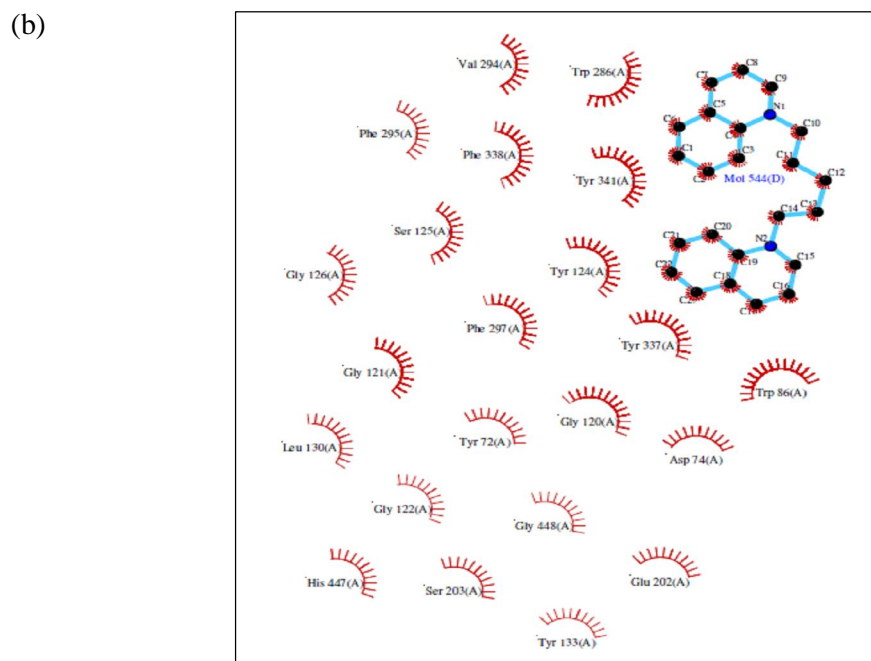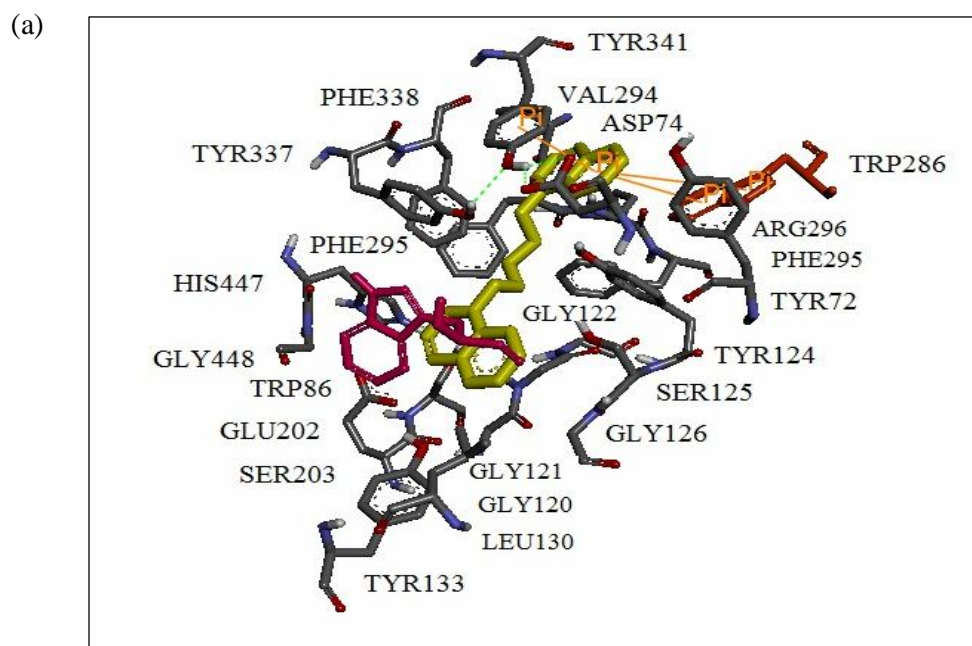
(a)

(b)

Figure 5.3: a) 3D representation of hAChE complex with compound **V18** (ZINC01668161) (yellow) at the PAS and CAS region of the AChE. **b)** Ligplot analysis to show the molecular interactions (hydrophobic and hydrogen bonds) between the ligand and the protein.

(a)

(b)

Figure 5.4: a) 3D representation of hAChE complex with compound **V21** (ZINC02190312) (blue) at the PAS and CAS region of the AChE. **b)** Ligplot analysis to show the molecular interactions (hydrophobic and hydrogen bonds) between the ligand and the protein.
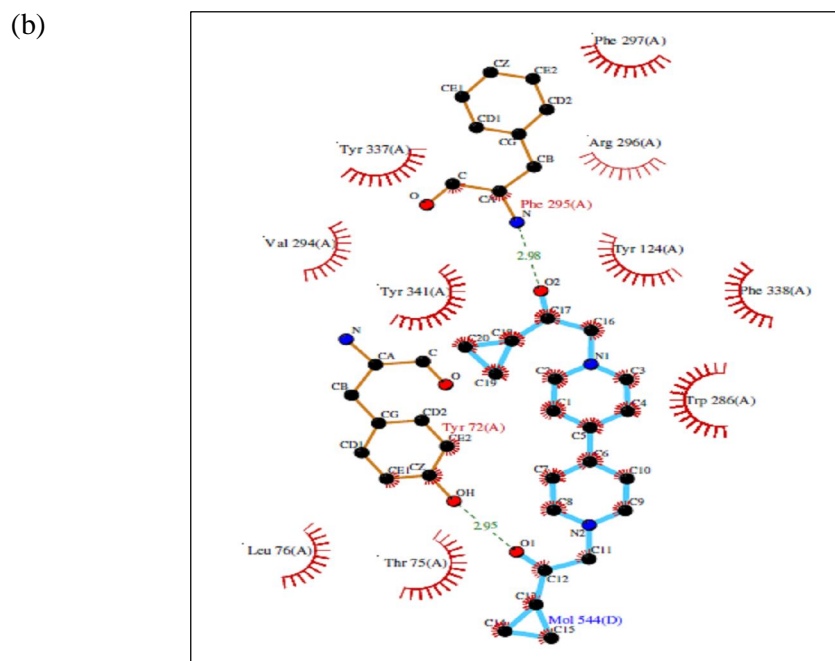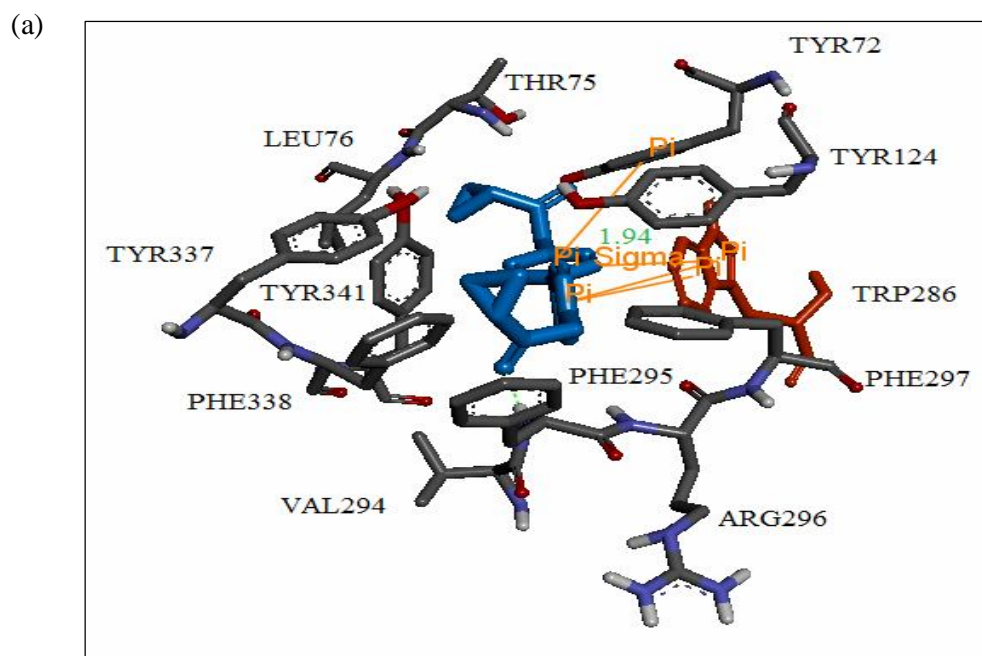
Compounds **V1**, **V12**, **V18** and **V21** showed inhibition of 27 %, 48 %, 90 % and 38 % at a final concentration of 10 μM, respectively. These compounds were further tested in various concentrations (0–100 μM) to estimate the IC_{50} value. The IC_{50} of **V1**, **V12** and **V21** were found to be 12.44 μM, 10.43 μM and 14.69 μM, respectively. The IC_{50} of **V18** was determined as 1.54 μM and this value was comparable to the value previously reported for **V18**, 4 μM (Komloova et al., 2011).

Molecular interaction study **(Tables 3.6 & 5.2) (see figures 5.3 (a) & (b))** has shown that compound **V18** bound to CAS and PAS of the enzyme near the aromatic residue Trp86 and Trp286, respectively. Residues that mainly involved in hydrophobic interaction are Tyr72, Asp74, Trp86, Gly120, Gly121, Gly122, Tyr124, Ser125, Gly126, Leu130, Tyr133, Glu202, Ser203, Trp286, Val294, Phe295, Phe297, Tyr337, Phe338, Tyr341, His447 and Gly448. In addition to the hydrophobic contacts, pi-pi interactions were also found between the compound **V18** and the residues Trp286 and Tyr341 which increase the anticholinesterase activity of this compound.

Docking studies on compounds **V1**, **V12** and **V21** **(Tables 3.6 & 5.2) (see figures 5.1, 5.2** and **5.4)** has indicated that these compounds are PAS binders. Molecular investigation has shown that the residues Trp286, Phe297, Phe338, Val294 and Tyr341 are mainly involved in hydrophobic contacts between these compounds and the enzyme. Pi-sigma interaction has been found between the compounds **V1 (C18)** and **V21 (C7)** with the residue Trp286. Besides pi-sigma interaction, pi-pi interaction was observed between the compound **V18** with the residues Trp286 and compound **V21** with the residues Trp286 and Tyr72.

5.3.2 Amyloid beta (Aβ) peptide aggregation assay

The compounds that showed the greatest AChE inhibitory activity (**V1**, **V2**, **V12**, **V18** and **V21**) were tested for their ability to inhibit Aβ peptide aggregation employing the thioflavin T fluorescence method and using propidium, a known inhibitor acting at the AChE peripheral site, as a standard compound.

Table 5.3: Inhibition of self-induced Aβ peptide aggregation by selected compounds.

No.	Zinc ID	Aβ peptide aggregation
		% Inhibition at 10 μM [a]
V1	ZINC04293012	60
V2	ZINC00033528	22
V12	ZINC04293010	51
V18	ZINC01668161	10
V21	ZINC02190312	8
	Propidium*	83[b]

[a] Values are expressed as mean of triplicate, [b] Tested at 8.2 µM, * Standard inhibitor

The results summarized in **Table 5.3** indicate that compounds **V1** and **V12** inhibited Aβ peptide aggregation at 10 µM at a level which is comparable to that of the standard inhibitor propidium, which caused 83 % inhibition at final concentration of 8.2 µM.

5.4 CONCLUSION

Compounds identified in the virtual screening study were tested using the Ellman assay to evaluate their inhibitory activity against AChE. Four of the compounds (**V1**, **V12**, **V18** and **V21**) were found to be potent inhibitors of AChE, with IC_{50} values in the range 1–15 μM.

Inhibition studies on self-induced Aβ peptide aggregation showed that two compounds (**V1** and **V12**) can exert more than 50 % inhibition on Aβ aggregation at a final concentration of 10 μM. Since these compounds are PAS binding ligands of AChE, they have the potential to interact with the Aβ binding site thus inhibiting AChE-induced beta amyloid aggregation.

CHAPTER 6: EVALUATION OF 2´-HYDROXY-AND 2´-METHOXY CHALCONES AS INHIBITORS OF ACETYLCHOLINESTERASE ACTIVITY AND AMYLOID BETA PEPTIDE AGGREGATION

6.1 INTRODUCTION

Chalcones, or 1,3-diaryl-2-propen-1-ones, are compounds belonging to the flavonoid family and posses important biological activities such as anthelmintic, antibacterial, amoebicidal, antiviral, insectidal, antiprotozoal, anticancer, cytotoxic, antiulcer and immunosuppressive activities (Dimmock et al., 1999). It also has been reported that chalcones have the potential to inhibit acetylcholinesterase (AChE) (Amor et al., 2005; Aurangzen Hasan, 2005). Even though chalcones have been tested for anticholinesterase activity, there are no reports of chalcones that bind specifically to the peripheral anionic site (PAS) of AChE.

In this study, we describe the evaluation of the anticholinesterase activity of a series of chalcones using the Ellman colorimetric assay. Since three-dimensional structure information of the complex structure of ligands and AChE is available in the Protein Data Bank (PDB), a docking model built with AutoDock 4.0 was generated for active chalcones and the protein-ligand binding interactions were studied in order to identify whether those chalcone that inhibited AChE could bind to the PAS of AChE. The compounds that showed the best AChE inhibitory potency were also tested to assess their ability to inhibit amyloid beta (Aβ) peptide aggregation employing the thioflavin T fluorescence method.

6.2 MATERIALS AND METHODS

The compounds were synthesized by Dr. Chee from Department of Chemistry, University of Malaya (Chee, 2011).

6.2.1 Anticholinesterase assay

Refer to **section 4.2**

6.2.2 Docking studies

6.2.2.1 Preparation of protein file

The AChE crystal structure, Human AChE (hAChE) in complex with fasciculin II (2.76 Å) (PDB ID: 1b41) was extracted from the PDB as a pdb file. The heteroatoms and water molecules were removed using Discovery Studio Visualizer 3.1 (Accelrys, Inc, Sandiego, CA, USA). Hydrogens were added and double coordinates were corrected using Hyper chem Pro 6.0 software. Then, again hydrogens were added, non-polar hydrogens were merged and the missing atoms were repaired using AutoDock Tools 1.5.2 software. Finally, the kollman charges were added and AutoDock 4 type atoms were assigned to the protein.

6.2.2.2 Preparation of ligand file

3-Dimensional structural models of compounds **C12**, **C14**, **C15** and **C18** were built using Chem Bio-3D software and saved in MOL2 format. These compounds were prepared in protonated form where appropriate for physiological pH. Then, they were minimized through the Hyper chem Pro 6.0 software (Geometry optimization – MM$^+$) to the lowest energy.

6.2.2.3 Molecular docking

Compounds **C12**, **C14**, **C15** and **C18** were docked to the hAChE structure in complex with fasciculin II (2.76 Å) (PDB ID: 1b41), using AutoDock 4.0. Docking was carried out using the hybrid Lamarckian Genetic Algorithm, with an initial population of 150 randomly placed individuals and a maximum number of 2500000 energy evaluations. Spacing was set to 0.375 and rmstol value was set to 2.0. Grid box was created by adjusting the defaults value to cover the entire protein. Ligand - protein interactions were analyzed using Viewer Lite, Discovery Studio Visualizer 3.1 and Lig plot 4.4.2 softwares.

6.2.3 Aβ peptide aggregation assay
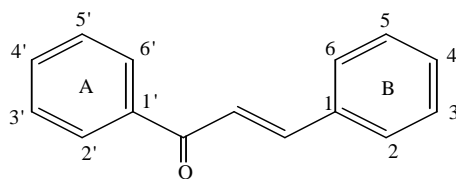
Refer to section **4.3**

6.3 RESULTS AND DISCUSSION

6.3.1 Anticholinesterase activity

The anticholinesterase activity of the prepared chalcones was determined at 10 µM using the method of Ellman et al. (1961) and the results are shown in **Table 6.1**. The IC_{50} values of the active compounds were also determined and were found to be 40–350 µM.

Compounds **C4**, **C8**, **C11**, **C12**, **C14**, **C15**, **C17** and **C18** have a hydroxyl group on ring A and showed cholinesterase inhibitory activity in the micro molar range. The present study indicated that a hydroxyl group on ring A *ortho* to the side chain is essential for inhibitory activity of chalcones towards AChE. This is supported by the earlier work of Aurangzen Hasan (2005) where it has been proven that hydroxyl group on ring A *ortho* to the side chain is responsible for AChE inhibitory activity.

Compounds **C12, C14, C18** and **C15** with halogen substituents (Cl/Br) on ring B showed good activity compared to other chalcones. This indicates that halogen groups on ring B may be important for cholinesterase inhibitory activity. In detail, compound **C18** with bromo substitution at position C-4 showed better inhibitory activity compared to compounds **C14** and **C15**. This shows that a halogen group specifically on C-4 on ring B seems to be an important requirement for optimal AChE inhibition of compounds bearing methoxyl substituents at positions C-4´ and C-6´.

Table 6.1: Structural data and anticholinesterase activity of chalcones 1–27.

Cpd.	2′	3′	4′	5′	6′	2	3	4	5	6	% Inhibition at 10 µM [a]	IC$_{50}$ ± SEM (µM)
C1	OH	H	H	H	H	H	H	H	H	H	11	
C2	OH	H	H	H	H	H	H	CH$_3$	H	H	-	
C3	OH	H	H	H	H	H	H	OCH$_3$	H	H	6	
C4	OH	H	H	H	H	H	H	N(CH$_3$)$_2$	H	H	28	266 ± 48
C5	OH	H	H	H	H	H	H	Br	H	H	-	
C6	OH	H	H	H	H	H	H	Cl	H	H	-	
C7	OH	H	H	H	H	H	O-CH$_2$-O		H	H	1	
C8	OH	H	H	H	H	H	OCH$_3$	OH	H	H	22	209 ± 102
C9	OH	H	H	H	H	H	OCH$_3$	OCH$_3$	OCH$_3$	H	-	
C10	OH	H	H	H	H	H	OCH$_3$	OCH$_3$	H	H	10	
C11	OH	H	H	H	H	H	OH	OH	H	H	29	177 ± 21
C12	OH	H	H	H	H	Br	H	H	H	H	38	55 ± 12
C13	OH	H	H	H	H	OH	Cl	H	Cl	H	-	
C14	OH	H	OCH$_3$	H	OCH$_3$	OH	Cl	H	Cl	H	51	73 ± 22
C15	OH	H	OCH$_3$	H	OCH$_3$	Br	H	H	H	H	23	85 ± 16
C16	OH	H	OCH$_3$	H	OCH$_3$	H	O-CH$_2$-O		H	H	5	
C17	OH	H	OCH$_3$	H	OCH$_3$	H	H	CH$_3$	H	H	23	354 ± 133
C18	OH	H	OCH$_3$	H	OCH$_3$	H	H	Br	H	H	30	41 ± 13
C19	OH	H	OCH$_3$	H	OCH$_3$	H	OCH$_3$	OCH$_3$	H	H	8	
C20	OH	H	OCH$_3$	H	OCH$_3$	H	OCH$_3$	OH	H	H	10	
C21	OH	H	OCH$_3$	H	OCH$_3$	H	H	OCH$_3$	H	H	7	
C22	OH	H	OCH$_3$	H	OCH$_3$	H	H	N(CH$_3$)$_2$	H	H	5	
C23	OH	H	OCH$_3$	OCH$_3$	H	H	OCH$_3$	OCH$_3$	H	H	10	
C24	OCH$_3$	H	OCH$_3$	OCH$_3$	H	H	OCH$_3$	OCH$_3$	H	H	1	
C25	OCH$_3$	H	OCH$_3$	H	OCH$_3$	H	OH	OH	H	H	6	
C26	OCH$_3$	H	OCH$_3$	H	OCH$_3$	H	OCH$_3$	OCH$_3$	H	H	3	
C27	OCH$_3$	H	OCH$_3$	H	OCH$_3$	H	H	H	H	H	2	

[a] Values are expressed as mean of triplicate, - = No activity observed at 10 µM

6.3.2 Docking studies

To investigate possible ligand - AChE interactions, docking studies were performed to generate binding model for the chalcones **C4**, **C8**, **C11**, **C12**, **C14**, **C15**, **C17** and **C18** towards hAChE.

Table 6.2: Correlation between the experiment and computational K_i values for the anticholinesterase activity of chalcones 1–27.

Compound	Experimental data	Computed data	
	$K_i \pm SEM$ (µM)	K_i (µM)	Binding site
C4	133 ± 24	60.64	PAS
C8	105 ± 51	104.15	PAS
C11	89 ± 11	45.21	PAS & CAS
C12	28 ± 6	22.56	PAS
C14	37 ± 11	102.29	PAS
C15	43 ± 8	48.79	PAS
C17	177 ± 67	180.72	PAS
C18	21 ± 7	56.78	PAS
Tacrine*	0.13 ± 0.01	20.51	CAS
Propidium*	5.7 ± 0.7	95.81	PAS

PAS = Peripeheral anionic site, CAS = Catalytic site, *Standard inhibitor of AChE

The hydroxyl group on ring A *ortho* to the side chain of compound **C18** forms a hydrogen bond to Ser293 (2.78 A°) and Ser293 (2.73 A°). This compound is a PAS binding ligand as it interacts mainly with the residue Trp286 at the PAS of the enzyme **(Fig. 6.5 a & b)**. Residues such as His287, Gln291, Val294, Phe295, Arg296, Phe297 and Phe338 are contributing for van der waals interaction while pi-sigma (1.874 A°) interaction was formed between the ligand and the residue Leu289.

It has been observed that hydroxyl group of compound **C12** forms a hydrogen bond to the residue Tyr72 (1.981 A°) **(Figure 6.2a)**. It was also found to have pi-pi interaction with the residue Trp286 and hydrophobic interactions with several other

residues such as Tyr72, Tyr124, Trp286, Val 294, Phe295, Phe297, Tyr337, Phe338 and Tyr341 at PAS region of AChE **(Figure 6.2b)**. Meanwhile, residues such as Tyr124, Phe297, Tyr337, Phe338 and Tyr341 are also involved in Van der waals interaction.

The hydroxyl group on ring A *ortho* to the side chain of compound C14 forms a hydrogen bond to Asp74 (3.10 A°). Meanwhile, another hydrogen bond was observed between the hydroxyl group on ring B *ortho* to the side chain of compound **C14** with Tyr124 (3.05 A°). There was a hydrophobic contact between the ligand and the residues Leu76, Tyr124, Trp286 and Tyr341 indicating that this ligand is a PAS binder **(Figure 6.3b)**. Docking investigation has also found that the residues Phe297, Phe338 and Tyr341 are involved in Van der waals interaction and the residue Trp286 contributes to pi-sigma interaction **(Figure 6.3a)**.

As shown in **Figure 6.4b**, the hydroxyl group on ring A *ortho* to the side chain of compound **C15** forms two hydrogen bonds. One is with Tyr72 (2.77 Å) and another is with Asp74 (2.91 Å). This compound is a PAS binding ligand since there is a hydrophobic contact between the ligand and the residues Leu76, Trp286, Phe297, Tyr337, Phe338 and Tyr341 which involves the PAS region of AChE. Further investigation has also shown that residues Tyr124, Phe297, Tyr337, Tyr338 and Tyr341 are involved in van der waals interaction and Trp286 favorable for pi-pi interaction. Docking studies on compounds **C4**, **C8**, **C11** and **C17** indicated that compound **C11** is both PAS and CAS binding ligand whereas compounds **C4**, **C8** and **C17** are PAS binders.

A correlation study was carried out to investigate the relationship between the experimental and docking study **(Figure 6.1)**. The study has shown a correlation ($R^2 =$

0.33) for the present series of compounds. The docking analysis has roughly predicted the binding locations for compounds which have been tested in this study. The r^2 value can be improved further by increasing the number of compounds being tested in this study.
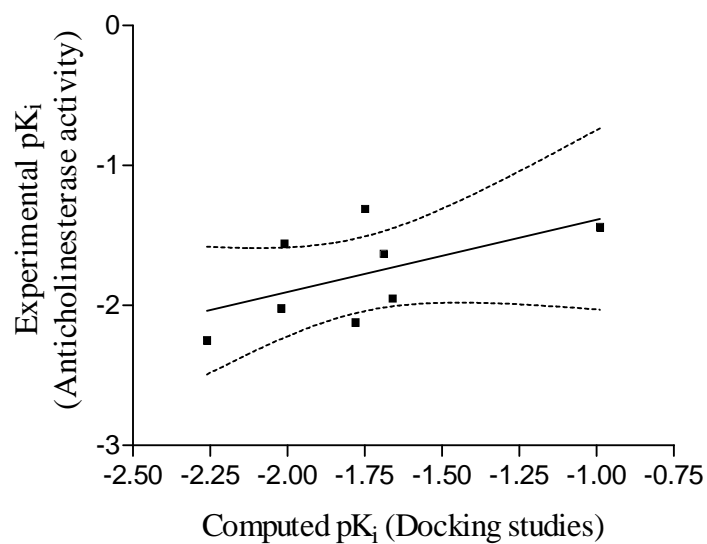

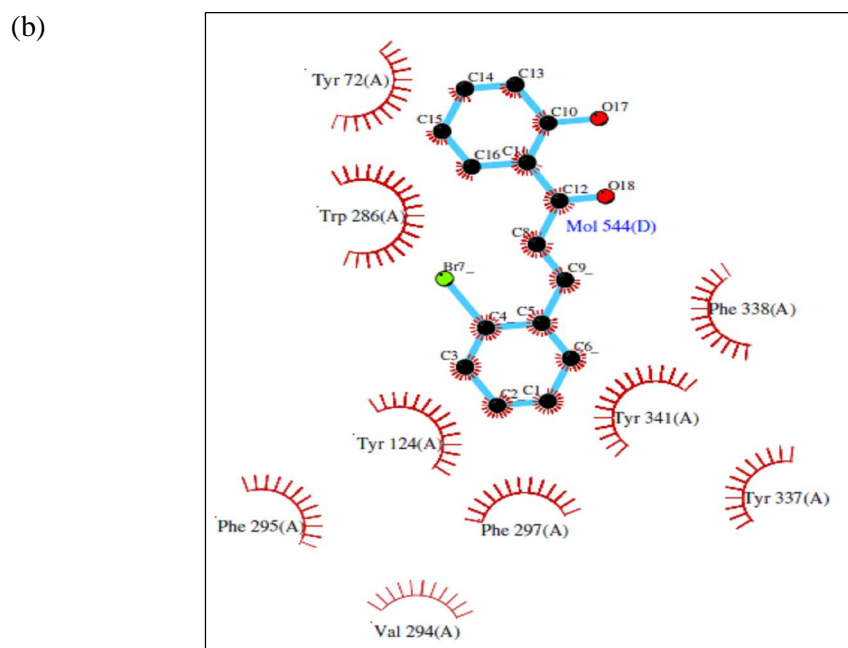**Figure 6.1:** Correlation plot of experimental pK_i (anticholinesterase activity) vs computed pK_i (docking studies).
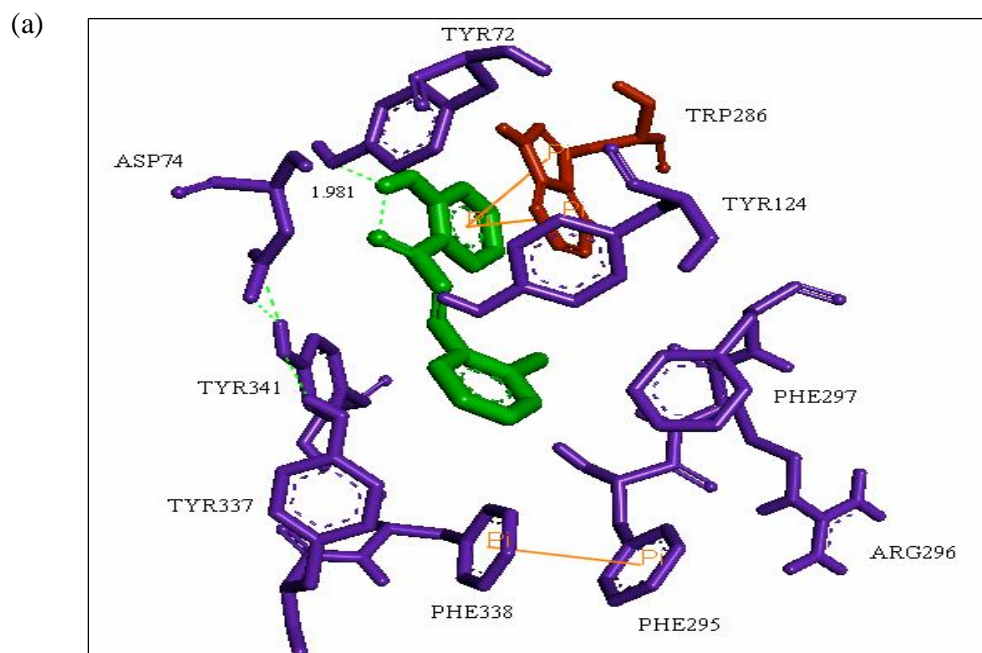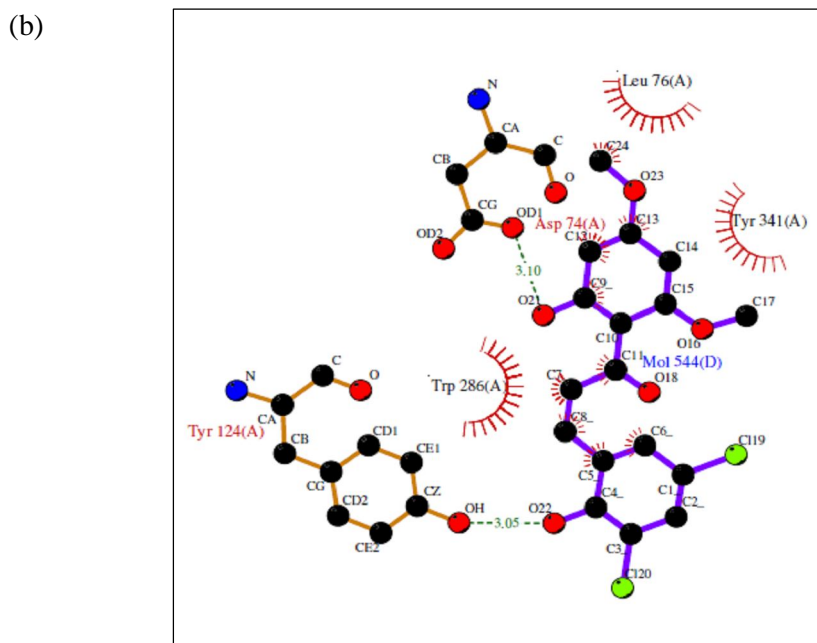
(a)

(b)

Figure 6.2: a) 3D representation of hAChE complex with compound **C12** (green) at the PAS region of the AChE. **b)** Ligplot analysis to show the molecular interactions (hydrophobic and hydrogen bonds) between the ligand and the protein.
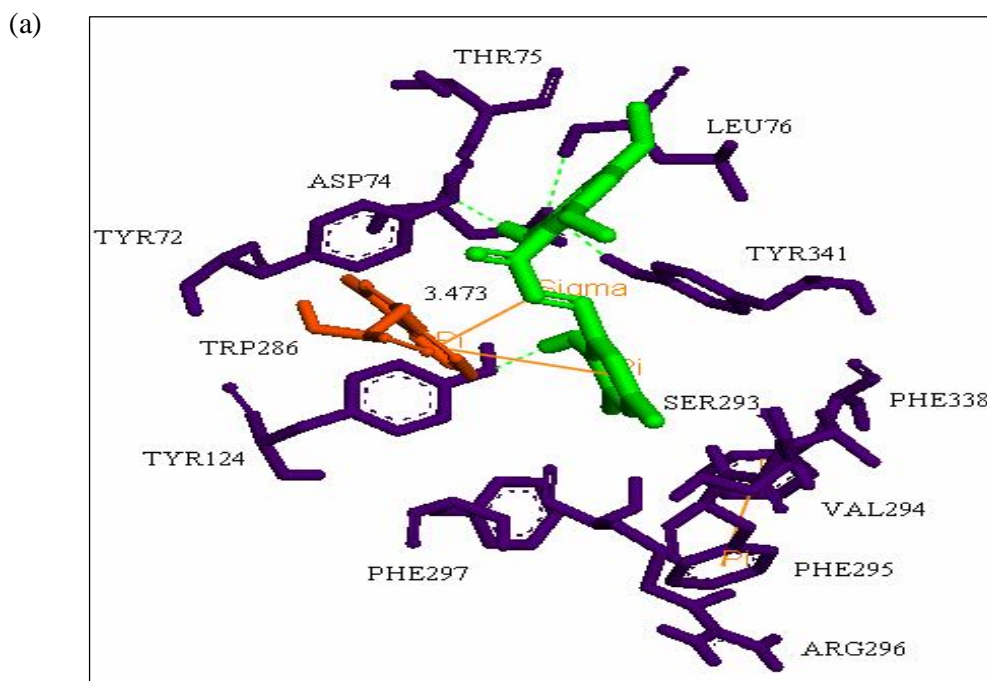
(a)

(b)

Figure 6.3: a) 3D representation of hAChE complex with compound **C14** (green) at the PAS region of the AChE. **b)** Ligplot analysis to show the molecular interactions (hydrophobic and hydrogen bonds) between the ligand and the protein.

Figure 6.4: a) 3D representation of hAChE complex with compound **C15** (green) at the PAS region of the AChE. **b)** Ligplot analysis to show the molecular interaction (hydrophobic and hydrogen bonds) between the ligand and the protein.
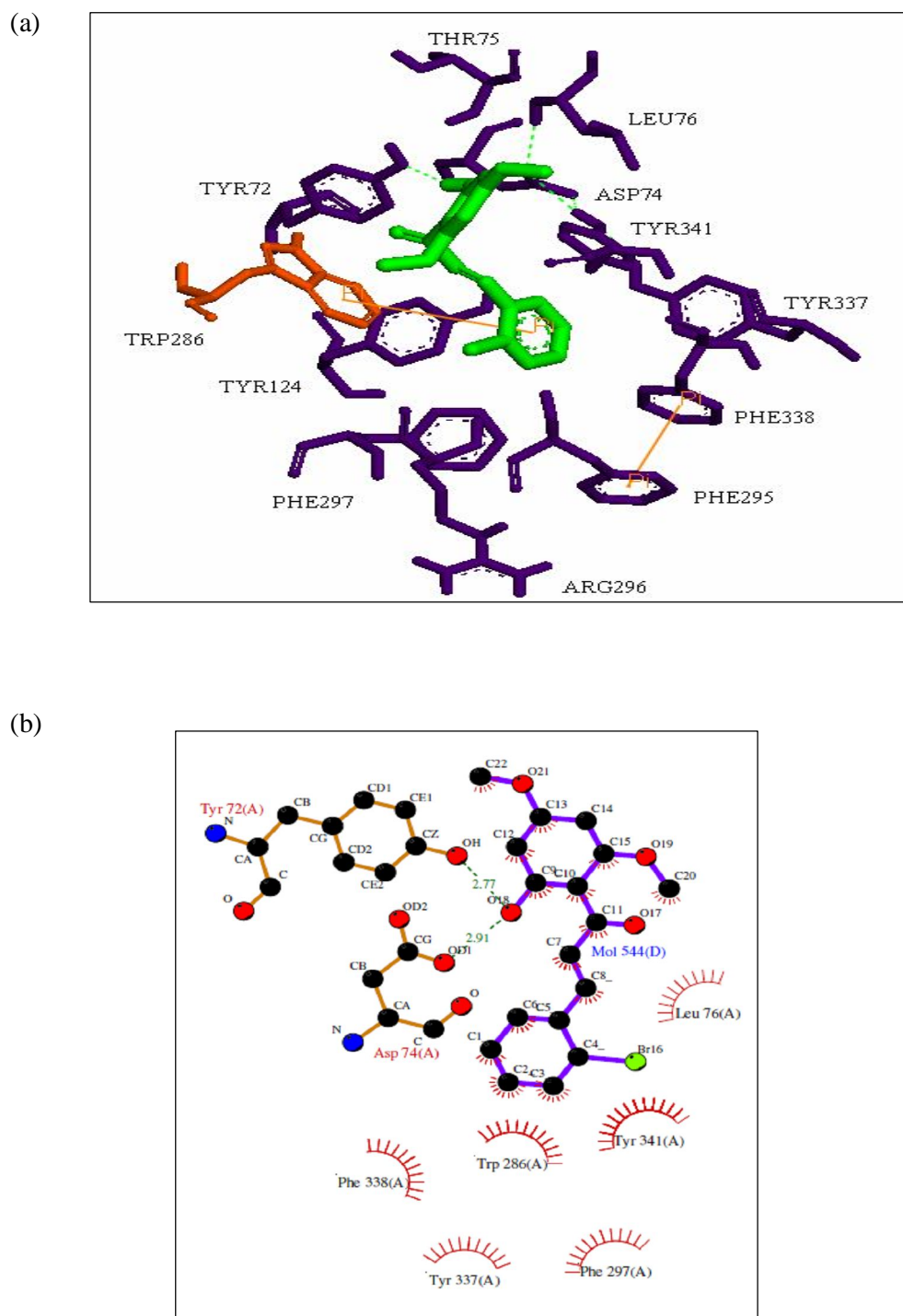
(a)

(b)

Figure 6.5: a) 3D representation of hAChE complex with compound **C18** (green) at the PAS region of the AChE. **b)** Ligplot analysis to show the molecular interactions (hydrophobic and hydrogen bonds) between the ligand and the protein.
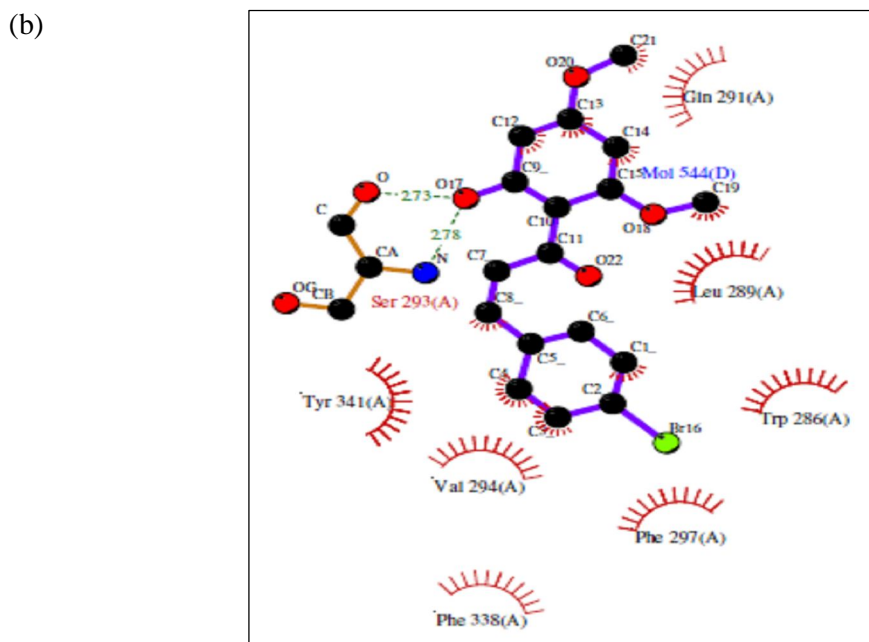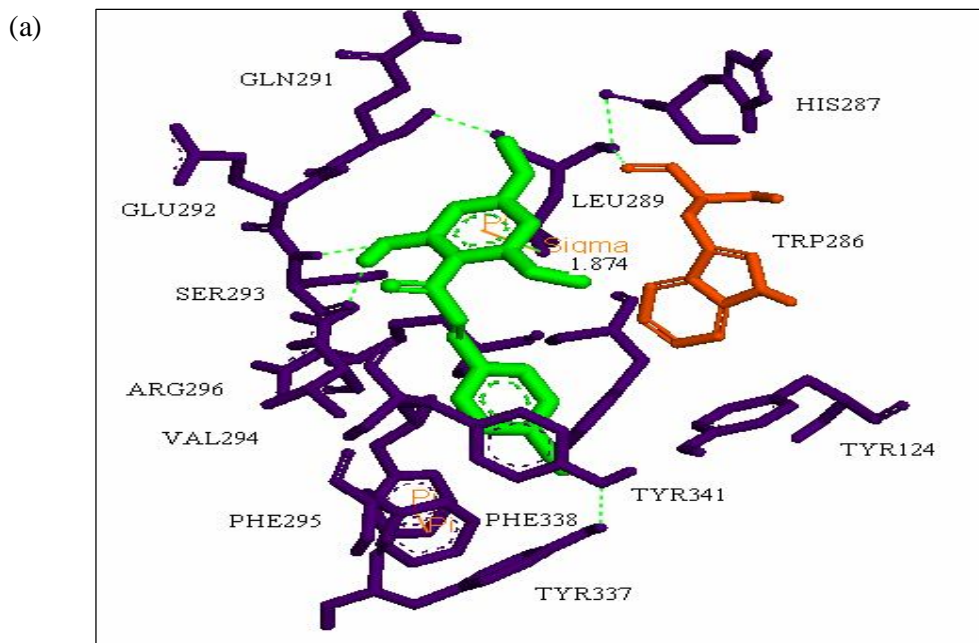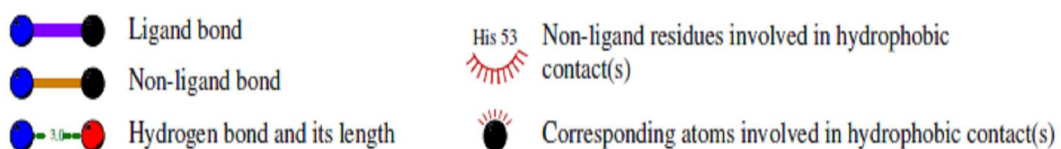
- Ligand bond
- Non-ligand bond
- Hydrogen bond and its length

His 53 — Non-ligand residues involved in hydrophobic contact(s)

— Corresponding atoms involved in hydrophobic contact(s)

6.3.3 Aβ PEPTIDE AGGREGATION ASSAY

The compounds that showed the greatest AChE inhibitory activity [compounds **C4**, **C8**, **C11**, **C12**, **C15**, **C17** and **C18** (compound **C14** wasn't tested due to insufficient amount)] were selected to assess their ability to inhibit Aβ peptide aggregation employing the thioflavin T fluorescence method. Propidium, a known inhibitor acting at the AChE peripheral site was used as a standard compound. The results summarized in **Table 6.3** indicated that compounds **C4**, **C11**, **C15** and **C18** inhibited the Aβ peptide aggregation at 10 µM at a level which is comparable to as potent as propidium, which caused 80 % inhibition at a final concentration of 8.2 µM.

Table 6.3: Inhibition of self-induced Aβ peptide aggregation by compounds with the greatest AChE inhibitory activity.

Compound	Aβ peptide aggregation % Inhibition at 10 µM [a]
C4	52
C8	5
C11	42
C12	17
C14	NE
C15	45
C17	3
C18	79
Propidium*	80[b]

[a] Values are expressed as mean of triplicate, * Standard inhibitor, [b] Tested at 8.2 µM, NE = not estimated

6.4 CONCLUSION

In conclusion, the overall docking analysis for the 8 compounds (**C4**, **C8**, **C11**, **C12**, **C14**, **C15**, **C17** and **C18**) which were found to inhibit AChE showed that these compounds bind at the PAS region of AChE except for compound **C11** which is both a PAS and CAS binding ligand. Molecular docking studies for compounds **C14**, **C15** and **C18** have further demonstrated the importance of hydroxyl group on ring A *ortho* to the side chain which is mainly involved in forming a hydrogen bond with protein residues. The most active compounds **C12**, **C14**, **C15** and **C18** were found to form hydrogen bonds with Tyr72, Asp74, Tyr124, Ser293, Phe295 and Arg296. Leu76, Trp286, Phe297, Tyr337, Phe338 and Tyr341 are seem to be an important residues as they are interact with these ligands by hydrophobic interactions. Furthermore, inhibition studies on self-induced Aβ aggregation has found that compound **C18** can exert an antiaggregation effect. In the present study, the combination of experimental and computational approach has successfully shown that some chalcones have the potential to inhibit amyloid beta aggregation thus preventing or delaying the degeneration of cholinergic neurons.

CHAPTER 7: GENERAL CONCLUSION AND FUTURE PERSPECTIVES

In the current study, a number of crystal structures of acetylcholinesterase (AChE) were extracted from the Protein Data Bank (PDB) and docked with known ligands to find a suitable structure for virtual screening. The blind docking results using a structure obtained from human acetylcholinesterase (hAChE) in complex with fasciculin II (PDB ID: 1b41) showed that most of the peripheral anionic site (PAS) binding ligands bound near the aromatic residue Trp286. This structure was found to be the most suitable for identifying PAS ligands and therefore was chosen for virtual screening.

The selected protein structure was then docked with a library of 830 commercially available ligands using computational procedures in order to identify potential anticholinesterase compounds and the lowest binding energy was exhibited by compound **V1**. About 21 compounds with a lowest binding energy range from -8.72 kcal/mol to -5.60 kcal/mol were selected for testing.

An assay to measure AChE inhibitory activity was optimised and used to evaluate the compounds identified from the virtual screening. Several compounds showed good activity with IC_{50} values in the range 1–15 µM. The most potent inhibitor, compound **V18**, inhibited AChE with IC_{50} of 1.54 µM. Molecular modeling studies showed this compound bound to the catalytic site (CAS) and PAS of the enzyme near the aromatic residues Trp86 and Trp286, respectively.

A self-induced amyloid beta (Aβ) peptide aggregation assay was optimised and used to evaluate the compounds with good AChE inhibitory activity. They were found

to inhibit Aβ peptide aggregation at 10 µM in the range 8 % to 60 % with compound **V1** showing the highest activity.

The anticholinesterase activity, and molecular interactions of a series of chalcones were also investigated in this study. Docking studies has indicated that the active compounds **C4**, **C8**, **C12**, **C14**, **C15**, **C17** and **C18** are PAS binders whereas compound **C11** is both a PAS and CAS binding ligand. Chalcones with greatest AChE inhibitory potency (**C4**, **C8**, **C11**, **C12**, **C14**, **C15**, **C17** and **C18)** were selected to assess their ability to inhibit Aβ peptide aggregation. The results indicated that these compounds gave inhibition at 10 µM in a range varying from 5 % to 79 %. Compound **C18** was found to be as potent as propidium, which caused 80 % inhibition at a final concentration of 8.2 µM.

In summary, we have identified some promising PAS-binding anticholinesterase compounds which show high inhibitory activity towards AChE and self-induced Aβ aggregation. Since other PAS-binding ligands such as propidium, and decamethonium have been found to inhibit AChE-induced Aβ aggregation, it can be hypothesized that the active compounds from this study might also have a significant effect in modulating this pathway. Therefore, further studies are required to investigate the effect of these compounds towards AChE-induced Aβ peptide aggregation and determine the inhibition mode of these compounds.

REFERENCES

Ahmed, E., Nawaz, S. A., Malik, A. & Choudhary, M. I. (2006) Isolation and cholinesterase-inhibition studies of sterols from *Haloxylon recurvum. Bioorganic & Medicinal Chemistry Letters.* **16**, 573–580.

Alhomida, A. S., Al-Rajhi, A. A., Kamal, M. A. & Al-Jafari, A. A. (2000) Kinetic analysis of the toxicological effect of tacrine (Cognex) on human retinal acetylcholinesterase activity. *Toxicology.* **147**, 33–39.

Alonso, D., Dorronsoro, I., Rubio, L., Munoz, P., Garcia-Palomero, E., Del Monte, M., Bidon-Chanal, A., Orozco, M., Luque, F. J., Castro, A., Medina, M. & Martinez, A. (2005) Donepezil-tacrine hybrid related derivatives as new dual binding site inhibitors of AChE. *Bioorganic & Medicinal Chemistry.* **13**, 6588–6597.

Amenta, F., Parnetti, L., Gallai, V. & Wallin, A. (2001) Treatment of cognitive dysfunction associated with Alzheimer's disease with cholinergic precursors. Ineffective treatments or inappropriate approaches?. *Mechanisms of Ageing and Development.* **122**, 2025–2040.

Amor, E. C., Villasenor, I. M., Nawaz, S. A., Hussain, M. S. & Choudhary, M. I. (2005) A dihydrochalcone from *Syzygium samarangense* with anticholinesterase activity. *Philippine Journal of Science.* **134**, 105–111.

Ashani, Y., Grunwald, J., Kronman, C., Velan, B. & Shafferman, A. (1994) Role of tyrosine-337 in the binding of Huperzine-a to the active-site of human acetylcholinesterase. *Molecular Pharmacology.* **45**, 555–560.

Ata, A., Iverson, C. D., Kalhari, K. S., Akhter, S., Betteridge, J., Meshkatalsadat, M. H., Orhan, I. & Sener, B. (2010) Triterpenoidal alkaloids from *Buxus hyrcana* and their enzyme inhibitory, anti-fungal and anti-leishmanial activities. *Phytochemistry.* **71**, 1780–1786.

Atta Ur, R., Parveen, S., Khalid, A., Farooq, A. & Choudhary, M. I. (2001) Acetyl and butyrylcholinesterase-inhibiting triterpenoid alkaloids from *Buxus papillosa. Phytochemistry.* **58**, 963–968.

Aurangzeb Hasan, K. M. K., Mohammed Sher, Ghulam M. Maharvi, Sarfraz A. Nawaz, M.I. Choudhary, Atta-Ur-Rahman, & Claudiu T. Supuran (2005) Synthesis and inhibitory potential towards acetylcholinesterase, butyrylcholinesterase and lipoxygenase of some variably substituted chalcones. *Journal of Enzyme Inhibition and Medicinal Chemistry.* **20**, 41–47.

Bartolini, M., Bertucci, C., Cavrini, V. & Andrisano, V. (2003) Beta-Amyloid aggregation induced by human acetylcholinesterase: Inhibition studies. *Biochemical Pharmacology.* **65**, 407–416.

Belluti, F., Piazzi, L., Bisi, A., Gobbi, S., Bartolini, M., Cavalli, A., Valenti, P. & Rampa, A. (2009) Design, synthesis, and evaluation of benzophenone derivatives as novel acetylcholinesterase inhibitors. *European Journal of Medicinal Chemistry.* **44**, 1341–1348.

Bourne, Y., Taylor, P. & Marchot, P. (1995) Acetylcholinesterase Inhibition by Fasciculin - crystal-structure of the complex. *Cell.* **83**, 503–512.

Brookmeyer, R., Johnson, E., Ziegler-Graham, K. & Arrighi, H. M. (2007) Forecasting the global burden of Alzheimer's disease. *Alzheimers & Dementia.* **3**, 186–191.

Chee, C. F. (2011) Synthesis of bioactive cyclohexenyl chalcones and flavonoid derivatives. PhD, University of Malaya.

Choudhary, A. I., Devkota, K. P., Nawaz, S. A., Ranjit, R. & Atta-Ur-Rahman (2005) Cholinesterase inhibitory pregnane-type steroidal alkaloids from *Sarcococca hookeriana*. *Steroids.* **70**, 295–303.

Choudhary, M. I., Shahnaz, S., Parveen, S., Khalid, A., Majeed Ayatollahi, S. A., Atta Ur, R. & Parvez, M. (2003) New triterpenoid alkaloid cholinesterase inhibitors from *Buxus hyrcana*. *Journal of Natural Products.* **66**, 739–742.

Chung, Y. K., Heo, H. J., Kim, E. K., Kim, H. K., Huh, T. L., Lim, Y., Kim, S. K. & Shin, D. H. (2001) Inhibitory effect of ursolic acid purified from *Origanum majorana* L. on the acetylcholinesterase. *Molecules and Cells.* **11**, 137–143.

Davies, P. & Maloney, A. J. (1976) Selective loss of central cholinergic neurons in Alzheimer's disease. *Lancet.* **2**, 1403.

De Ferrari, G. V., Canales, M. A., Shin, I., Weiner, L. M., Silman, I. & Inestrosa, N. C. (2001) A structural motif of acetylcholinesterase that promotes amyloid beta-peptide fibril formation. *Biochemistry.* **40**, 10447–10457.

Dimmock, J. R., Elias, D. W., Beazely, M. A. & Kandepu, N. M. (1999) Bioactivities of chalcones. *Current Medicinal Chemistry.* **6**, 1125–1149.

Dvir, H., Silman, I., Harel, M., Rosenberry, T. L. & Sussman, J. L. (2010) Acetylcholinesterase: From 3D structure to function. *Chemico-Biological Interactions.* **187**, 10–22.

Eichler, J., Anselment, A., Sussman, J. L., Massoulie, J. & Silman, I. (1994) Differential effects of "peripheral" site ligands on Torpedo and chicken acetylcholinesterase. *Molecular Pharmacology.* **45**, 335–340.

Ellman, G. L., Courtney, K. D., Andres, V., Jr. & Feather-Stone, R. M. (1961) A new and rapid colorimetric determination of acetylcholinesterase activity. *Biochemical Pharmacology.* **7**, 88–95.

Fan, P., Hay, A. E., Marston, A. & Hostettmann, K. (2008) Acetylcholinesterase-inhibitory activity of linarin from *Buddleja davidii*, structure-activity relationships of related flavonoids, and chemical investigation of *Buddleja nitida*. *Pharmaceutical Biology.* **46**, 596–601.

Filho, J.M.B., Medeiros, K.C.P., Diniz, M.D.F.F.M., Batista, L.M., Athayde-Filho, P.F, Silva, M.S., Da-Cunha, E.V.L., Almeida, J.R.G.S & Quintans Junior L.J.Q. (2006) Natural products inhibitors of the enzyme acetylcholinesterase. *Brazilian Journal of Pharmacognosy.* **16**, 258-285.

Fodale, V., Quattrone, D., Trecroci, C., Caminiti, V. & Santamaria, L. B. (2006) Alzheimer's disease and anaesthesia: Implications for the central cholinergic system. *British Journal of Anaesthesia.* **97**, 445–452.

Friesner, R. A., Banks, J. L., Murphy, R. B., Halgren, T. A., Klicic, J. J., Mainz, D. T., Repasky, M. P., Knoll, E. H., Shelley, M., Perry, J. K., Shaw, D. E., Francis, P. & Shenkin, P. S. (2004) Glide: A new approach for rapid, accurate docking and scoring. 1. Method and assessment of docking accuracy. *Journal of Medicinal Chemistry.* **47**, 1739–1749.

Harel, M., Kleywegt, G. J., Ravelli, R. B., Silman, I. & Sussman, J. L. (1995) Crystal structure of an acetylcholinesterase-fasciculin complex: Interaction of a three-fingered toxin from snake venom with its target. *Structure.* **3**, 1355–1366.

Harel, M., Quinn, D. M., Nair, H. K., Silman, I. & Sussman, J. L. (1996) The X-ray structure of a transition state analog complex reveals the molecular origins of the catalytic power and substrate specificity of acetylcholinesterase. *Journal of the American Chemical Society.* **118**, 2340–2346.

Harel, M., Schalk, I., Ehret-Sabatier, L., Bouet, F., Goeldner, M., Hirth, C., Axelsen, P. H., Silman, I. & Sussman, J. L. (1993) Quaternary ligand binding to aromatic residues in the active-site gorge of acetylcholinesterase. *Proceedings of the National Academy of Sciences of the United States of America.* **90**, 9031–9035.

Houghton, P. J. & Howes, M. J. (2005) Natural products and derivatives affecting neurotransmission relevant to Alzheimer's and Parkinson's disease. *Neurosignals.* **14**, 6–22.

Inestrosa, N. C., Alvarez, A., Perez, C. A., Moreno, R. D., Vicente, M., Linker, C., Casanueva, O. I., Soto, C. & Garrido, J. (1996) Acetylcholinesterase accelerates assembly of amyloid-beta-peptides into Alzheimer's fibrils: Possible role of the peripheral site of the enzyme. *Neuron.* **16**, 881–891.

Inestrosa, N. C., Dinamarca, M. C. & Alvarez, A. (2008) Amyloid-cholinesterase interactions - Implications for Alzheimer's disease. *Febs Journal.* **275**, 625–632.

Jacobsen, J. S., Reinhart, P. & Pangalos, M. N. (2005) Current concepts in therapeutic strategies targeting cognitive decline and disease modification in Alzheimer's disease. *Journal of the American Society for Experimental NeuroTherapeutics (ASENT).* **2**, 612–626.

Jones, G., Willett, P., Glen, R. C., Leach, A. R. & Taylor, R. (1997) Development and validation of a genetic algorithm for flexible docking. *Journal of Molecular Biology.* **267**, 727–748.

Jung, M. & Park, M. (2007) Acetylcholinesterase inhibition by flavonoids from *Agrimonia pilosa. Molecules.* **12**, 2130–2139.

Kalauni, S. K., Choudhary, M. I., Khalid, A., Manandhar, M. D., Shaheen, F., Atta Ur, R. & Gewali, M. B. (2002) New cholinesterase inhibiting steroidal alkaloids

from the leaves of *Sarcococca coriacea* of Nepalese origin. *Chemical & Pharmaceutical Bulletin (Tokyo)*. **50**, 1423–1426.

Kang, S. Y., Lee, K. Y., Park, M. J., Kim, Y. C., Markelonis, G. J., Oh, T. H. & Kim, Y. C. (2003) Decursin from *Angelica gigas* mitigates amnesia induced by scopolamine in mice. *Neurobiology of Learning and Memory*. **79**, 11–18.

Khalid, A., Zaheer Ul, H., Anjum, S., Khan, M. R., Atta Ur, R. & Choudhary, M. I. (2004) Kinetics and structure-activity relationship studies on pregnane-type steroidal alkaloids that inhibit cholinesterases. *Bioorganic & Medicinal Chemistry*. **12,** 1995–2003.

Khurana, R., Coleman, C., Ionescu-Zanetti, C., Carter, S. A., Krishna, V., Grover, R. K., Roy, R. & Singh, S. (2005) Mechanism of thioflavin T binding to amyloid fibrils. *Journal of Structural Biology*. **151**, 229–238.

Kim, D. K., Lee, K. T., Baek, N. I., Kim, S. H., Park, H. W., Lim, J. P., Shin, T. Y., Eom, D. O., Yang, J. H. & Eun, J. S. (2004) Acetylcholinesterase inhibitors from the aerial parts of *Corydalis speciosa*. *Archives of Pharmacal Research*. **27**, 1127–1131.

Kimura, M., Akasofu, S., Ogura, H. & Sawada, K. (2005) Protective effect of donepezil against A beta(1-40) neurotoxicity in rat septal neurons. *Brain Research*. 1047, 72–84.

Komloova, M., Musilek, K., Horova, A., Holas, O., Dohnal, V., Gunn-Moore, F. & Kuca, K. (2011) Preparation, in vitro screening and molecular modelling of symmetrical bis-quinolinium cholinesterase inhibitors-implications for early Myasthenia gravis treatment. *Bioorganic & Medicinal Chemistry Letters*. **21**, 2505–2509.

Korabecny, J., Musilek, K., Zemek, F., Horova, A., Holas, O., Nepovimova, E., Opletalova, V., Hroudova, J., Fisar, Z., Jung, Y. S. & Kuca, K. (2011) Synthesis and in vitro evaluation of 7-methoxy-N-(pent-4-enyl)-1,2,3,4-tetrahydroacridin-9-amine-new tacrine derivate with cholinergic properties. *Bioorganic & Medicinal Chemistry Letters*. **21,** 6563–6566.

Kryger, G., Harel, M., Giles, K., Toker, L., Velan, B., Lazar, A., Kronman, C., Barak, D., Ariel, N., Shafferman, A., Silman, I. & Sussman, J. L. (2000) Structures of recombinant native and E202Q mutant human acetylcholinesterase complexed with the snake-venom toxin fasciculin-II. *Acta Crystallographica Section D: Biological Crystallography*. **56**, 1385–1394.

Kuntz, I. D., Blaney, J. M., Oatley, S. J., Langridge, R. & Ferrin, T. E. (1982) A Geometric Approach to Macromolecule-Ligand Interactions. *Journal of Molecular Biology*. **161**, 269–288.

Kvaltinova, Z., Lukovic, L., Machova, J. & Fatranska, M. (1991) Effect of the steroidal alkaloid buxaminol-E on blood pressure, acetylcholinesterase activity and (3H)quinuclidinyl benzilate binding in cerebral cortex. *Pharmacology*. **43**, 20–25.

Kwon, Y. E., Park, J. Y., No, K. T., Shin, J. H., Lee, S. K., Eun, J. S., Yang, J. H., Shin, T. Y., Kim, D. K., Chae, B. S., Leem, J. Y. & Kim, K. H. (2007) Synthesis, in vitro assay, and molecular modeling of new piperidine derivatives having dual inhibitory potency against acetylcholinesterase and Abeta(1-42) aggregation for Alzheimer's disease therapeutics. *Bioorganic & Medicinal Chemistry.* **15**, 6596–6607.

Levine, H. (1993) Thioflavine-T interaction with synthetic Alzheimers-Disease beta-amyloid peptides - detection of amyloid aggregation in solution. *Protein Science.* **2**, 404–410.

Levine, H., 3rd. (1997) Stopped-flow kinetics reveal multiple phases of thioflavin T binding to Alzheimer beta (1-40) amyloid fibrils. *Archives of Biochemistry and Biophysics.* **342**, 306–316.

Li, L. T., Liu, Y. Q., Wang, L. J., Cheng, Y. Q., Saito, M., Yamaki, K. & Qiao, Z. H. (2009) Isoflavone content and anti-acetylcholinesterase activity in commercial douchi (a traditional chinese salt-fermented soybean food). *Jarq-Japan Agricultural Research Quarterly.* **43**, 301–307.

Liu, S. J., Yang, L., Jin, Z., Huang, E. F., Wan, D. C. C., Lin, H. Q. & Hu, C. (2009) Design, synthesis, and biological evaluation of 7H-thiazolo[3,2-b]-1,2,4-triazin-7-one derivatives as novel acetylcholinesterase inhibitors. *Arkivoc*. 333–348.

Mizutani, M. Y. & Itai, A. (2004) Efficient method for high-throughput virtual screening based on flexible docking: Discovery of novel acetylcholinesterase inhibitors. *Journal of Medicinal Chemistry.* **47**, 4818–4828.

Morris, G. M., Goodsell, D. S., Halliday, R. S., Huey, R., Hart, W. E., Belew, R. K. & Olson, A. J. (1998) Automated docking using a Lamarckian genetic algorithm and an empirical binding free energy function. *Journal of Computational Chemistry.* **19**, 1639–1662.

Munoz-Ruiz, P., Rubio, L., Garcia-Palomero, E., Dorronsoro, I., Del Monte-Millan, M., Valenzuela, R., Usan, P., De Austria, C., Bartolini, M., Andrisano, V., Bidon-Chanal, A., Orozco, M., Luque, F. J., Medina, M. & Martinez, A. (2005) Design, synthesis, and biological evaluation of dual binding site acetylcholinesterase inhibitors: New disease-modifying agents for Alzheimer's disease. *Journal of Medicinal Chemistry.* **48**, 7223–7233.

Naiki, H., Higuchi, K., Hosokawa, M. & Takeda, T. (1989) Fluorometric determination of amyloid fibrils in vitro using the fluorescent dye, thioflavin T1. *Analytical Biochemistry.* **177**, 244–249.

Naiki, H., Higuchi, K., Matsushima, K., Shimada, A., Chen, W. H., Hosokawa, M. & Takeda, T. (1990) Fluorometric examination of tissue amyloid fibrils in murine senile amyloidosis: Use of the fluorescent indicator, thioflavine T. *Laboratory Investigation.* **62**, 768–773.

Naiki, H., Higuchi, K., Nakakuki, K. & Takeda, T. (1991) Kinetic analysis of amyloid fibril polymerization in vitro. *Laboratory Investigation.* **65**, 104–110.

Pakaski, M., Rakonczay, Z., Fakla, I., Papp, H. & Kasa, P. (2000) In vitro effects of metrifonate on neuronal amyloid precursor protein processing and protein kinase C level. *Brain Research.* **863**, 266–270.

Pera, M., Roman, S., Ratia, M., Camps, P., Munoz-Torrero, D., Colombo, L., Manzoni, C., Salmona, M., Badia, A. & Clos, M. V. (2006) Acetylcholinesterase triggers the aggregation of PrP 106-126. *Biochemical & Biophysical Research Communications.* **346**, 89–94.

Racchi, M., Mazzucchelli, M., Porrello, E., Lanni, C. & Govoni, S. (2004) Acetylcholinesterase inhibitors: Novel activities of old molecules. *Pharmacological Research.* **50**, 441–451.

Racchi, M., Uberti, D., Govoni, S., Memo, M., Lanni, C., Vasto, S., Candore, G., Caruso, C., Romeo, L. & Scapagnini, G. (2008) Alzheimer's disease: New diagnostic and therapeutic tools. *Immunity & Ageing.* **5**, 7.

Radic, Z., Duran, R., Vellom, D. C., Li, Y., Cervenansky, C. & Taylor, P. (1994) Site of fasciculin interaction with acetylcholinesterase. *Journal of Biological Chemistry.* **269**, 11233–11239.

Rarey, M., Kramer, B., Lengauer, T. & Klebe, G. (1996) A fast flexible docking method using an incremental construction algorithm. *Journal of Molecular Biology.* **261**, 470–489.

Reddy, A. S., Pati, S. P., Kumar, P. P., Pradeep, H. N. & Sastry, G. N. (2007) Virtual screening in drug discovery -- a computational perspective. *Current Protein & Peptide Science.* **8**, 329–351.

Rollinger, J. M., Hornick, A., Langer, T., Stuppner, H. & Prast, H. (2004) Acetylcholinesterase inhibitory activity of scopolin and scopoletin discovered by virtual screening of natural products. *Journal of Medicinal Chemistry.* **47**, 6248–6254.

Rouleau, J., Iorga, B. I. & Guillou, C. (2011) New potent human acetylcholinesterase inhibitors in the tetracyclic triterpene series with inhibitory potency on amyloid beta aggregation. *European Journal of Medicinal Chemistry.* **46**, 2193–2205.

Sabate, R., Lascu, I. & Saupe, S.J. (2008) On the binding of Thioflavin-T to HET-s amyloid fibrils assembled at pH 2. *Journal of Structural Biology.* doi:10.1016/j.jsb.2008.02.002.

Schaeffer, E. L., Figueiro, M. & Gattaz, W. F. (2011) Insights into Alzheimer disease pathogenesis from studies in transgenic animal models. *Clinics.* **66,** 45–54.

Shen, C. & Murphy, R.M. (1995) Solvent effects on self-assembly of β-amyloid peptide. *Biophysical Journal.* **69**, 640–651.

Shoichet, B. K. (2004) Virtual screening of chemical libraries. *Nature.* **432**, 862–865.

Silman, I. & Sussman, J. L. (2008) Acetylcholinesterase: How is structure related to function?. *Chemico-Biological Interactions.* **175**, 3–10.

Soreq, H., Benaziz, R., Prody, C. A., Seidman, S., Gnatt, A., Neville, L., Liemanhurwitz, J., Levlehman, E., Ginzberg, D., Lapidotlifson, Y. & Zakut, H. (1990) Molecular-cloning and construction of the coding region for human acetylcholinesterase reveals a G+C-rich attenuating structure. *Proceedings of the National Academy of Sciences of the United States of America.* **87**, 9688–9692.

Soto, C. (1999) Plaque busters: strategies to inhibit amyloid formation in Alzheimer's disease. *Molecular Medicine Today.* **5**, 343–350.

Sussman, J. L., Harel, M., Frolow, F., Oefner, C., Goldman, A., Toker, L. & Silman, I. (1991) Atomic structure of acetylcholinesterase from *Torpedo californica*: a prototypic acetylcholine-binding protein. *Science.* **253**, 872–879.

Tang, B. L. (2005) Alzheimer's disease: channeling APP to non-amyloidogenic processing. *Biochemical & Biophysical Research Communications.* **331**, 375–378.

Terry, A. V. & Buccafusco, J. J. (2003) The cholinergic hypothesis of age and Alzheimer's disease-related cognitive deficits: Recent challenges and their implications for novel drug development. *Journal of Pharmacology and Experimental Therapeutics.* **306**, 821–827.

Vardy, E. R., Catto, A. J. & Hooper, N. M. (2005) Proteolytic mechanisms in amyloid-beta metabolism: Therapeutic implications for Alzheimer's disease. *Trends In Molecular Medicine.* **11**, 464–472.

Yamamoto, Y., Ishihara, Y. & Kuntz, I. D. (1994) Docking analysis of a series of benzylamino acetylcholinesterase inhibitors with a phthalimide, benzoyl, or indanone moiety. *Journal of Medicinal Chemistry.* **37**, 3141–3153.

Yan, H., Zhang, H. Y. & Tang, X. C. (2007) Involvement of M1-muscarinic acetylcholine receptors, protein kinase C and mitogen-activated protein kinase in the effect of huperzine A on secretory amyloid precursor protein-alpha. *Neuroreport.* **18**, 689–692.

Zhang, H. Y., Liang, Y. Q., Tang, X. C., He, X. C. & Bai, D. L. (2002) Stereoselectivities of enantiomers of huperzine A in protection against beta-amyloid(25-35)-induced in PC12 and NG108-15 cells and cholinesterase inhibition in mice. *Neuroscience Letters.* **317**, 143–146.